REPORT NO. FRA/OR&D 76-290

FEASIBILITY OF FLAW DETECTION IN RAILROAD WHEELS USING ACOUSTIC SIGNATURES

K. Nagy
R. D. Finch

UNIVERSITY OF HOUSTON
Department of Mechanical Engineering
Houston TX 77004

OCTOBER 1976

FINAL REPORT

Prepared for

U.S. DEPARTMENT OF TRANSPORTATION
FEDERAL RAILROAD ADMINISTRATION
Office of Research and Development
Washington DC 20590

NOTICE

This document is disseminated under the sponsorship of the Department of Transportation in the interest of information exchange. The United States Government assumes no liability for its contents or use thereof.

NOTICE

The United States Government does not endorse products or manufacturers. Trade or manufacturers' names appear herein solely because they are considered essential to the object of this report.

Technical Report Documentation Page

1. Report No.	2. Government Accession No.	3. Recipient's Catalog No.
FRA/OR&D 76-290		

4. Title and Subtitle	5. Report Date
FEASIBILITY OF FLAW DETECTION IN RAILROAD WHEELS USING ACOUSTIC SIGNATURES	October 1976
	6. Performing Organization Code
7. Author(s)	8. Performing Organization Report No.
K. Nagy and R. D. Finch	DOT-TSC-FRA-76-6
9. Performing Organization Name and Address University of Houston* Department of Mechanical Engineering Houston TX 77004	10. Work Unit No. (TRAIS) RR631/R7314
	11. Contract or Grant No. DOT-FR-30002
12. Sponsoring Agency Name and Address U.S. Department of Transportation Federal Railroad Administration Office of Research and Development Washington DC 20590	13. Type of Report and Period Covered Final Report Aug. 1972 - Aug. 1974
	14. Sponsoring Agency Code

15. Supplementary Notes

*Under contract to: U.S. Department of Transportation
Transportation Systems Center
Kendall Square
Cambridge MA 02142

16. Abstract The feasibility study on the use of acoustic signatures for detection of flaws in railway wheels was conducted with the ultimate objective of development of an intrack device for moving cars. Determinations of the natural modes of vibrating wheels under various conditions are reported. Differences in acoustic signatures are found between good and cracked wheels, including spectral changes and variations in the time decay of sound. Various sounds occurring in normal railroad practice, such as rolling noise on welded rail and over joints and retarder screech were investigated. It was concluded that special purpose impacters will have to be used for a servicable device. Pattern recognition techniques were used for selecting good and bad wheels with a computerized processing scheme. A laboratory demonstration system has been constructed and found to be 85% reliable when system malfunctions are discounted.

17. Key Words	18. Distribution Statement
Railroad Wheels Acoustic Signature Defect Detection	DOCUMENT IS AVAILABLE TO THE U.S. PUBLIC THROUGH THE NATIONAL TECHNICAL INFORMATION SERVICE, SPRINGFIELD, VIRGINIA 22161

19. Security Classif. (of this report)	20. Security Classif. (of this page)	21. No. of Pages	22. Price
Unclassified	Unclassified	206	

Form DOT F 1700.7 (8-72) Reproduction of completed page authorized

PREFACE

The wheel is one of the most critical components of a car or locomotive in that a failure often results in a major derailment causing significant damage and operational losses. The availability of effective methods to determine if wheels have developed cracks is a potentially effective way to control such losses. The objective of this work was to evaluate an inspection method for the detection of wheel cracks.

The authors would like to express their sincere appreciation and thanks to the following:

Dr. B. D. Cook and other members of the Acoustics group, including Messrs. H. Dhingra, M. Jamal, D. Dousis, A. Chaudhari, K. Shrivastava, and B. Nagarkar for their assistance and efforts during the experimental work.

Mr. M. Duckler for his contribution to the design of the automatic impacter.

Messers. B. Smith, J. Baklik, D. Dogett, and L. Farley for assistance with the experimental equipment.

Mr. Don Bray and Mr. Roger Steele for vigorous and helpful contract monitoring.

The Southern Pacific Railroad Company for the loan of wheels, access to railroad property, and friendly advice.

METRIC CONVERSION FACTORS

Approximate Conversions to Metric Measures

Symbol	When You Know	Multiply by	To Find	Symbol
		LENGTH		
in	inches	2.5	centimeters	cm
ft	feet	30	centimeters	cm
yd	yards	0.9	meters	m
mi	miles	1.6	kilometers	km
		AREA		
in^2	square inches	6.5	square centimeters	cm^2
ft^2	square feet	0.09	square meters	m^2
yd^2	square yards	0.8	square meters	m^2
mi^2	square miles	2.6	square kilometers	km^2
	acres	0.4	hectares	ha
		MASS (weight)		
oz	ounces	28	grams	g
lb	pounds	0.45	kilograms	kg
	short tons (2000 lb)	0.9	tonnes	t
		VOLUME		
tsp	teaspoons	5	milliliters	ml
Tbsp	tablespoons	15	milliliters	ml
fl oz	fluid ounces	30	milliliters	ml
c	cups	0.24	liters	l
pt	pints	0.47	liters	l
qt	quarts	0.95	liters	l
gal	gallons	3.8	liters	l
ft^3	cubic feet	0.03	cubic meters	m^3
yd^3	cubic yards	0.76	cubic meters	m^3
		TEMPERATURE (exact)		
°F	Fahrenheit temperature	5/9 (after subtracting 32)	Celsius temperature	°C

Approximate Conversions from Metric Measures

Symbol	When You Know	Multiply by	To Find	Symbol
		LENGTH		
mm	millimeters	0.04	inches	in
cm	centimeters	0.4	inches	in
m	meters	3.3	feet	ft
m	meters	1.1	yards	yd
km	kilometers	0.6	miles	mi
		AREA		
cm^2	square centimeters	0.16	square inches	in^2
m^2	square meters	1.2	square yards	yd^2
km^2	square kilometers	0.4	square miles	mi^2
ha	hectares (10,000 m^2)	2.5	acres	
		MASS (weight)		
g	grams	0.035	ounces	oz
kg	kilograms	2.2	pounds	lb
t	tonnes (1000 kg)	1.1	short tons	
		VOLUME		
ml	milliliters	0.03	fluid ounces	fl oz
l	liters	2.1	pints	pt
l	liters	1.06	quarts	qt
l	liters	0.26	gallons	gal
m^3	cubic meters	35	cubic feet	ft^3
m^3	cubic meters	1.3	cubic yards	yd^3
		TEMPERATURE (exact)		
°C	Celsius temperature	9/5 (then add 32)	Fahrenheit temperature	°F

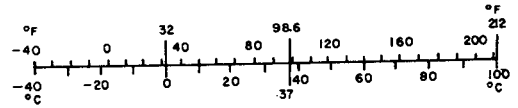

TABLE OF CONTENTS

TABLE OF CONTENTS (CONT'D)

LIST OF ILLUSTRATIONS

LIST OF ILLUSTRATIONS (CONTINUED)

LIST OF ILLUSTRATIONS (CONTINUED)

LIST OF ILLUSTRATIONS (CONTINUED)

LIST OF TABLES

EXECUTIVE SUMMARY

In this report, a laboratory demonstration system is described which is 75 - 85% reliable in detecting large cracks in wheels. The system works by recognizing the difference in the sound of a cracked wheel. In a sense it could be described as an automation of the art of carmen who can pick out bad wheels by their sound from a hammer blow.

In the automated system a hammer is actuated by a wheel as it moves along the track. A microphone is used to detect the sound. The electrical signal from the microphone is analyzed in terms of its frequency (or tonal) content and in terms of how quickly or slowly it (and the sound) dies away. These data are then processed by a minicomputer which has been programmed to recognize the various patterns of sounds or acoustic signatures as they are termed in this report. The minicomputer makes a decision as to whether or not the wheel is bad.

The background research reported here has been directed at answering such practical questions as the effects on the acoustic signature of wheel size and geometry, wheel load, surface covering, such as grease and dirt layers, and the various types of defects and cracks. It is concluded that the system works well enough in the laboratory to justify development of a prototype field installation.

There are presently under development other systems for in-track flaw detection method, one being the ultrasonic surface wave (USW) technique. One of the authors of this report was involved with pioneering research on the USW technique, which has the inherent

limitation that it can only find flaws within a shallow depth below the surface of the wheel tread. On the other hand, the acoustic signature technique, while it has not yet been field tested, has the potential of finding major flaws anywhere on the wheel. The reliability of the acoustic signature technique can be improved with the use of more sophisticated computer programming for pattern recognition. In addition the development of programs for recognition of various sounds could be applied to other problems such as detecting flat spots or shattered rims or air hose leaks.

1. INTRODUCTION

1.1 STATEMENT OF PROBLEM

Well developed nondestructive test methods are in use for monitoring product quality during the manufacture of railway wheels, including ultrasonic, magnetic particle, dye penetrant, and eddy current inspection techniques. However, there are no reliable, economical methods for finding in-service wheels with plate cracks. Today most flawed wheels on rolling stock are found by visual inspection. A considerable number of wheels have heavy coats of grease and grime in the plate area of the wheel, and thus, if large cracks are present, they may not be visible. The principal types of wheel cracks and their importance in derailments have been discussed in a previous report [3].

A need exists for an automoated railway wheel test facility that is capable of detecting flawed wheels on a passing train. The operation of such a test station would be economical only if it did not interfere with normal railway service, if it operated automatically, and if its reliability was such that it did not produce erroneous results, with railway personnel performing only necessary maintenance or repair. By locating such automated inspection stations at key railway junctions, a high percentage of cars could be monitored.

1.2 PRIOR WORK AND CURRENT OBJECTIVES

Some effort has been made by several groups to develop the principles of such automatic inspection stations. Two promising techniques are ultrasonic and acoustic signature methods. In the ultrasonic method, a pulse is sent into the wheel as it rolls over a transducer. Bray and Dalvi [1-5] initiated this work with one-fourth scale model wheels. Dalvi succeeded in producing surface waves on the tread of a stationary one-fourth scale wheel and detecting various machined flaws on the tread both with pulse echo and attenuation techniques. Scanning Systems, Inc., have built a prototype system based on the same principle. Their system was field tested in the fall of 1973 with a good success rate in detecting thermal cracks on the tread of rolling wheels. The system, however, is effective only for cracks that are within about 3/8 inch of the surface of the tread. Bray succeeded in detecting plate flaws using ultrasonic pulses and this work has been extended by Batelle Northwest.

In the acoustic signature method (where acoustic signature means the characteristic sound or vibration emitted by an object), a wheel is excited so that the radiated sound from the wheel may be distinguished from background noise. When a crack is introduced, the acoustic signature will change.

The acoustic signature method is gaining in acceptance as a nondestructive test method. Some of the early work relating to flaw detection of various aircraft components was done by Shroer, et al [6]. Signature analysis is also used in detection of flawed bearings [7].

The first experiments aimed at evaluating the feasibility of the acoustic signature method as a railway wheel flaw detection device were performed by Nagy with one-fourth scale wheels [8]. The experiment consisted of an examination of the audio frequency acoustic radiation from an excited wheel. Several ways of exciting wheels were experimented with and finally it was found that the most reproducible results were obtained with a random noise input.

Some results of third octave band spectral analysis of sound from such model wheels are shown in Figure 1.1. There were two good wheels and the dotted areas indicate the differences between the spectral levels of the good wheels and a bad wheel (which had a simulated plate flaw). The differences between the good and bad wheel spectra were much greater than the differences between the spectra of the good wheels and so it was felt that the acoustic signature technique would also be a feasible flaw detection method. These results were confirmed with narrow band analysis which showed shifts of resonant

INDICATES DIFFERENCE BETWEEN FLAWED WHEEL AND TWO GOOD WHEELS.

INDICATES DIFFERENCE BETWEEN TWO GOOD WHEELS.

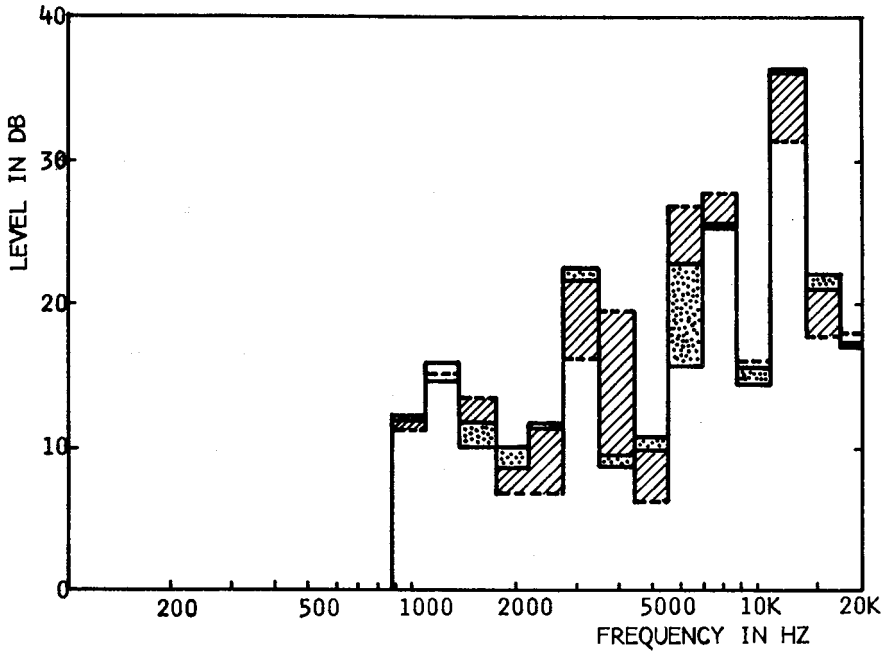

Fig. 1.1 1/3 Octave Comparative Graph for Three Model Wheels, Random Noise Tests (Dashed line indicates flawed wheel spectra)

frequencies and amplitude changes. Most of the changes induced by flaws in the spectra of the model wheels lie roughly in the 1.5 - 20 kHz range. Using the usual scaling law, this corresponds to a frequency range of roughly 400 Hz to 5000 Hz in full sized wheels.

Although they were promising, the results of the experiments with one-fourth scale model wheels did not yield enough data for the design of a prototype flaw detection device. The experiments performed were limited by the fact that the flaws were machined into the wheels. A machined flaw is only an approximation to an in-service fatigue crack. The effects of load, grease layers, wear and geometrical variations also remained as unknown factors. It was also unclear from the earlier study if sounds arising from normal railroad practice could be used for signature analysis or whether a specially constructed transducer would be necessary.

The objective of the current research program was to extend the earlier work to a feasibility study on full size wheels, some of which had real flaws acquired through normal use.

1.3 SYSTEM DESCRIPTION

A system to detect flaws using acoustic signatures is illustrated schematically in Fig. 1.2. The excitation might

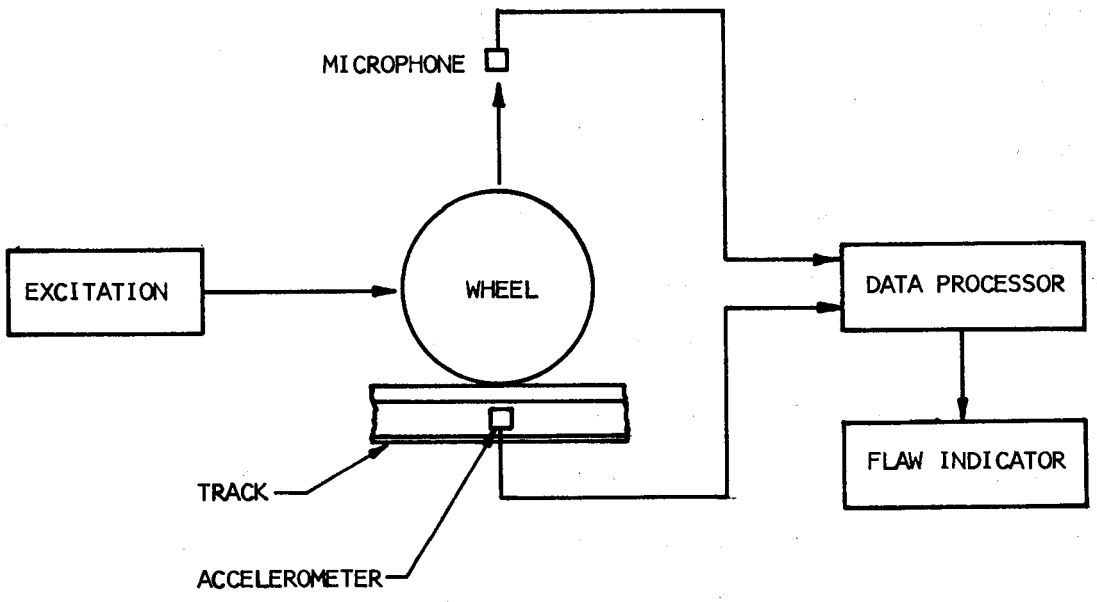

Fig. 1.2 Schematic of Flaw Indicator System Components

consist of a single impact (hammer blow or passage over a joint), continuous shaking due to surface roughness of the track as in rolling, or slip-stick action as in the cases of retarder action, braking or in passage around a curve. The vibratory mechanical energy of the excited wheel is partially degraded by sound radiation into the air and vibration of the track. (There are other nonacoustic forms of energy loss in addition, of course.) These two forms of acoustic energy could be detected by a microphone or track mounted accelerometer, respectively. The transduced signal would be interpreted by a data processing unit and a decision made as to whether or not the wheel is flawed. Finally some sort of flaw indicator would be actuated if necessary.

1.3.1 Design Questions

In order to prove feasibility and to produce an optimum system, information is required on a number of pertinent questions. The central point of the system is obviously the wheel, faulty or otherwise. Since the vibrational response of any object is determined by its impedance (mass and stiffness reactance, damping and modal coupling), it would be desirable to have a complete knowledge of these quantities as a function of frequency, and then to know how they are affected by the presence of flaws of various types and sizes. It should then,

in principle, be possible to predict the vibrational response of the wheel under various forms of excitation. Clearly the best form of excitation would be that whose forcing function has a wide frequency band in the range in which there are the greatest impedance differences between good and bad wheels. Selection of the best detection method is then simply a matter of finding which has maximum sensitivity to the wheel vibration in the same frequency range. The choice of data processing method consists of determining the differences between signatures of good and bad wheels in the most reliable manner. Finally the constraints of achieving convenient and reliable hardware have to be met.

1.3.2 Procedures

There are basically two ways in which these design questions may be resolved. For lack of better terminology, we shall call these the deterministic and statistical approaches.

In the deterministic approach one would attempt to calculate the impedances of good and bad wheels, with experimental verification, and then predict the wheel response under forcing functions typical of various types of excitation. Selection of detection devices and data processing schemes then could be determined to achieve maximum differentiation of good and bad wheel signatures.

Alternatively, the purely statistical approach would be to set up a prototype system, varying excitation methods and detection devices by trial and error. By sampling large numbers of wheels, the statistical patterns of signatures from good and bad wheels could be established and data processing schemes evolved to maximize the reliability of recognizing bad wheels.

The major problem with the deterministic method is the difficulty of obtaining precise knowledge of the impedance functions. Here one has to resort to partial knowledge. For instance, it is possible to determine the resonance frequencies of good and bad wheels (at which the reactance becomes zero) both experimentally and theoretically. The damping can also be measured, as a function of frequency. It is only possible to conjecture the nature of the forcing functions of the various excitation methods from experimental tests. On the other hand, the basic problem with using a purely statistical approach is that of obtaining a sufficient number of flawed wheels among large numbers of good wheels.

In practice, it appears that a combination of the deterministic and statistical approaches is desirable, due to the difficulties of trying to follow either one in a rigorous manner. Thus, the understanding implicit in the deterministic

approach, in so far as it exists, can be used as a guide in deciding which trials to undertake in statistical data gathering.

In the following chapters, the status of knowledge bearing on the key design problems is outlined. The starting point is a discussion of the determination of wheel resonances, firstly with approximate models and then by using a finite element method. The results of these theoretical studies are then compared with experimental and field data, and the principal differences between good and bad wheel signatures determined. The efficacy of various excitation and detection methods is then discussed and data processing methods are reviewed. Finally, a laboratory demonstration system and its performance is described. Experimental and computational details are presented in appendices.

2. THE RAILWAY WHEEL

2.1 INTRODUCTION

As explained in the preceding chapter, it would be desirable to be able to determine theoretically the response of a wheel to various forcing functions. If such a theory could be developed, it would serve several very practical purposes. For example, it is difficult to collect a sample of wheels with all the variations of flaw sizes and types that might eventually be encountered by a working device. With a reliable theory, however, the behavior of such variations could be simulated. The problem is that the theory is not easily developed.

We start by considering various elementary models and proceed to a finite element analysis. Although the theory has not been advanced as far as is desirable, it still yields some useful insights.

2.2 ELEMENTARY THEORY

2.2.1 Introduction

The railway wheel consists of a heavy rim, connected to the hub with a plate section (see Fig. 2.1) and may be modeled as a ring or as a plate. In Fig. 2.1 such ring and plate

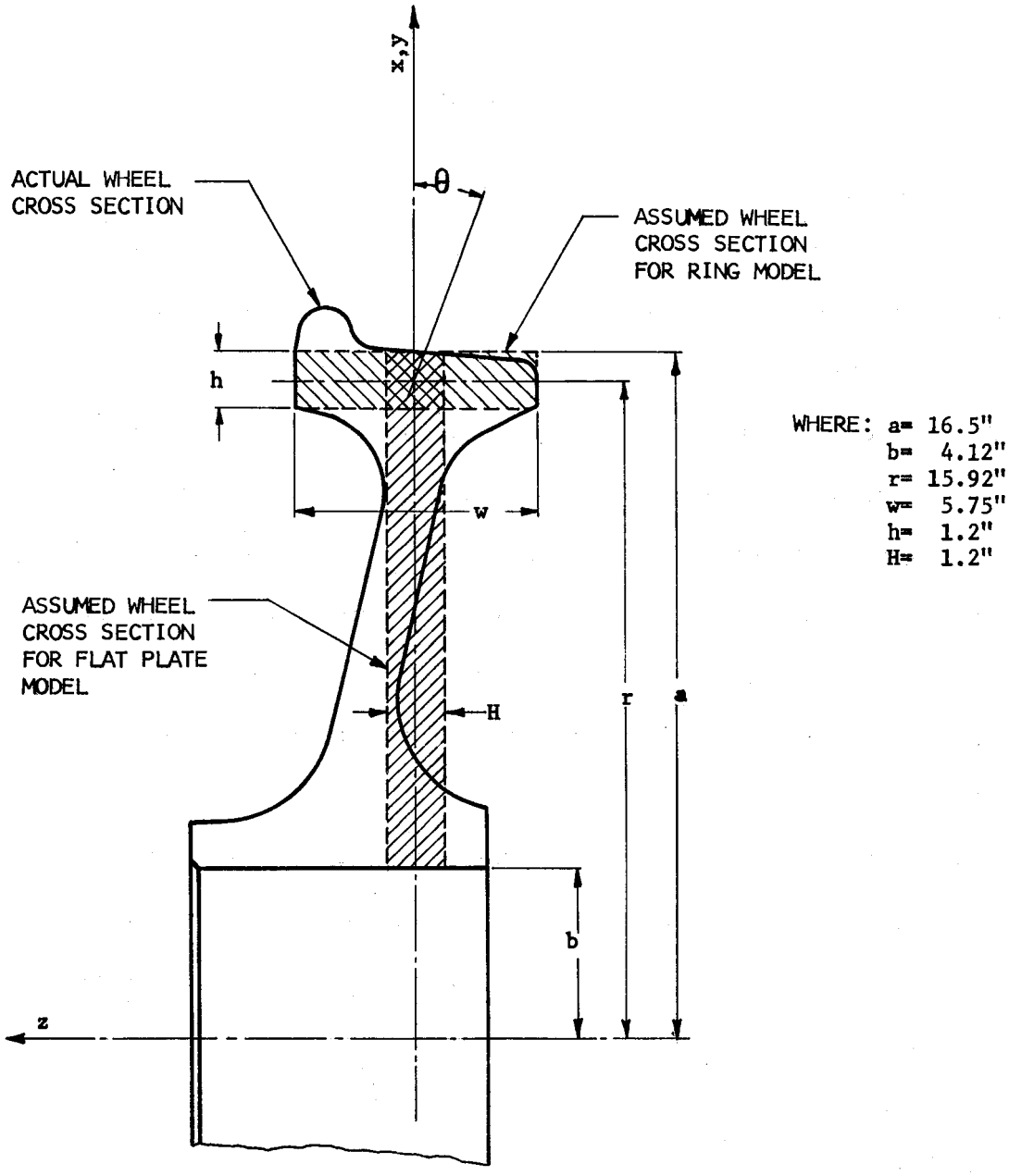

Fig. 2.1 Assumed and Actual Wheel Cross Sections

model outlines are superimposed over the actual cross section of the wheel. Bray [1] used ring and plate models in his original study of ultrasonic propagation. In the feasibility study of acoustic flaw detection in wheels using one-fourth scale models, Nagy made an attempt to model the railway wheel as a flat annular plate [8]. Although results from these elementary models are not in close quantitative agreement with experimental values, helpful qualitative insights are gained. A considerable amount of research has been done on vibration of annular plates by workers interested in high speed turbines, high speed saw blades, and related problems. Stappenbeck [9] compared the impact excited railroad wheel resonances with those of a ring and apparently had greater success than with the flat plate model.

2.2.2 Vibrations of Annular Plates and Circular Rings

The theory of vibration of thin annular plates was originally developed in the early 1920's by Southwell [10]. In the usual development it is assumed that transverse normal and shear strains can be neglected. Normal stresses are also assumed to be zero at the middle surface of the plate. With these assumptions, the equation of motion for free vibrations is given by:

$$\frac{EI}{\rho H(1-\nu^2)} \nabla^2 \nabla^2 w = - \frac{\partial^2 w}{\partial t^2} \qquad (1)$$

where $w(x,y)$ = displacement,

ρ = mass density,

E = Young's modulus,

I = moment of inertia of plate per unit width,

H = thickness of plate,

ν = Poisson's ratio,

t = time,

and ∇ = Laplacian operator.

Solutions to Eq. (1) are found by separation of variables. Assuming the annular plate to be clamped at its inner radius b and free at its outer radius a, the Eigenvalues λ_{nm}, were tabulated by Leissa [11] for various ratios of b/a. The resonant frequencies are then given by:

$$f_{nm} = \frac{\lambda^2_{nm}}{2\pi a^2} \sqrt{\frac{EI}{\rho H(1-\nu^2)}} \qquad \begin{matrix} \text{for } n = 1, 2, 3, \ldots \\ m = 1, 2, 3, \ldots \end{matrix} \qquad (2)$$

where f_{nm} = eigenfrequencies,

λ_{nm} = eigenvalues,

and a = the outer radius of the annular plate.

Timoshenko [12] gives a review of the fundamental theory of a vibrating circular ring. The modes of vibration of the ring

may be grouped as follows: radial or extensional modes, torsional modes and flexural modes. The following assumptions are made in the derivations:

a. The ring has a constant cross section.

b. The dimensions of the cross section are small when compared with the ring radius, r. (see Fig. 2.1).

c. The cross section is symmetrical with respect to the plane of the ring.

For the case of radial or extensional vibrations, the equation of motion is:

$$\ddot{u} + \frac{E}{\rho r^2} u = 0 \ , \qquad (3)$$

where u = the radial displacement.

The frequency of the fundamental radial mode is found to be:

$$f = \frac{1}{2\pi} \sqrt{\frac{E}{\rho r^2}} \qquad (4)$$

Higher extensional modes analogous to longitudinal vibrations of prismatic bars are given by:

$$f_n = \frac{1}{2\pi} \sqrt{\frac{E}{\rho r^2}} \sqrt{1+n^2} \quad \text{for } n = 0, 1, 2, 3, \ldots \qquad (5)$$

For the case of torsional vibrations, the equation of motion is:

$$\ddot{\theta} + \frac{E I_x}{\rho r^2 I_p} \theta = 0 \qquad (6)$$

where θ = the angle of rotation with respect to the plane of the ring;

I_x = the moment of inertia of cross section with respect to an axis parallel to the plane of the ring;

and I_p = the polar moment of inertia of cross section.

The frequencies of the torsional modes are given by:

$$f_n = \frac{1}{2\pi}\sqrt{\frac{E\,I_x}{\rho r^3\,I_p}}\sqrt{1+n^2} \quad \text{for } n = 0, 1, 2, 3,... \qquad (7)$$

Flexural vibrations of circular rings are of two different types; in one, all displacements are parallel to the plane of the ring, in the other displacements in the plane of the ring as well as displacements normal to it and twist occur. The resonant frequencies for these two cases respectively are given by the following equations. For in-plane flexure the resonant frequencies are given by:

$$f_n = \frac{1}{2\pi}\sqrt{\frac{EI_z}{\rho A r^4}}\sqrt{\frac{n^2(1-n^2)^2}{(n^2+1)}} \quad \text{for } n = 1, 2, 3,.. \qquad (8)$$

where A = the cross sectional area,

I_z = the moment of inertia of cross section with respect to an axis normal to the plane of the ring.

For out-of-plane flexure the resonant frequencies are given by:

$$f_n = \frac{1}{2\pi}\sqrt{\frac{E\,I_x}{\rho A r^4}}\sqrt{\frac{n^2(n^2-1)^2}{(n^2+1+\nu)}} \quad \text{for } n = 1, 2, 3,.. \qquad (9)$$

where I_x = moment of inertia of cross section with respect to an axis in the plane of the ring.

2.2.3 Approximation of Wheel Resonances by Elementary Theories

In Table 2.1 resonance frequencies calculated using the elementary theories discussed in the preceeding section are tabulated for the annular plate, the flexural modes perpendicular to the plane of the circular ring along with experimentally obtained values for a 33-inch good wheel. The in-plane flexural modes occur at considerably lower frequencies than the out-of-plane flexural modes and do not appear to correspond to any mode actually observed in the wheel. Resonance frequencies were also calculated for the extensional and torsional modes of the circular ring model, and were found to occur at much higher frequencies than the flexural modes, and consequently they are omitted from these tabulations.

The resonances obtained with the elementary models differ in value from actual wheel resonances. It is to be expected

TABLE 2.1. LIST OF RESONANCES CALCULATED WITH ELEMENTARY WHEEL MODELS

Modes with Plate Model				Modes with Ring Model (Flexural Modes Perpendicular to Plane of Ring)			Experimental Resonances for 33" Wheel	
m	m	freq. in Hz.	approx. shape	n	freq. in Hz	approx. shape	freq. in Hz	approx. shape
1	0	275						
0	0	290		1	0			
2	0	346		2	549		420	
3	0	578		3	1579		1093	
0	1	1856		4	3049		1890	
1	1	1943		5	4948		2417	
2	1	2218		6	7272			
3	1	2706		7	10021			

that resonant frequencies obtained with an annular plate model should be lower than experimentally obtained values for a similar size railway wheel since the wheel has a conical plate section which is reinforced by a heavy rim. Savin and Fleishman [13] investigated the dynamic behavior of circular plates reinforced with concentric circular ribs. Their results showed that increasing the "relative rigidity" of the rib will increase the resonant frequencies, whereas increasing the "relative mass" of the rib will cause a decrease in the resonant frequencies. Similarly, the stiffness of a free ring should be less than that of a ring restrained by a heavy web section.

Although the simple annular plate model or the ring model are inadequate for accurate prediction of wheel resonances, it is of considerable interest to determine whether the vibration of a railway wheel is more similar to an annular plate or to a circular ring.

Stappenbeck [9] experimented with 765 mm diameter street car wheels. Having obtained experimental resonance frequencies and mode shapes, he reported that those which were excited the most intensely were the ones with 2, 3, 4,... nodal diameters and no nodal circles. He examined the frequency ratios of these prominent resonances and compared them to frequency ratios for a circular ring.

For the flexural modes of a circular ring the resonance frequencies are given by Eq. (9) which may be rewritten as follows:

$$f_n = \frac{n(n-1)}{\sqrt{n^2+1+\nu}} B \quad \text{for } n = 1, 2, 3, \ldots \qquad (10)$$

where

$$B = \frac{1}{2\pi} (EI_x/\rho A r^4)^{\frac{1}{2}}$$

When $n = 1$, $f_1 = 0$, in which case the ring translates in a rigid body mode. When $n = 2$ the ring performs the fundamental mode of flexural vibration. The ratios of the frequencies of higher order modes to the fundamental are found to be: 1.0, 2.86, 5.51, 8.94, 13.3, ... for $n = 2, 3, 4, 5, 6, \ldots$ respectively.

In Fig. 2.2 are shown a frequency spectrum obtained experimentally by Stappenbeck for 765 mm diameter wheels under impact and a spectrum obtained by multiplying the lowest resonance that Stappenbeck found by the ring flexural model frequency ratios. This implies that the constant B in Eq. 10 has to be decreased to take account of the presence of the plate. Thus there is some correspondence between actual and calculated resonances indicating ring-like behavior of the wheel, under impact. Stappenbeck further states that the resonance frequencies of the rim, as above are very close to that of the wheel,

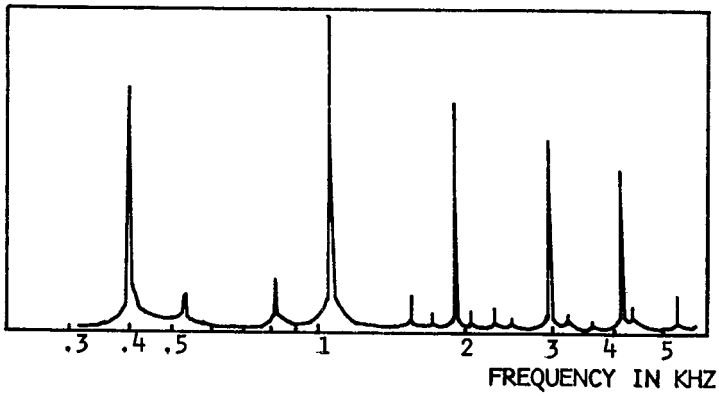

STAPPENBECK'S SPECTRUM FOR 765 MM DIAMETER STREETCAR WHEEL

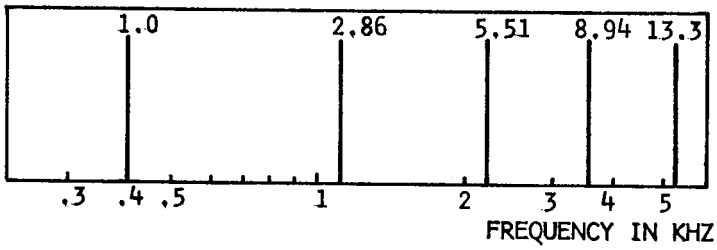

LINE SPECTRA OBTAINED BY MULTIPLYING THE LOWEST RESONANCE OBTAINED BY STAPPENBECK WITH THE RING FREQUENCY RATIOS.

Fig. 2.2 Approximation of Wheel Resonances with Elementary Ring Theory

although it is unclear if he observed this experimentally.

It must be concluded that exact resonance frequencies for modes of vibration of a railway wheel cannot be obtained by an annular plate or a ring model. But there are similarities between the behaviors of these simple models and the railway wheel.

2.2.4 Changes in Resonant Frequencies Due to Imperfections

Previous work on the vibration of annular plates was aimed toward turbine wheels, saw blades, and other high speed rotating equipment. The objective of these studies was to determine the effects on the vibration characteristics of the plate when imperfections were introduced, whether intentionally or accidentally. A brief review is given in the following of some of this work with mention of those aspects which have been found to have parallels in railway wheel vibration.

Mote [14] analysed the free vibration of centrally clamped circular saw blades by the Rayleigh-Ritz technique. He found that clamping stresses and stresses induced by centrifugal force will affect the resonant frequencies. Similarly, thermal gradients introduced at the outer edge of the saw blade altered the values of resonant frequencies. Mote also found that symmetrical modes of vibration (modes with nodal

curves on concentric circles) were not excited experimentally. Williams [15] has shown that for a perfectly homogeneous vibrating disk the angular position of the nodal diameters depends solely on the position of the exciting force. However, the presence of cracks or discontinuities eliminates the indeterminacy of position of the nodal diameters, which then take on perferred positions. For each mode (with at least one nodal diameter) there are two perferred nodal positions. Based on experiments performed with thin disks having holes or added masses Tobias [16,17] found that the resonant frequencies will change. He cites a paper written by Zenneck [18] who explains these changes by the change in the kinetic energy of the plate. Tobias noted that imperfections in stiffness should produce frequency changes by altering the strain energy of the plate. It is apparent from his work that the frequency change for one of a pair of perferred nodal positions is small, while quite large for the other. The numerical value of resonance change also increases with increasing mode number, but the percentage change is almost constant for the various modes.

The railroad wheel also bears a similarity to a bell. The sounds of bells have been studied extensively and it is interesting to note that beat tones in bells are eliminated by grinding away amounts of the bell metal at points on the periphery of the rim. Occurrence of beat frequencies was

noted for plates [16,17] as well as for bells. It was also observed by Rayleigh [19] that the lowest mode of bells is usually somewhat subdued, and the sound output is from the higher modes of flexural vibration. He attributes this to the stiffness of the cupped portion or mount of the bell.

2.3 RESONANCES WITH A FINITE ELEMENT PROGRAM AND EXPERIMENTAL RESULTS

2.3.1 Introduction

Accurate information on wheel resonances is required to predict resonance changes as a crack grows in size. This task is difficult to do experimentally since it is not possible to collect a set of wheels with the same type of crack, at its various stages of growth, due to limitations in time. The finite element method of analysis [20,21] appears to be the easiest way to tackle the problem theoretically. For convenience, it was decided to use the ANSYS Engineering Analysis Computer Program evolved from the work of Swanson. Unfortunately the cost of computer time limited the study to the cases of an unflawed wheel and one with a large simulated plate crack.

In the finite element method of analysis, the continuum of the structure to be analysed is separated by imaginary surfaces into a number of finite elements. These elements are interconnected at a discrete number of points or "nodes"

situated on their boundaries. The displacements of the nodal points are the basic unknown parameters of the problem. Functions are chosen to determine the state of displacement within each finite element in terms of its nodal displacements. The displacement functions also define the state of strain within an element in terms of nodal displacements. If the nodal force-displacement relationships for each element are known, then the force-displacement relationship may be obtained for the entire structure using matrix methods. The general form of the stiffness matrix for each element is

$$[k]\ \{u\} = \{f\} \tag{1}$$

where

$[k]$ is the element stiffness matrix,

$\{u\}$ is the vector of element nodal displacements, and

$\{f\}$ is the vector of element nodal forces.

For the total structure

$$[K]\ \{U\} = \{F\} \tag{2}$$

Where

$$[K] = \sum_{i>1}^{n} [k] \tag{3}$$

$[K]$ is the total structure stiffness matrix,

$\{U\}$ is a vector of all the nodal displacements in the structure,

and $\{F\}$ is a vector of all corresponding nodal forces. The equation of motion for a structure expressed in matrix notation is:

$$[M]\{\ddot{U}\} + [C]\{\dot{U}\} + [K]\{U\} = \{F(t)\} \qquad (4)$$

where

[M] is the structure mass matrix,

[C] is the structure damping matrix,

and $\{F(t)\}$ is the mode forcing function.

If it is assumed that the structure is undamped and there is no force applied, Eq. (4) reduces to

$$[M]\{\ddot{U}\} + [K]\{U\} = 0 \qquad (5)$$

for free vibrations. If it is assumed that these free vibrations will be harmonic and of the form:

$$\{U\} = \{U_n\}\cos\omega_n t \quad \text{for } n = 1, 2, 3, \ldots$$

then Eq. (5) becomes:

$$\left(-\omega_n^2 [M] + [K]\right)\{U_n\} = 0 \qquad (6)$$

which is an eigenvalue problem with n values of ω^2 and n vectors $\{U_n\}$ which satisfy Eq. (6).

The ANSYS Program has two options for solving the eigenvalue problem. In one option, after forming the matrices [M] and [K], the Eq. (6) is solved by Jacobi iteration [22] to yield a complete set of eigenvectors and eigenvalues. In the other option, a "matrix condensation" (Guyan reduction) technique is used. In this procedure, n "master" degrees of

freedom are specified to characterize the natural frequencies of the system. The mass and stiffness matrices are reduced to these master degrees of freedom and the eigenvalue problem is solved for the n degrees of freedom. These n eigenvectors are then expanded to the full set of structure displacement degrees of freedom.

2.3.2 Good Wheel Resonances

The principal task for the user of the ANSYS Program is the selection of the proper element type, the subdivision of the structure to be analyzed into elements, and the determination of coordinate dimensions for each node (see Appendix D). Figure 2.3 shows the computer generated plot of the elements that were used for modeling a 33-inch good wheel.

It was assumed that the wheel is rigidly fixed at the hub, is stress free, and is uniformly homogeneous with Youngs' modulus $E = 30 \times 10^6$ PSI and Poisson's ratio $\nu = 0.3$. The results of the computer run are summarized in Figs. 2.4 and 2.5. Figure 2.4 shows the calculated line spectrum and experimentally determined spectra for comparison. The experimental values were obtained as outlined in Appendix A, Section A.3.2.

In Fig. 2.5 are shown approximate mode shapes obtained

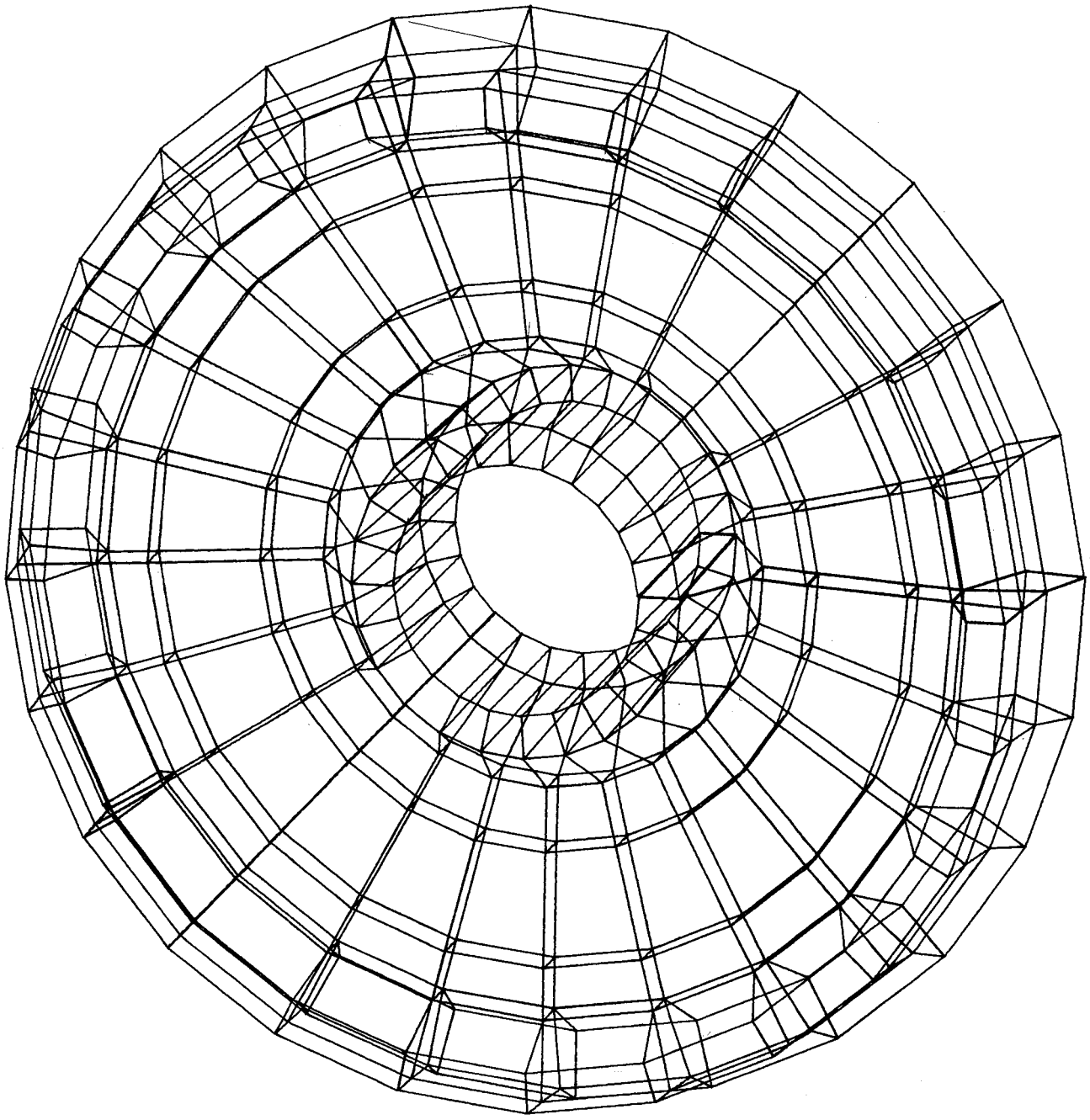

Fig. 2.3 Computer Generated Plot of Elements Used in ANSYS Program for Modeling a 33" Good Wheel

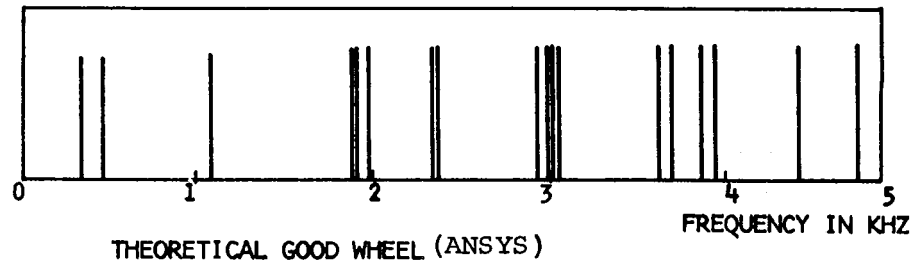

THEORETICAL GOOD WHEEL (ANSYS)

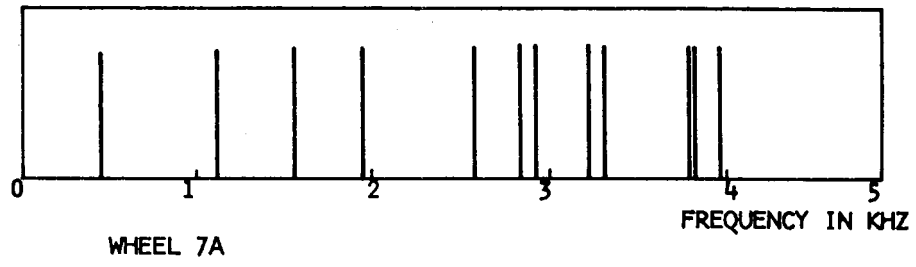

WHEEL 7A

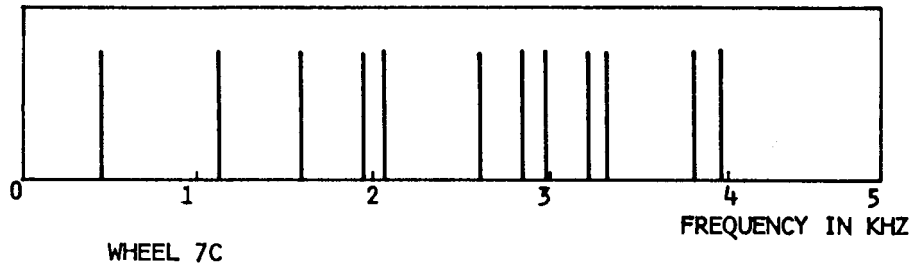

WHEEL 7C

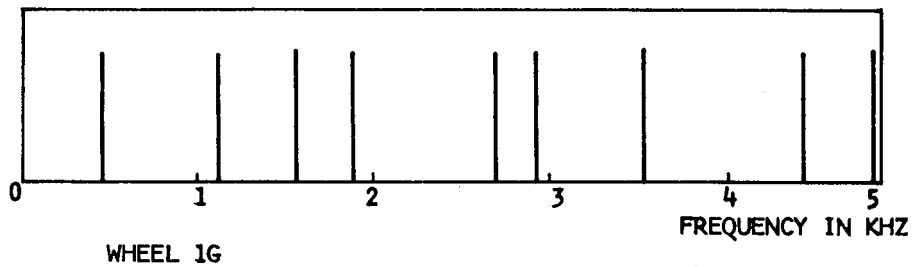

WHEEL 1G

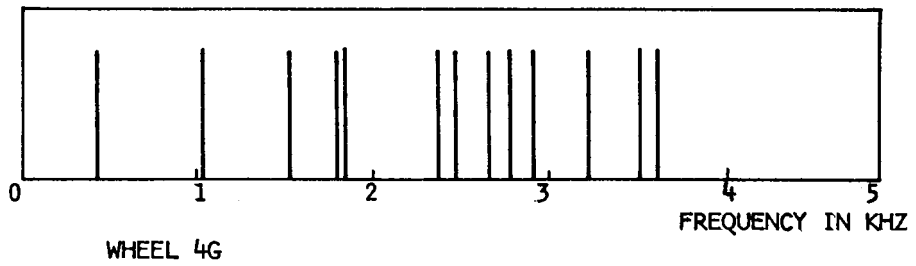

WHEEL 4G

Fig. 2.4 Line Spectra of Resonances Obtained from the ANSYS Program, Compared with Experimental Spectra for 33" Good Wheel, Obtained by Using a Rail-Mounted Accelerometer

NOTE: THE HUB IS FIXED FOR ALL MODE SHAPES

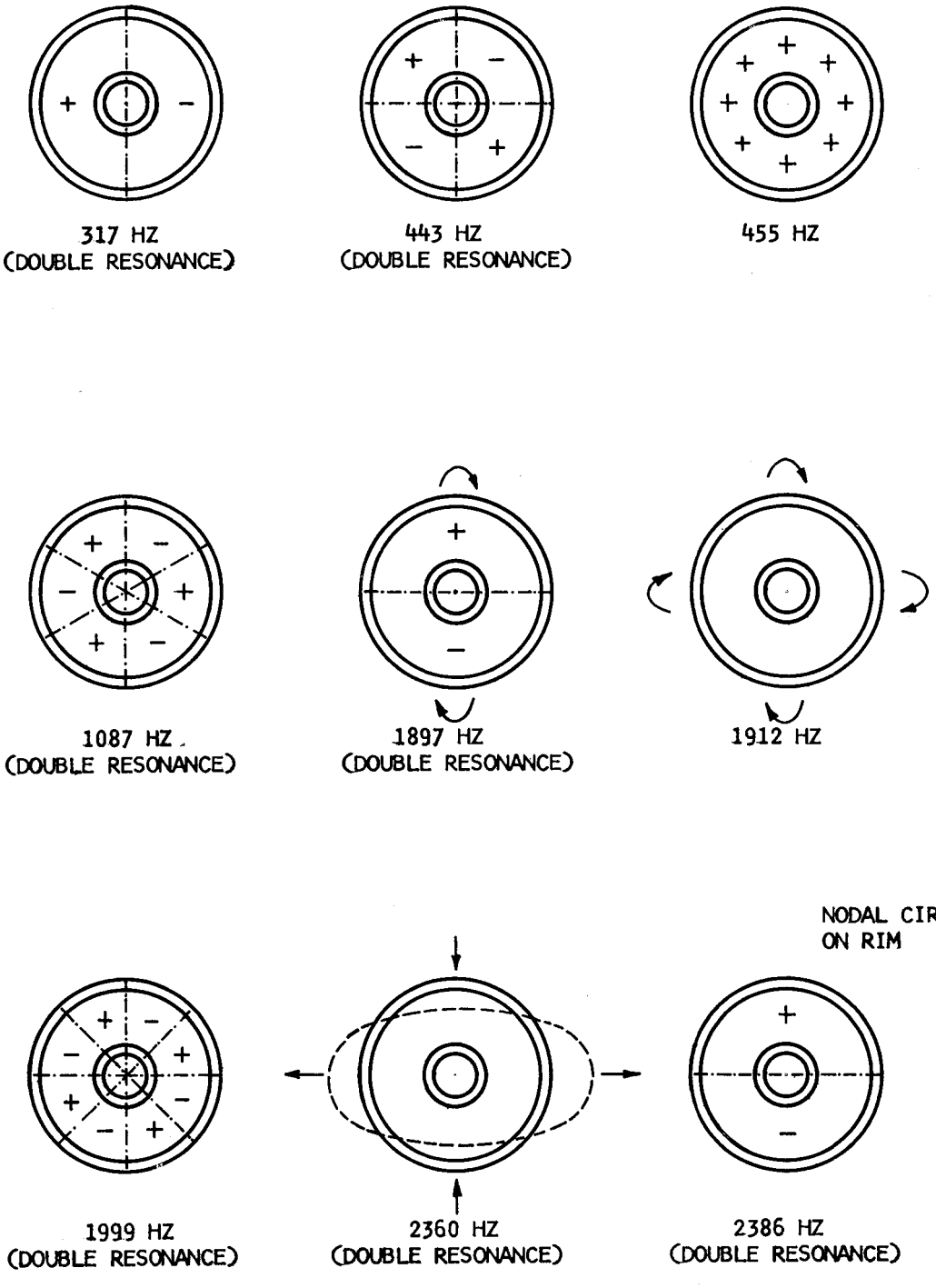

Fig. 2.5 Mode Shapes Obtained with ANSYS Program for 33" Good Wheel

with the ANSYS Program for a 33-inch diameter good wheel. In all of these modes the rim participates in the motion, except where noted otherwise. As an illustration of such a mode shape, a time average hologram is shown of a one-fourth scale model wheel vibrating in a modal configuration having two nodal diameters, in Fig. 2.6. This was obtained as outlined in Section A.3.4. Mode shapes in full sized wheels were confirmed by probing the vibrating wheel surface with an accelerometer.

The theoretically obtained resonances are in well spaced groups; however, some of the resonances within these groups are rather close. For example, the mode with two nodal diameters occurs at 443 Hz and the mode where all of the wheel moves one way occurs at 455 Hz. It is apparent from the theoretical calculations that for each mode of vibration which contains at least one nodal diameter, there are two preferred nodal positions shifted relative to each other. The angular shift is such that the nodes of one position are aligned with the antinodes of the other. This result is in agreement with the previously mentioned work of Tobias [16] who found that for an ideal disk the resonant frequency of nodal position pairs should be identical. It is also apparent that modes such as that occurring at 1897 Hz (see Fig. 2.5) where twisting motion of the rim takes place could not be predicted by thin

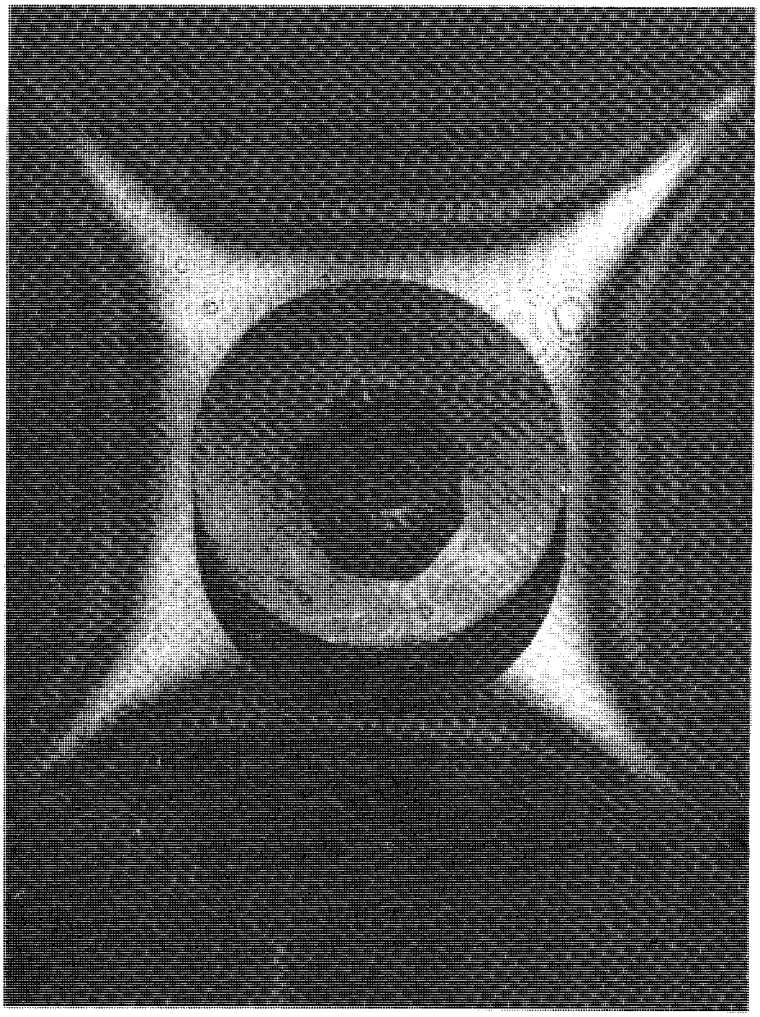

Fig. 2.6 Hologram of ¼ Scale Model Wheel Without Crack at 1798 Hz (corresponds to a frequency of 445 Hz in a full-sized wheel)

plate theory. On the other hand the mode at 2386 Hz, with a nodal circle on the rim could not be predicted by the ring theory, but is quite close to the corresponding thin plate mode, predicted at 1943 Hz (see Table 2.1).

To obtain experimental verification of these theoretical results tape recordings of accelerometer signals of wheel vibrations were analyzed with a narrow band real time analyzer (see Appendix A. 2.2). To facilitate easy comparison of theoretically obtained values of resonances to experimental data these amplitude vs. frequency plots were converted to line spectra in which the presence of a resonance is designated with a single line. In Fig. 2.4 line spectra from accelerometers on rails are shown for good wheels 7A and 7C which are new sheels mounted onto the same axle, for good wheels 1G and 4G which are mounted on axles with cracked wheels on the other side. Up to about 200 Hz there is good agreement between theory and experiment. In the line spectra for the experimental data there is a resonance at 1595 Hz which was not predicted theoretically. This resonance is presumed to be due to the rail (see section 3.5). The poor agreement between theoretical and experimental values at frequencies above 2000 Hz may be explained by the approximate nature of the theoretical model, which by necessity was composed of rather large elements to save computer time. The inaccuracy of the

theoretical model is expected to increase with increasing frequency.

The line spectra for good wheels 7A, 7C, and 1G look quite similar to each other with particularly good agreement between wheels 7A and 7C which are two new wheels mounted onto the same axle. The line spectra for wheel 1G somewhat differs from these two, but is still quite close at low frequencies. However, the line spectra for wheel 4G is markedly different from the three other experimental line spectra. This raised the question of just how good wheel 4G really is. While there are no visible large cracks on 4G, it is made of the same material as wheel 4B, is of the same design, manufactured at the same time by forging, and has the same mileage. Wheel 4G was cleaned with a powered wire brush and examined for any presence of cracks. It was found upon close examination that at a radius where the back hub fillet is tangent to the plate there is a one-half to three-fourths of an inch wide circumferential band of small cracks (each aligned perpendicular to the radial direction) in the mill scale layer which covers that area. Wheel 4B, the flawed wheel on the same axle, was cleaned in the same region and a similar band of small cracks found to exist there also. Furthermore, it appears that on wheel 4B the large plate crack originated in this region and then progressed outward towards the rim (Fig. 2.7).

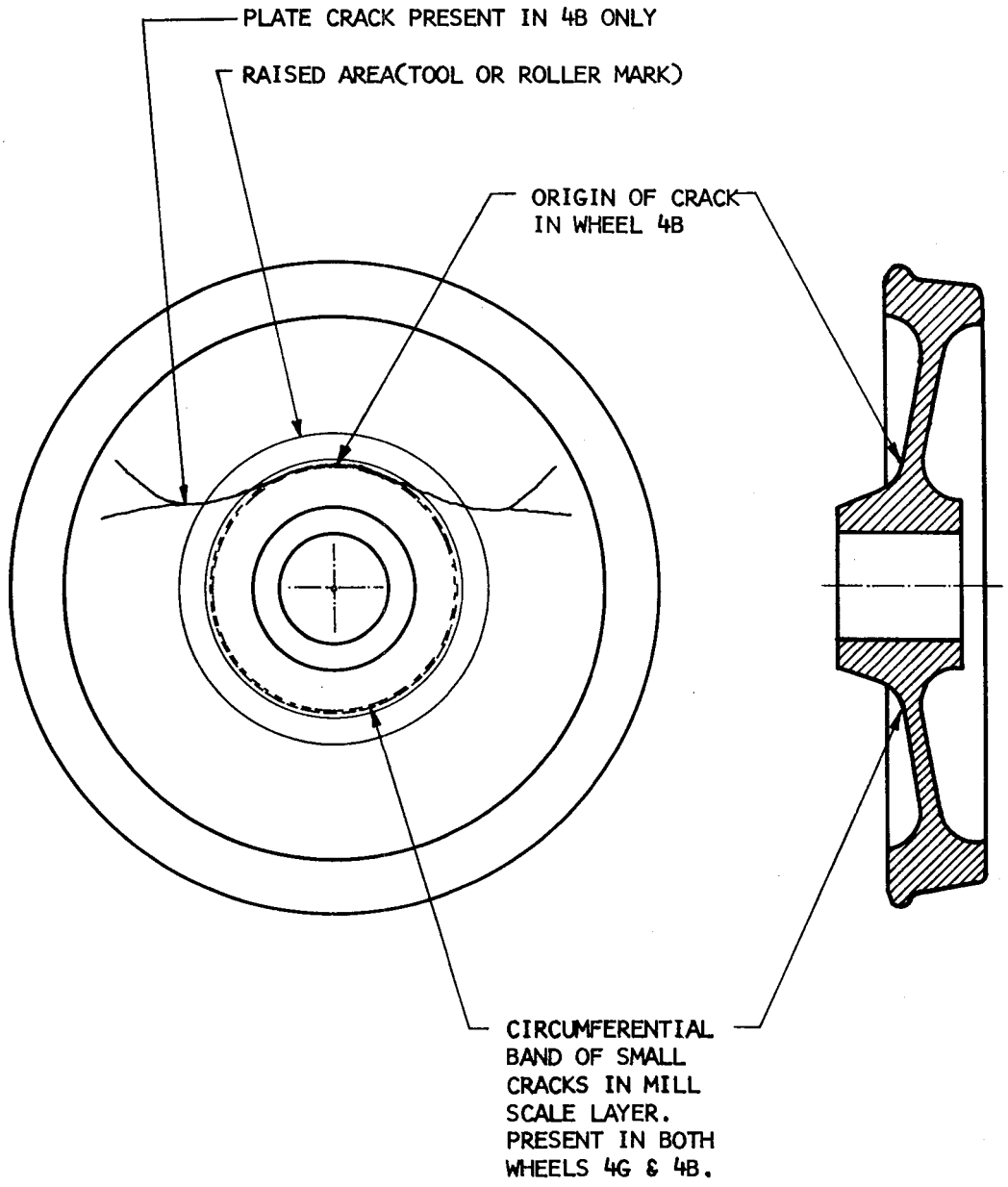

Fig. 2.7 Sketch of Cracks in Wheels 4G & 4B

2.3.3 Flawed Wheel Resonances

A large plate crack was modelled with the ANSYS Program, by providing double and disconnected nodes in the crack area (Fig. 2.8). The finite element model was otherwise identical to the one used for the good wheel analysis. A plate crack was chosen, since this type of flaw is not readily detectable at present by any operational NDT method. Fig. 2.9 shows a line graph of the calculated resonances along with a line graph of the resonances calculated for a good wheel. In Fig. 2.10 are shown some of the mode shapes that were obtained theoretically for a 33" flawed wheel.(See Appendix D for listings.)

It is apparent from Fig. 2.9 that the wheel with the plate flaw has far more resonances than the good wheel. This is due to the fact that the resonance values associated with the two preferred nodal positions of a particular mode of vibration have separated. Thus for each mode of vibration there are two separate resonances. This numerical difference, however, is not uniform. For example for the mode with one nodal diameter the two resonance values are 148.5 Hz and 255.13 Hz, whereas for the mode shape with two nodal diameters the two resonance values are 421.7 Hz and 429.6 Hz. Thus the presence of the crack affects various modes differently. This may be

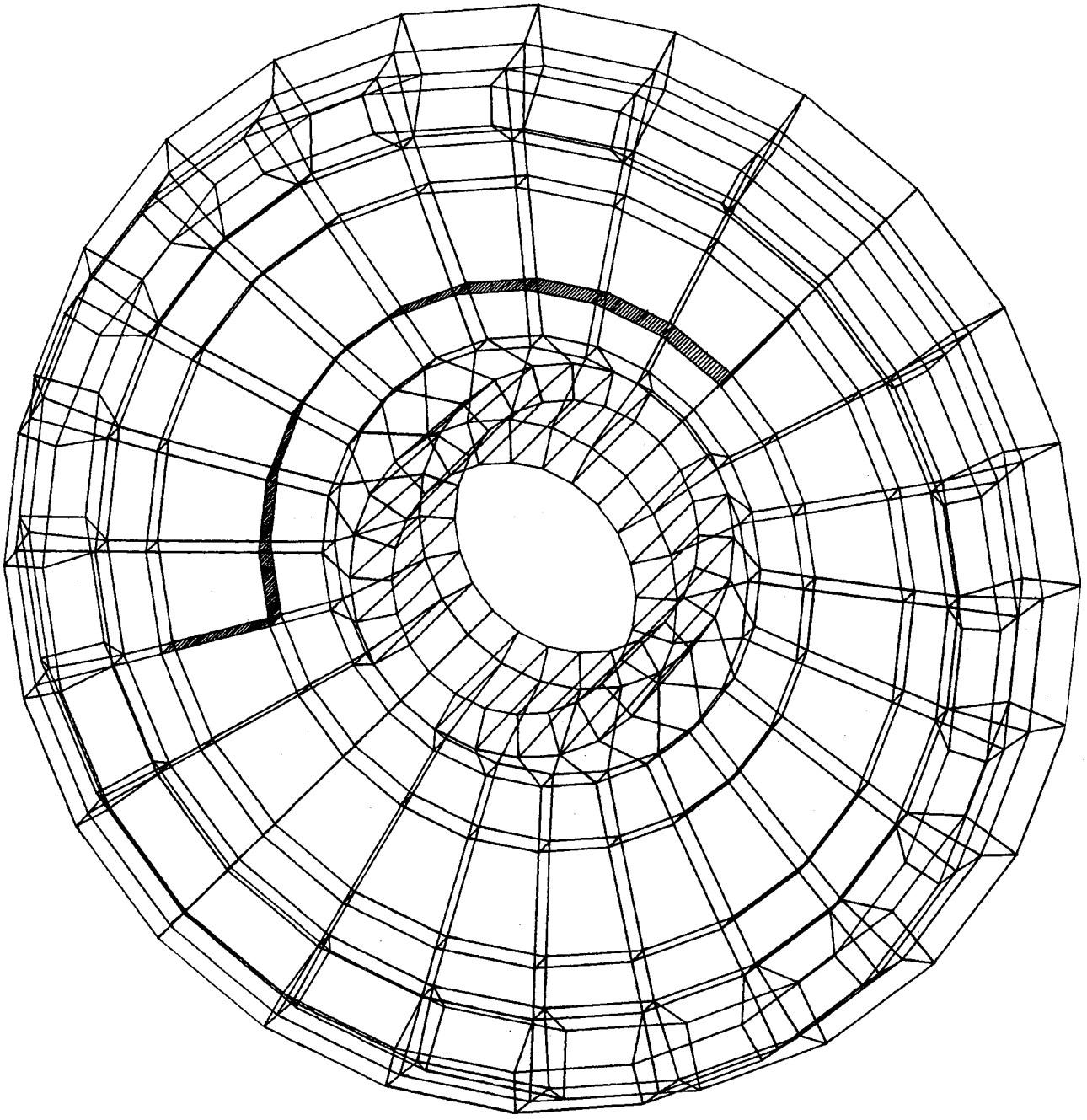

Fig. 2.8 Computer Generated Plot of Elements Used in ANSYS Program for Modeling a 33rd Flawed Wheel

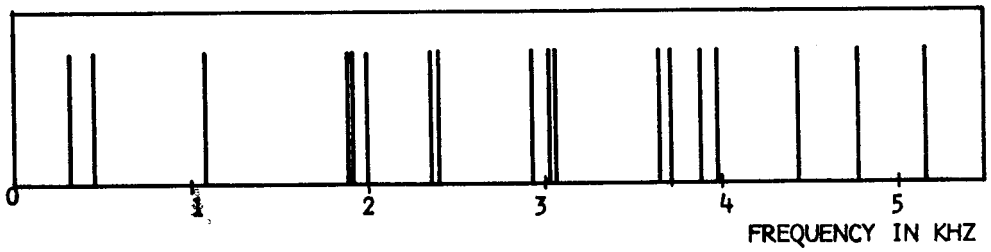

THEORETICAL RESONANCES OF A GOOD WHEEL

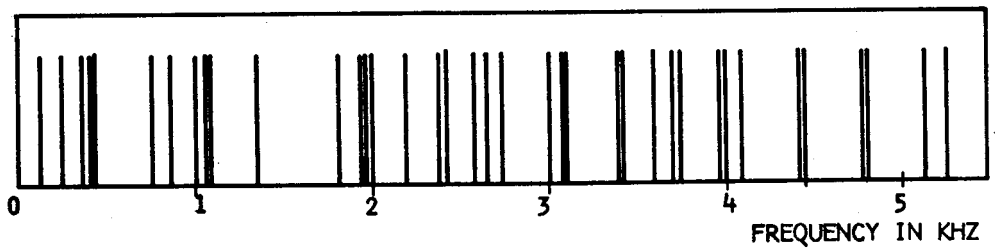

THEORETICAL RESONANCES OF A WHEEL WITH A PLATE FLAW

Fig. 2.9 Line Spectra of Resonances Obtained from the ANSYS Program for 33rd Good and Flawed Wheels

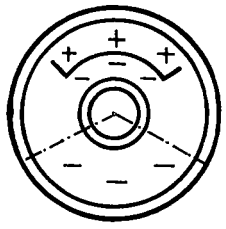

148.5 HZ

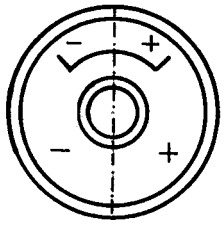

255.13 HZ

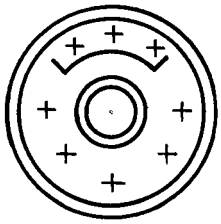

347.3 HZ

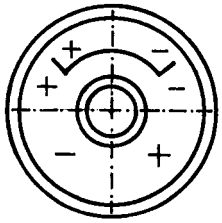

421.7 HZ

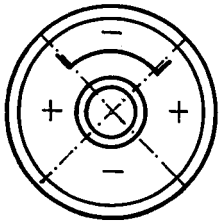

429.7 HZ

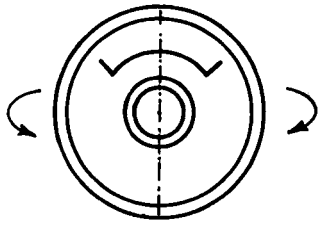

764.5 HZ

Fig. 2.10 Mode Shapes Obtained with ANSYS Program for 33" Wheel with Plate Crack

due to the size and angular orientation of the crack with respect to the mode shape. In all cases the mode shapes were oriented symmetrically about the crack. The simulated plate flaw is rather large (extending about one third of the way around the wheel) and the mode shapes that were obtained are dominated by the presence of the crack. At the lower, or "plate like" resonances, there is some similarity between good and bad wheel response (i.e., the presence of well defined nodal diameters) even though the crack faces have considerable relative motion, thus indicating modification of the mode shape. At the higher or "ring like" resonance, the effect of the crack is such that similarities to good wheel mode shapes disappear and it is not possible to even match mode shapes between good and bad wheels. A possible explanation is that the modes dominated by rim vibrations may be thought of as vibrations of a ring, partially restrained on its inside diameter. The presence of a plate crack locally alters this restraint, thus altering the mode shapes and resonance frequencies.

As an experimental test of the ANSYS program results, axle 4, one of whose wheels has a large plate crack, was studied with particular care. Each wheel was excited with the shaker, driven through the usual power amplifier but using a frequency synthesizer to provide a pure tone input of high

frequency stability, in order to distinguish between closely spaced resonances. As mentioned previously there is reason not to regard wheel 4C as a "good" wheel, but it does not contain a large crack as in 4B and thus affords some basis for comparison. Line spectra are shown in Fig. 2.11 for experimental resonance values for the two wheels. There is good qualitative agreement between theory and experiment in that the number of resonances increases considerably for wheel 4B. However, the quantitative agreement is poor due to the approximate nature of the theoretical model. To obtain exact theoretical models for flawed wheels would require an excessive amount of computer time.

The experimental data does show that the flawed wheel resonance pairs associated with a particular mode are separate frequencies. The good wheel has 4 resonances below 1000 Hz. This is in agreement with theory since it predicts 4 resonances below 1000 Hz. (See Fig. 2.5 and Appendix D, Section D3.) The bad wheel has 9 resonances in this region. Theory predicts 7 resonances for the bad wheel. This multiplication of resonances is found in other areas of the spectrum as well.

2.3.4 Effects of Load

Experiments to determine the effects of load were performed as outlined in Appendix A, Section A.3.2. Fig. 2.12

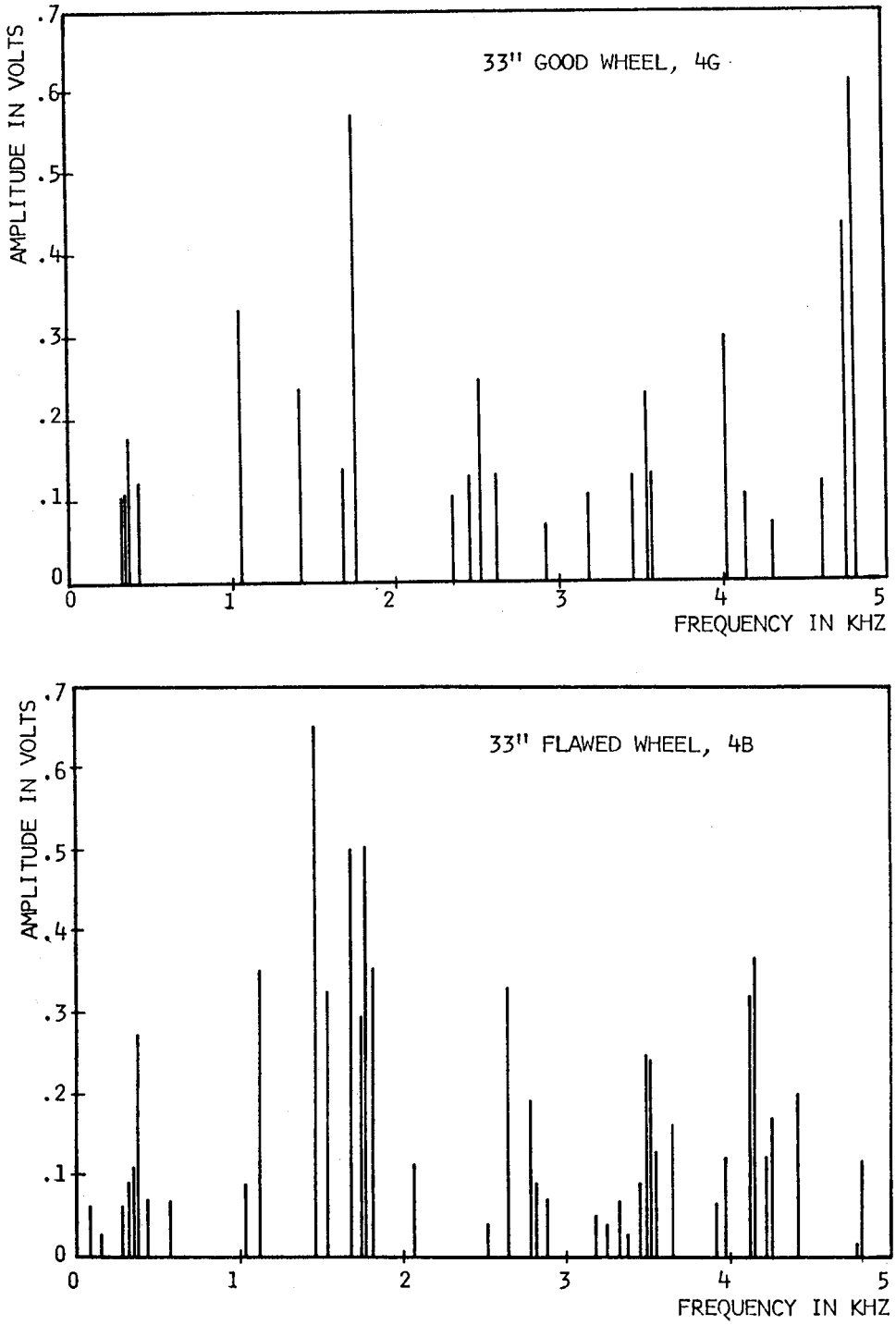

Fig. 2.11 Resonances of a 33" Good Wheel and 33" Wheel with a Plate Crack, Obtained Experimentally. Many more resonances are found in the cracked wheel, in qualitative agreement with theory

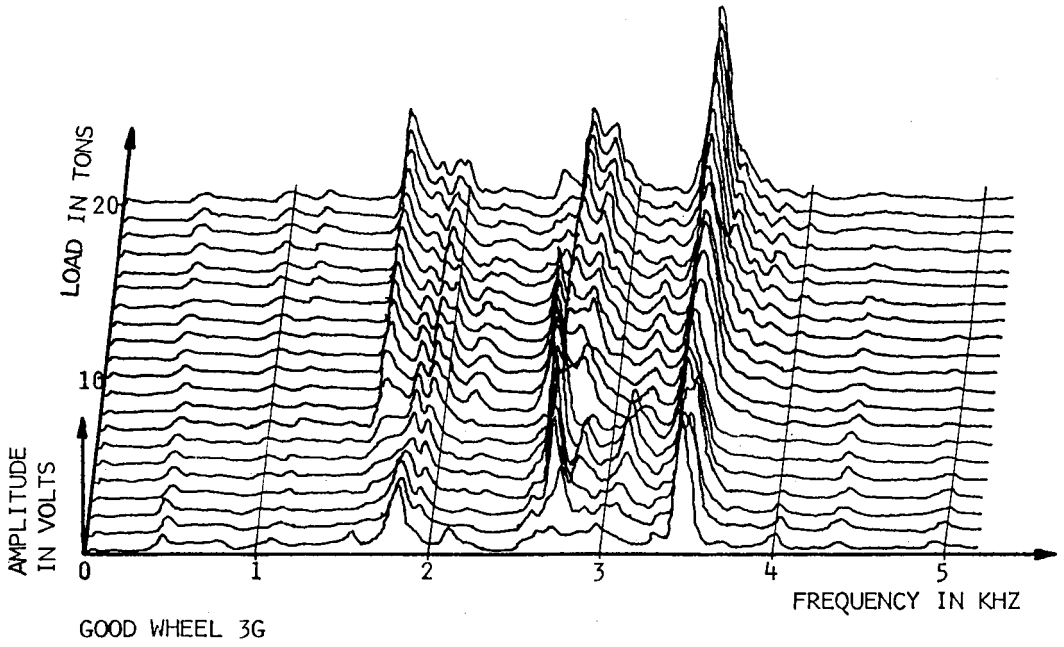

Fig. 2.12 Variation of Wheel Signature with Load for Wheel 3G
(Accelerometer Pickup)

shows a series of spectral analyses, each with increasing load. The traces are superimposed on one another but slightly offset to give a three dimensional perspective. Some resonances are enhanced by the load; some are diminished. Some shift slightly in frequency and some split into two separate resonance peaks.

On the other hand, if one does not use too fine discrimination, it is clear that the changes do not produce complete disorder in the three-dimensional plot. That there is a characteristic spectrum associated with a good wheel is further shown in Fig. 2.13. Here are two such three-dimensional plots for two new wheels on either side on an axle, each changing under load. Note that the general characteristics of the plots are similar. Now, however, consider Fig. 2.14. The upper plot is for a good used wheel. The lower plot is a badly cracked wheel on the other side of the same axle. There are pronounced shifts in the positions of the major resonances.

The same effect is shown in Fig. 2.15. These are line spectra in which the presence of a resonance at a particular frequency is marked by a line, and its amplitude by the height of the line. A 10-ton load does not affect the character of the spectrum anywhere near as much as the presence of a large crack, even though it produces some of the same changes in resonances.

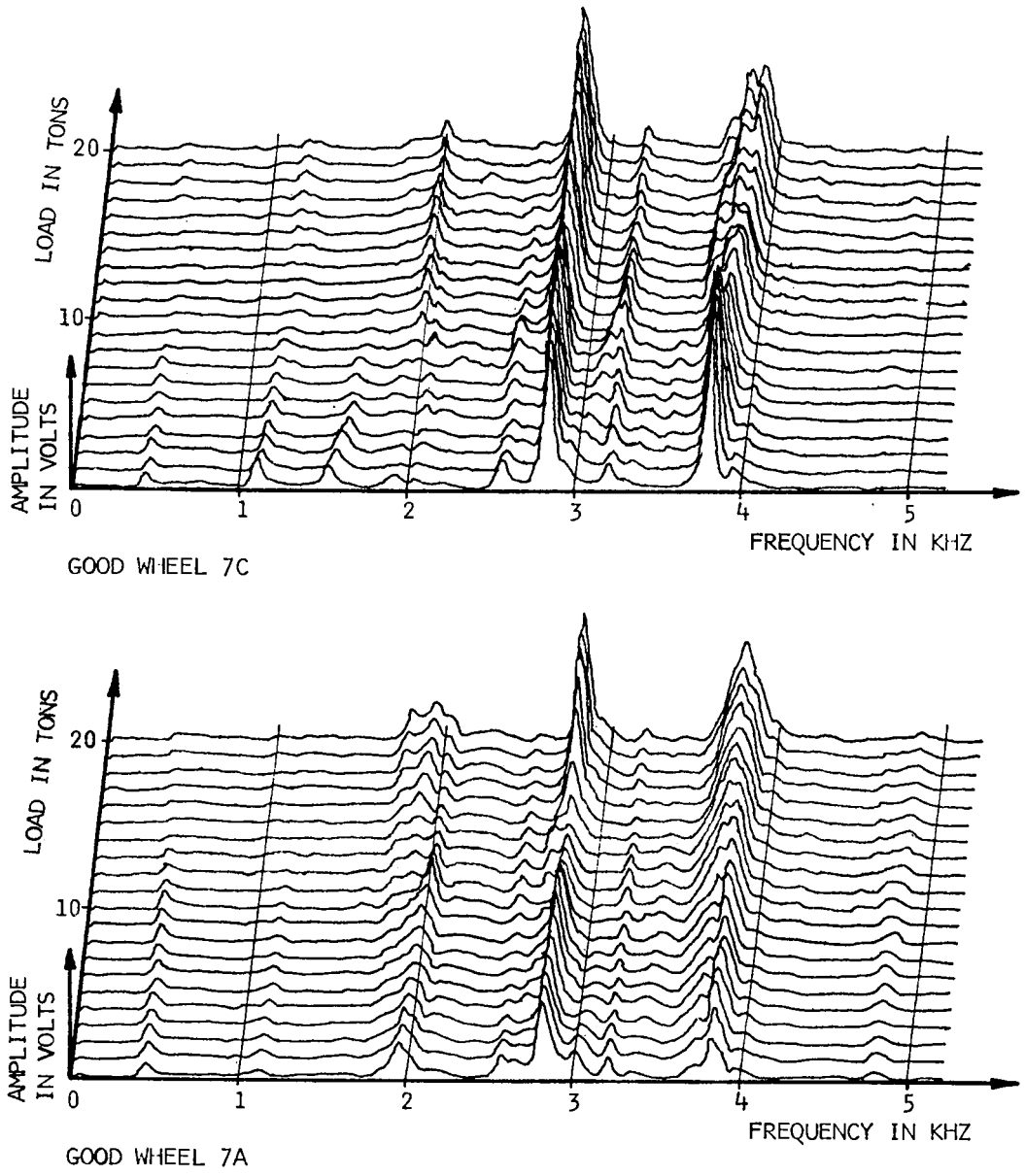

Fig. 2.13 Variation of Wheel Signature with Load for Wheels on Axle 7 (Accelerometer Pickup)

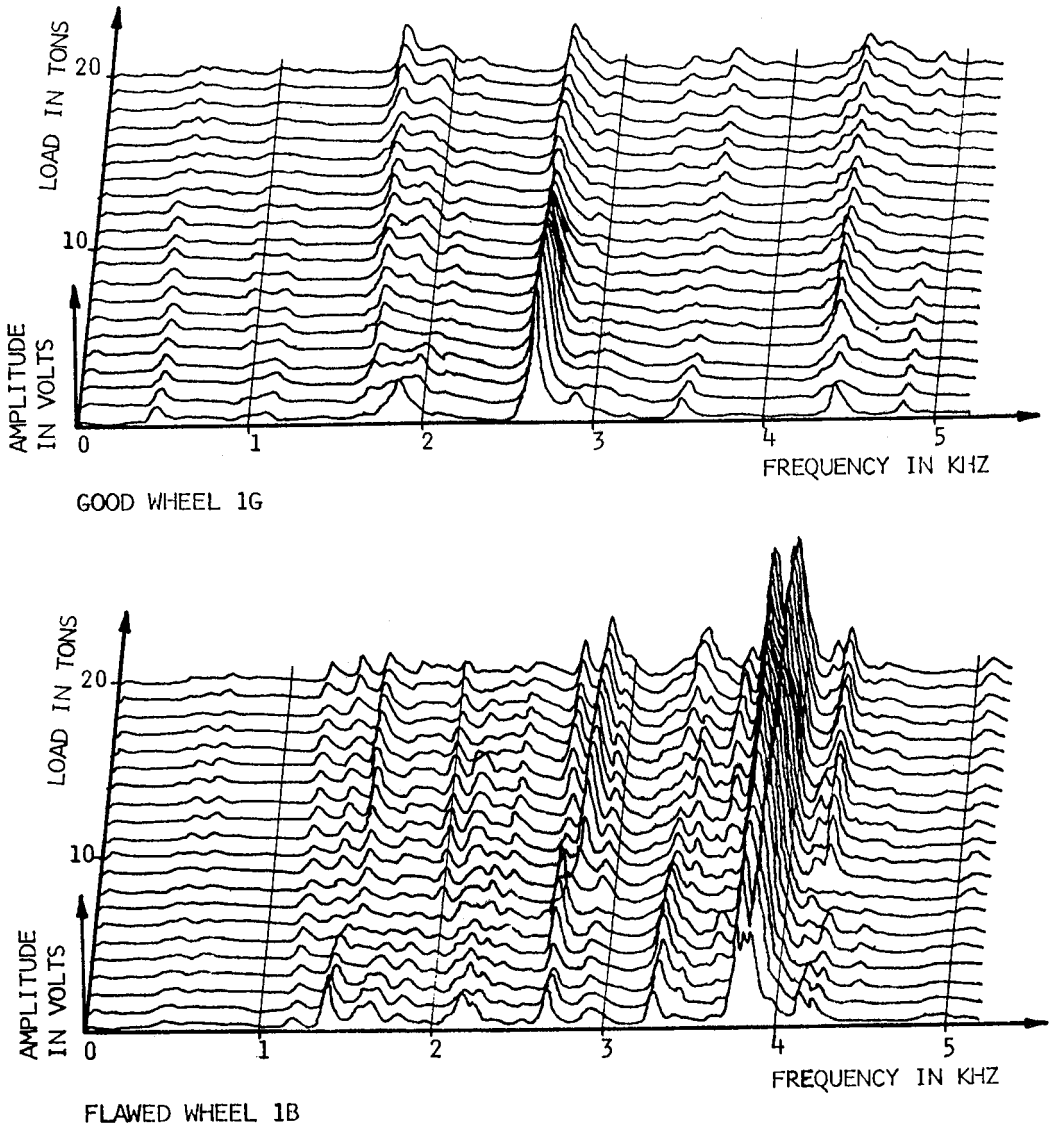

Fig. 2.14 Variation of Wheel Signature with Load for Wheels on Axle 1 (Accelerometer Pickup)

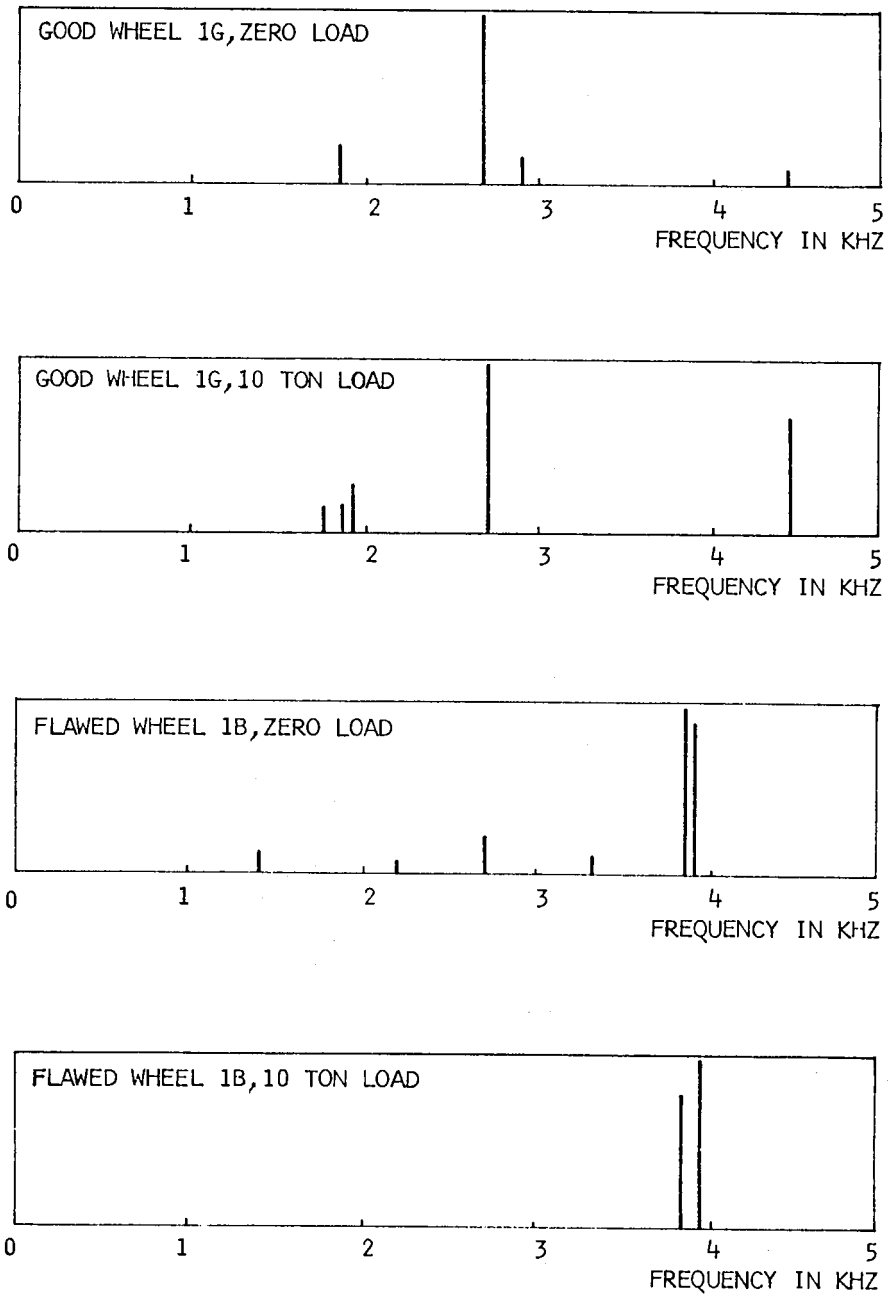

Fig. 2.15 Line Spectra for Wheels on Axle 1, under Zero and 10 Ton Load
(Wide Band Random Noise, Accelerometer Pickup)

2.3.5 Beating

Decaying sound emitted by a wheel that has been excited by a sharp blow on occasion will show a strong beating effect. The effect was observed at some of the resonances in the range of 1 to 3 KHz. (See Fig. 2.16.) Which resonance shows beating seems to depend on which area of the wheel is struck. Similar results have been obtained by Steele and Lotz [23] using a sonogram technique for data analysis.

The effect is due to two close resonances being equally excited, and the beat frequency is the difference between the two resonance frequencies. It is to be expected that as the frequency difference between the two close resonances increases, that this beat frequency will become higher and higher and finally unobservable. When a large flaw is present, the likelihood of coupled oscillation between two modes is diminished.

When autocorrelation of a wheel signature under continuous excitation by a shaker is made with bandpass filtering, the autocorrelation function can be used to find the beat frequency. Fig. 2.17 shows autocorrelations of sound excited by random noise shaker drive applied to wheels 7A and 7C (good wheels) and for wheels 4G and 4B. The autocorrelations are shown as functions of the delay time between samples. The beat frequencies which appear in the autocorrelation

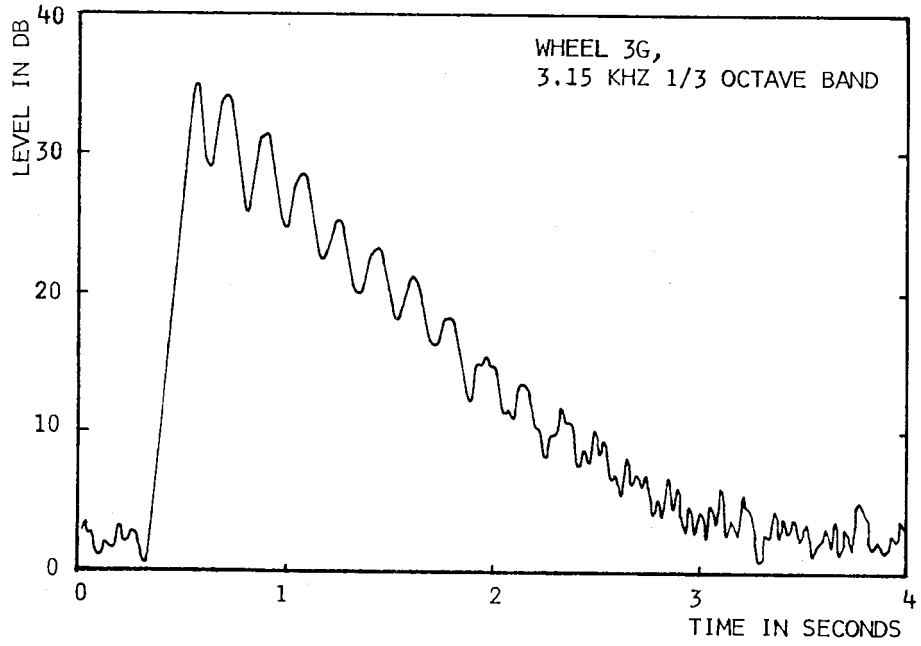

Fig. 2.16 Beating Effect as Shown by Sound Decay in the 3.15 kHz Center Frequency 1/3 Octave Band for a 33" Good Wheel 3G

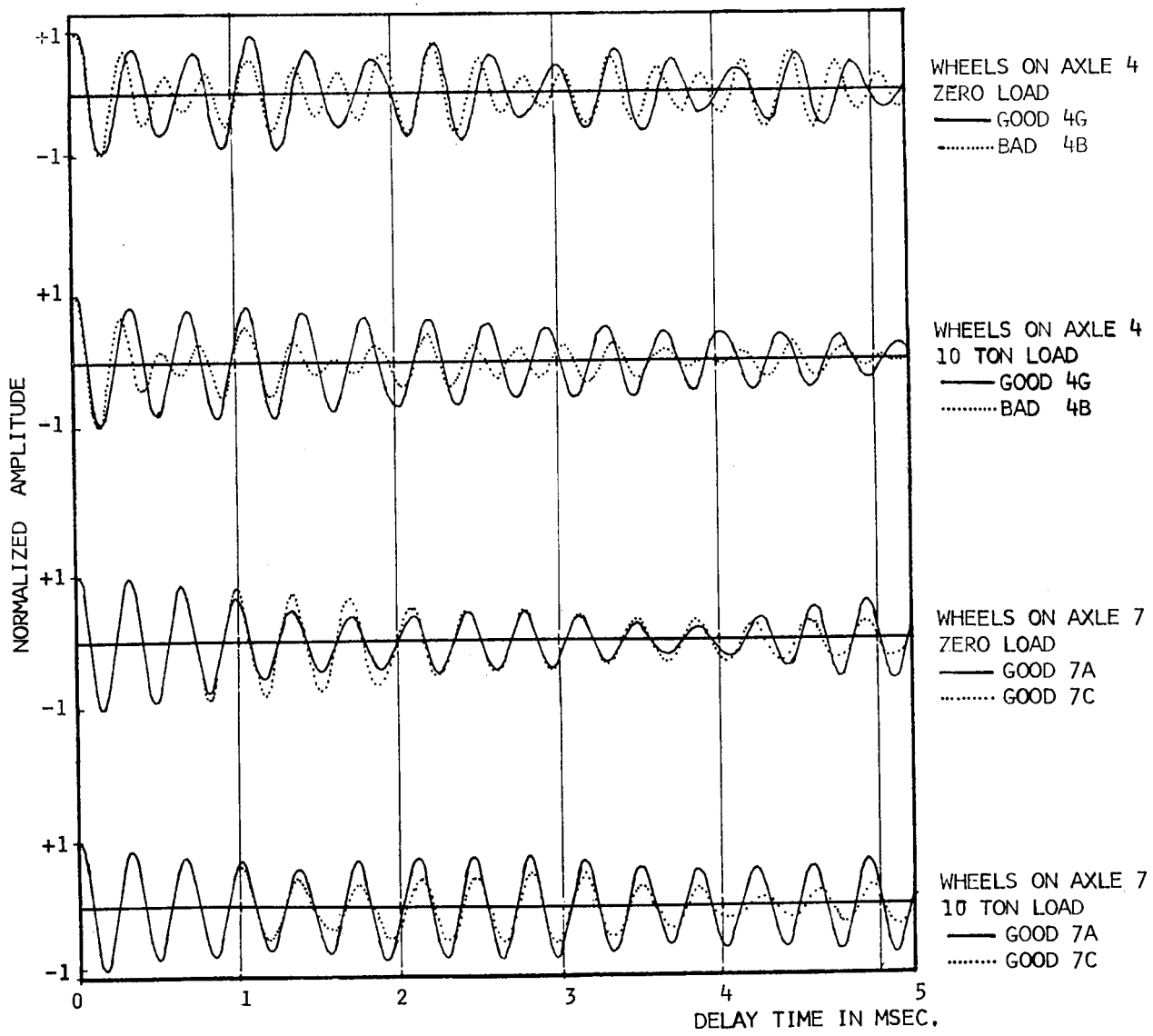

Fig. 2.17 Autocorrelation Functions for Signatures of Wheels 7A,7C,4G and 4B

function are obviously lower in the case of the good wheels than for bad ones. It is possible that this beating effect could be used as the basis of a flaw detection method. As distinct from observations of decay time only high beat frequencies will be found using this method.

2.4 DAMPING

Decay rates of sound were obtained for good and defective wheels, when they were excited by impact. (See Section A.3.1 for description of impact tests.) The minicomputer was used to take successive amplitude values of the decaying sound, and then decay rates in dB/sec. were calculated. In Table 2.2 are shown decay rates for all the 33" wheels on inventory for the 1/3 octave bands with center frequencies of 1, 2, 4, and 8 KHz. Decay rate was also obtained for the C weighted overall sound level. It is apparent from the table that greasy wheels have a higher decay rate than wheels without grease, and that faulty wheels have higher decay rates. This effect is also shown by oscillograms of decaying sound in Fig. 2.18 for wheels 3G and 3B which are good and bad greasy wheels on axle 3, and in Fig. 2.10 which are for good and bad wheels on axle 4. Wheel 7A is a new wheel with a coat of grease which was applied in the laboratory.

TABLE 2.2 LIST OF TIME DECAY RATES FOR WHEELS ON INVENTORY AT THE UNIVERSITY OF HOUSTON. UNITS ARE dB/SEC

Wheel	Center Frequencies of 1/3 Octave Bands				Overall Level C scale	Comments
	1k	2k	4k	8k		
1B	17	33	31	26	20	bad
1G	3	3	4	18	8	good
3B	20	36	27	17	12	bad,greasy
3G	10	29	15	0*	12	good,greasy
4B	4	19	24	28	12	bad
4G	3	21	10	19	8	good
7A	11	27	24	26	13	good,greasy
7C	3	9	10	18	8	good
8B	14	30	25	0*	19	bad
8G	4	4	14	16	5	good
9A	8	17	17	20	13	good
9C	12	13	16	26	17	small crack
10A	0*	14	6	18	10	good
10C	5	13	13	17	10	good
11A	2	6	9	12	6	good
11C	2	6	13	13	8	good

Note: The decay times were obtained by impacting the wheel with a hammer.

* Spurious result due to beating.

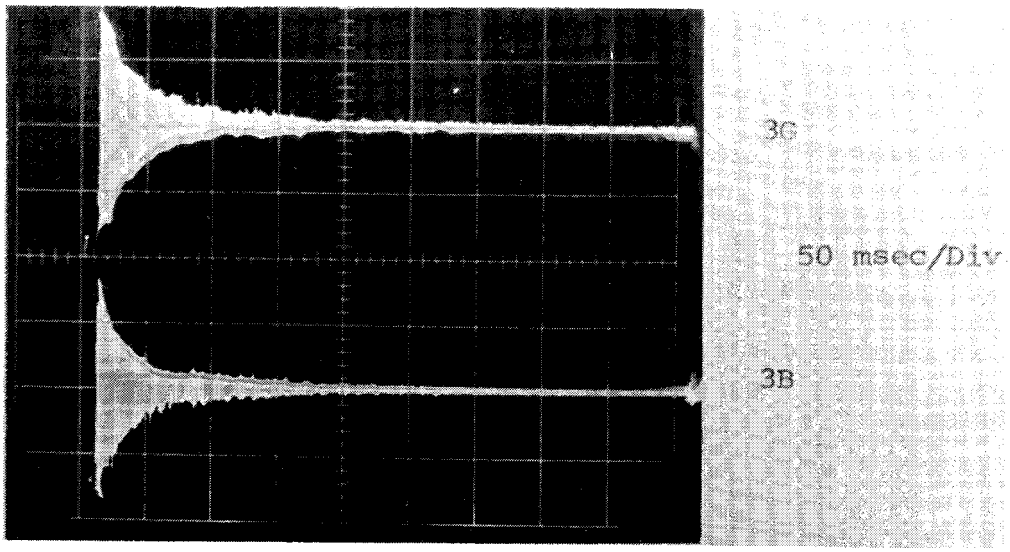

Fig. 2.18 Time Decay of Sound for Wheels on Axle 3

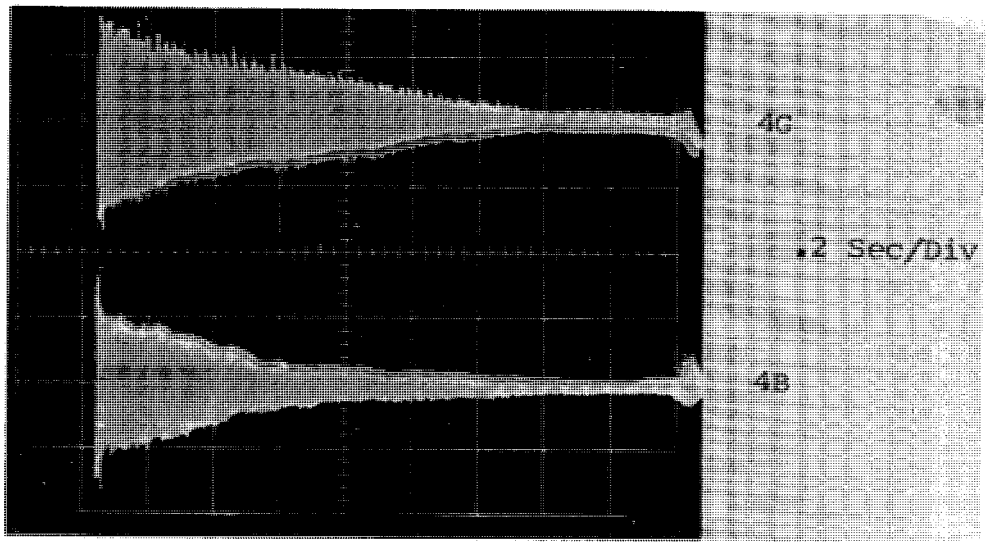

Fig. 2.19 Time Decay of Sound for Wheels on Axle 4

It is concluded from this study that fast decay rates tend to indicate bad wheels, but that greasy wheels have comparable values to those of flawed ones. In railway practice greasy wheels are primarily caused by leaking of lubricant from plain journal bearing type wheel bearing boxes. The current trend is to replace journal bearings with roller bearings.

3. EXCITATION AND DETECTION METHODS

3.1 INTRODUCTION

The best form of excitation should have a forcing function with a wide frequency band in the range in which there are the greatest impedance differences between good and bad wheels. The studies of wheel resonances and damping suggest that this frequency range lies from 1 KHz to about 5 KHz. In addition, the excitation should generate a vibration amplitude in the wheel sufficient for detection above other ambient noise. The excitation should be as reproducible as possible and independent of train velocity. Finally, the excitation needs to be reliable, safe, and inexpensive. The three principal forms of excitation will now be reviewed in the light of these criteria. From the viewpoint of safety it would obviously be desirable to use sounds generated in everyday railroad practice. Mainly for this reason a number of field recordings were made. Analysis of these recordings, as well as data from laboratory transducers, will be presented according to the type of forcing function.

3.2 RANDOM SHAKING

Rolling along continuous welded rail results in an

oscillating force input to the wheel whose frequency content depends on the spectral density of track surface roughness. At low speeds (say 10 mph), the frequency content of such a forcing function will be predominantly low frequency. This is illustrated in Fig. 3.1 which shows a 1/3 octave band analysis of airborne rolling noise from a train moving at about 10 mph on welded rail. The maximum of the radiated sound lies in the 300 to 500 Hz range and thus probably is associated with the three low frequency wheel modes. These findings are in general agreement with analyses made by workers concerned with railroad noise [24]. It is concluded that pure rolling (at least at the relatively low speeds required for operation of this system) is an unsatisfactory method of exciting the frequency range in which flaws produce most effect.

For laboratory purposes a shaker driven by random noise of wide frequency range is a useful and reproducible way to excite wheels. However to use such a device in field practice would require much greater force amplitudes than the 50-lb. maximum value in the present tests in order to achieve a reasonable signal to noise ratio. Together with the problems of housing and maintenance, this would appear to be a relatively expensive prospect.

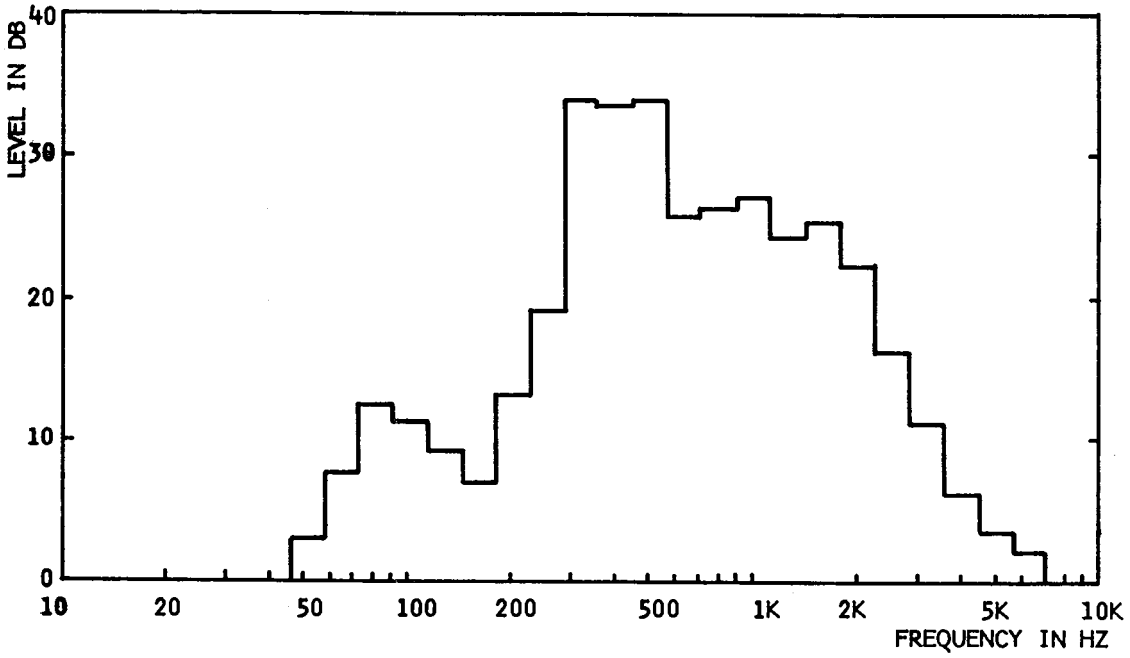

Fig. 3.1 Freight Train Rolling Noise, Microphone Pickup

3.3 SLIP-STICK EXCITATION

The screeching produced by wheels rounding curves, wheel retarders or brakes originates in a frictional action. Stappenbeck [9] argues that the difference in the coefficients of static and kinetic friction results in a periodic forcing function. Consequently it is to be expected that there will be a preferential excitation of those wheel modes closest in frequency to the strong pure tones of the forcing function. Stappenbeck found that the screeching noise from 28" train wheels on curves contained pronounced resonance lines at 420, 1059, and 1927 Hz. This result can be compared with the present results [20] from analysis of retarder screech. Fig. 3.2 shows a constant bandwidth analysis of retarder noise with pronounced resonances at 450, 600, 1000, and 2800 Hz. For comparison with Fig. 3.1, a 1/3 octave band analysis of screeching noise is shown in Fig. 3.3. The point to be made is that screech noise excites higher frequency wheel modes than rolling. One problem with slip-stick excitation as a source of sound for flaw detection is that it is not reproducible. Stappenbeck has noted, that the frequencies excited in a given wheel may change abruptly and that different may be excited in different wheels. These findings are confirmed by the present results. Fig. 3.4 shows a number of line

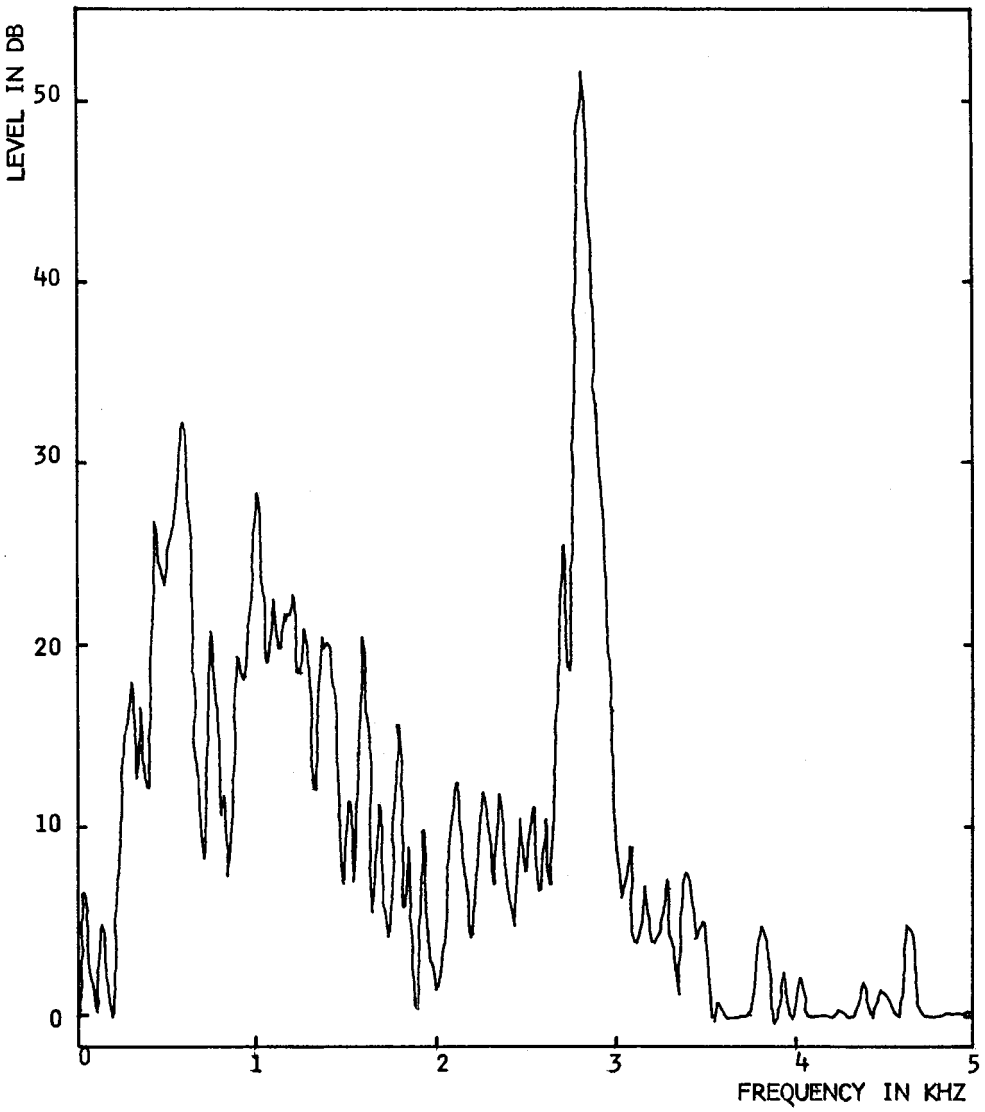

Fig. 3.2 Retarder Screech Noise, Narrow Band Spectrum, Microphone Pickup

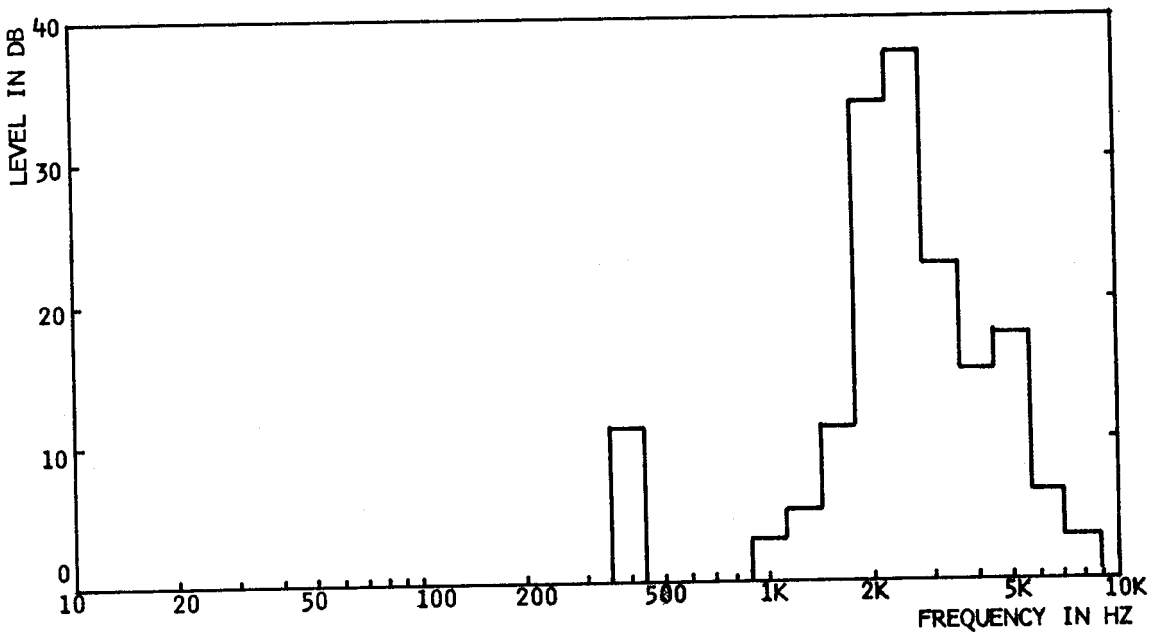

Fig. 3.3 Retarder Screech Noise, 1/3 Octave Spectrum, Microphone Pickup

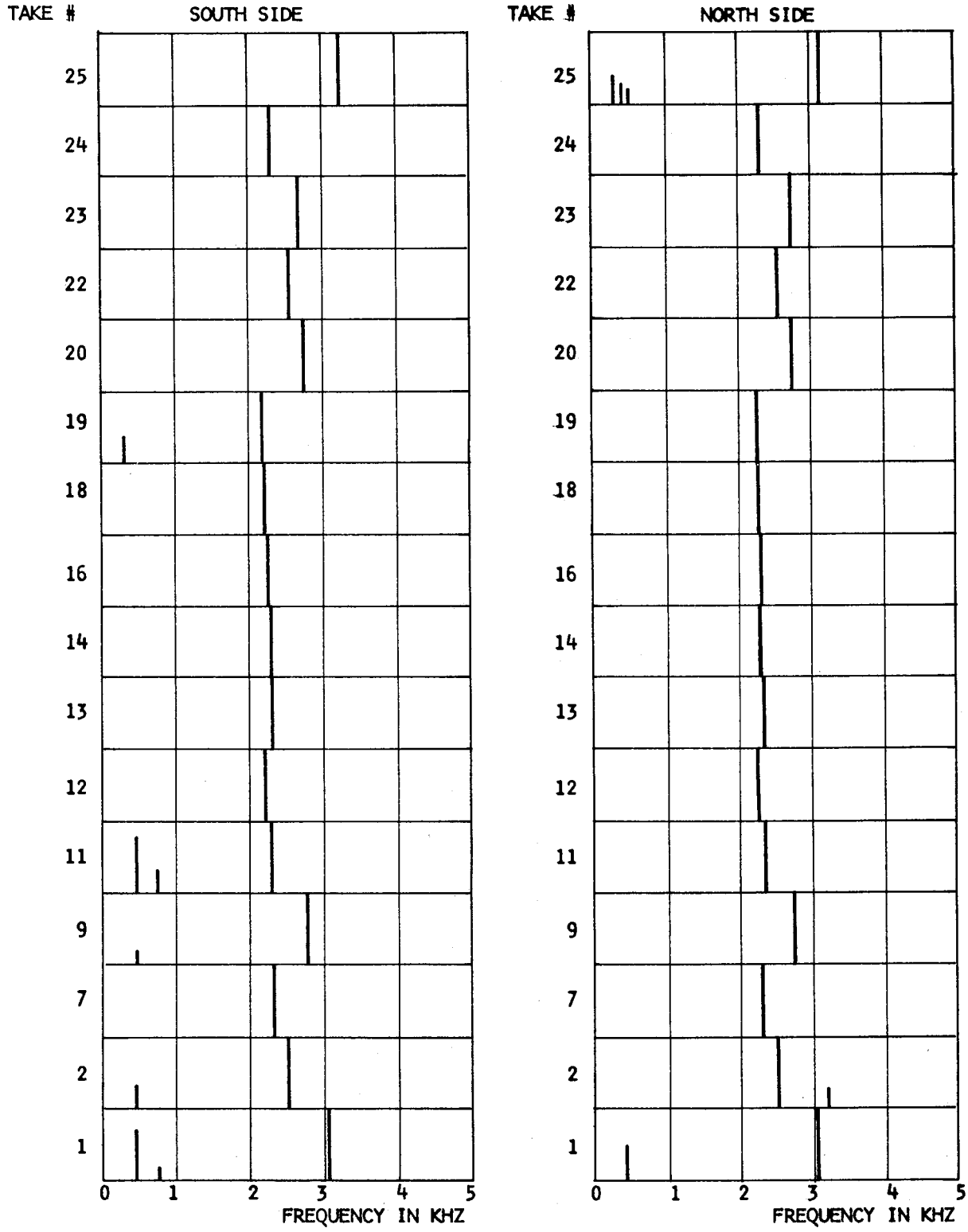

Fig. 3.4 Line Spectra for Screeching Noise from Retarder

spectra of retarder noise. Each pair of spectra consists of analysis of sound from wheels on either side of a given car. Successive "take numbers" represent different cars. While the spectra from either side are consistently similar, there are differences in which resonances are excited from car to car. A further problem is that some wheels are not excited at all. The reasons for these effects might be resolved through further research and means of obtaining more reproducible results devised. However, the fact is that, at present, slip-stick excitation does not seem to be the best candidate for a flaw detection device on the basis of lack of reproducibility and the relatively small number of resonances excited.

3.4 IMPACT EXCITATION

The last of the three principal types of excitation to be discussed brings us back to the maintenance man's hammer. As discussed in section 2.4, impact is the easiest way to measure damping. Moreover, it is also a convenient way to excite the resonances above 1000 Hz. Fig. 3.5 is a narrow band analysis of impact noise generated by hitting a wheel with a rod and, for comparison, Fig. 2.6 is a 1/3 octave band analysis of a similar impact. Impact occurs when a wheel crosses a joint and Fig. 3.7 is a 1/3 octave band analysis of such an event. Since in this case, the maximum output is still in the low frequency (500 Hz) bands, it is concluded

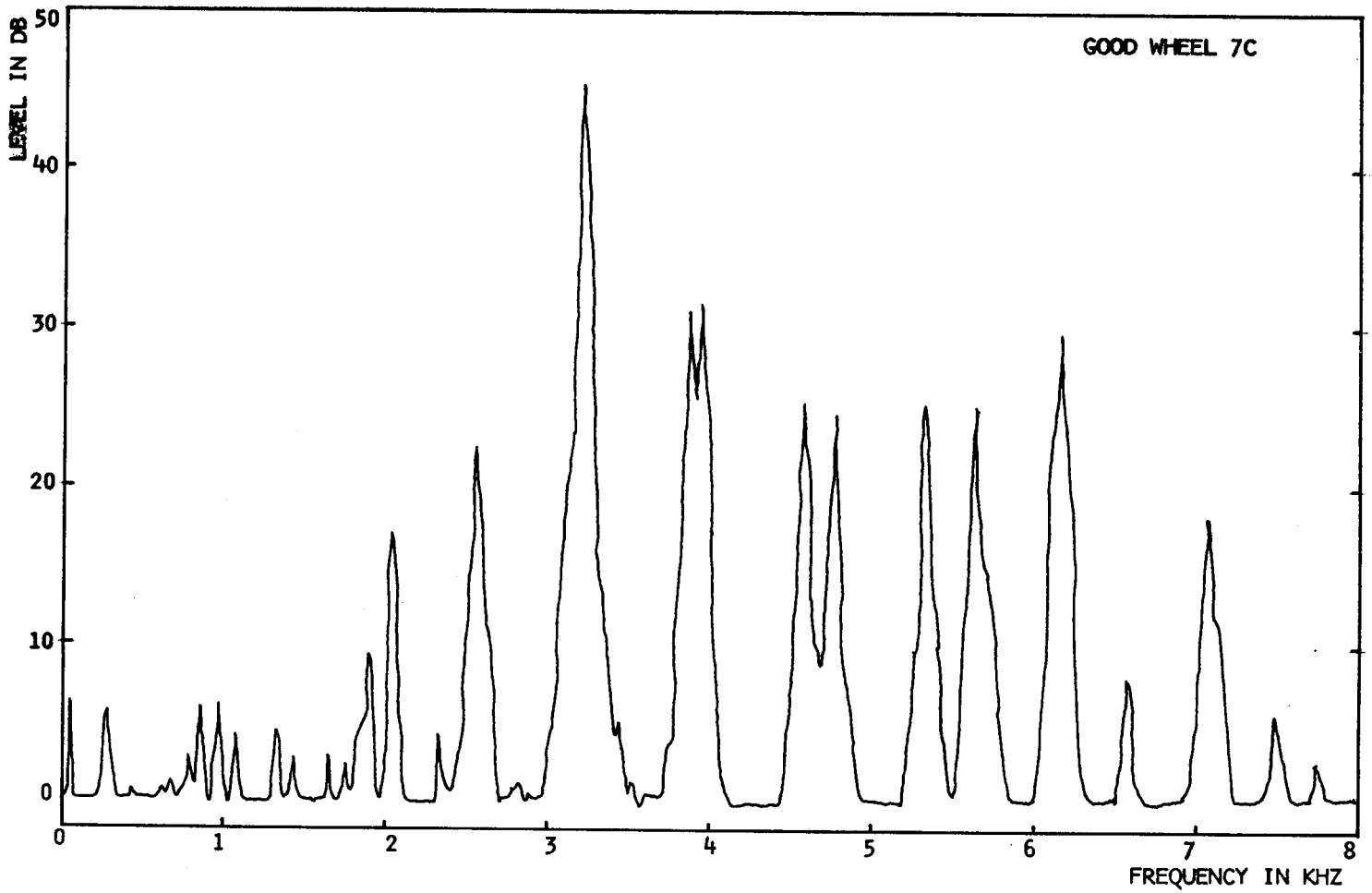

Fig. 3.5 Narrow Band Spectra of Impact Noise When Striking a Wheel with a Bar. **Wheel 7C, Microphone Pickup.** Note the relatively large number of resonances excited, as compared with retarder screech (Fig. 3.2)

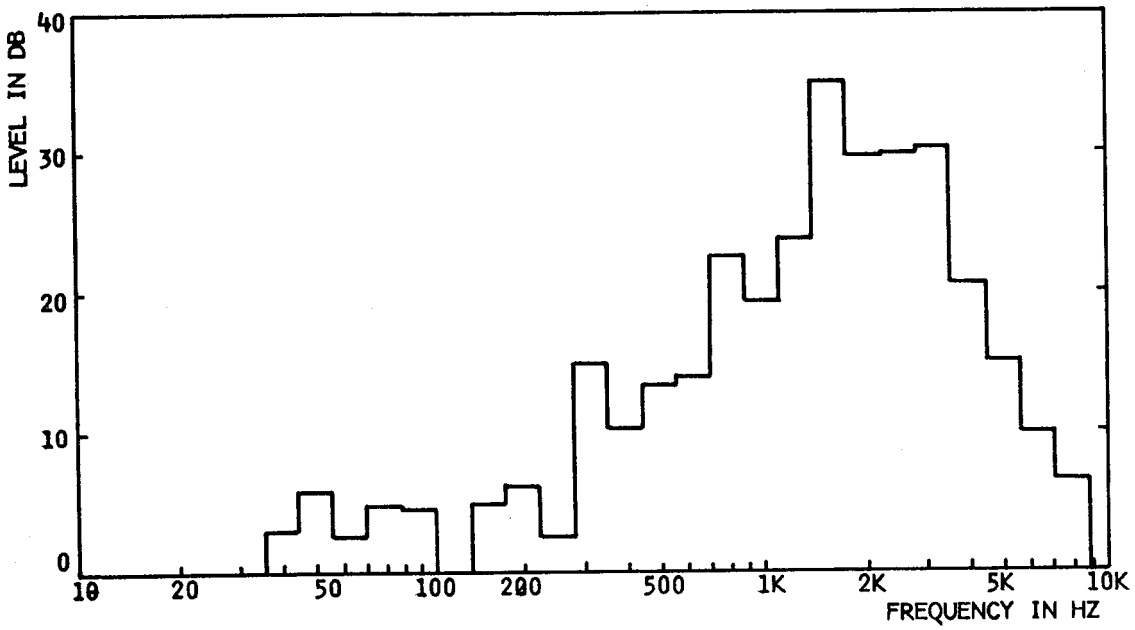

Fig. 3.6 1/3 Octave Spectra of Impact Noise When Striking a Wheel with a Bar (Microphone Pickup)

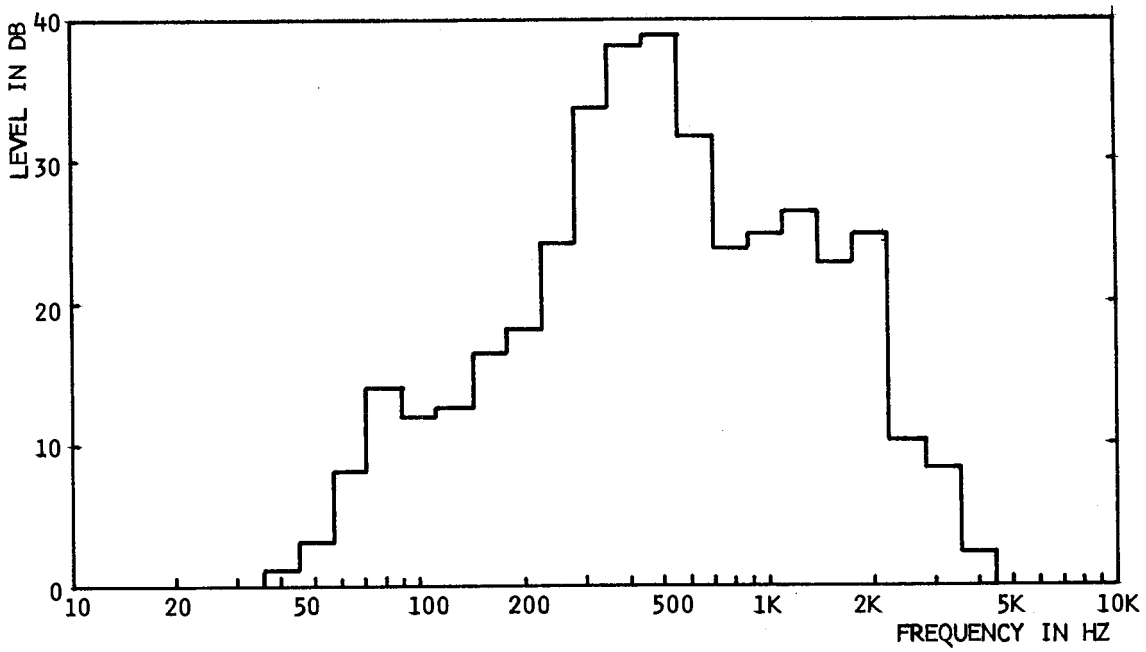

Fig. 3.7 1/3 Octave Spectra of Impact Noise When Hitting a Rail Joint (Microphone Pickup)

that the impact was not sufficient to completely mask rolling noise (see Fig. 3.1). The conclusion is that the best form of excitation is an impact, generating sound of sufficient intensity to exceed the background noise, since the spectral content of impact is much richer in the frequency range of interest than the other forms of excitation.

3.5 CHOICE OF DETECTION METHOD

The best detection device is basically a transducer with maximum sensitivity in the frequency range of interest, namely 1 to 5 KHz. There are a wide variety of inexpensive microphones and accelerometers to choose from so this element of the system is not a problem. The choice of detection method really depends on the radiation path and the need to isolate the signal from a given wheel.

If the radiation path is via the track to an accelerometer, the problem of track resonances is introduced. An experiment was performed in which random noise was used to drive the shaker, which was positioned at the top of the wheel on the tread. An accelerometer was positioned on the wheel's plate and then on the track. Fig. 3.8 shows a narrow band analysis of the two transduced signals. The track borne signal shows several resonances not found on the plate. (In other tests, the plate transducer was moved to different

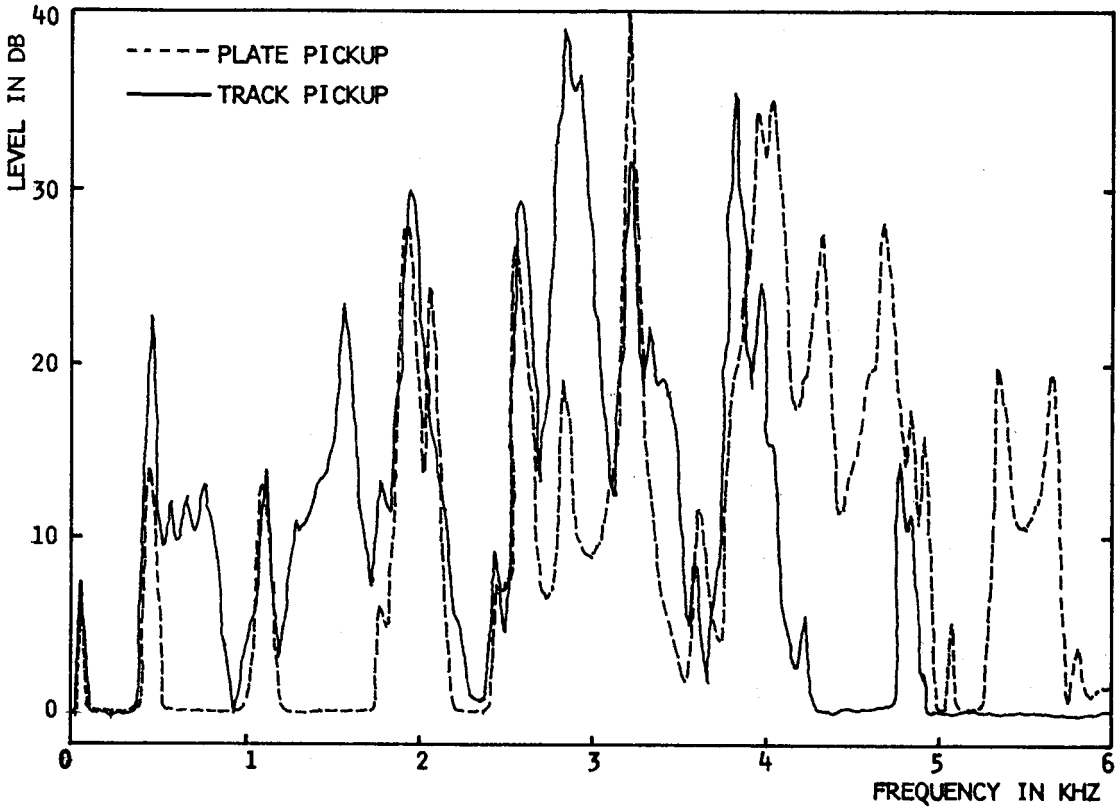

Fig. 3.8 Narrow Band Spectra for Plate and Track Pickup, for Random Noise Input, Wheel 7A. Where the track signal is greater than the wheel signal there is probably a track resonance; i.e., there are probable track resonances in the frequency regions 500-800 Hz, 1500 Hz, 2900 Hz and 3800 Hz

positions to ensure that it was not situated at a node.) Thus there seems to be evidence that track resonances occur at 500-700 Hz, 1600 Hz, 2800 Hz, and 3800 Hz. Since some of these resonances lie in the range of the wheel resonances of interest, the track borne vibration is obviously a less desirable detection method than the non resonant air-borne path.

The problem of isolation of the signal from an individual wheel will obviously be diminished if the excitation is confined to a given wheel, as with an automatic wheel impacter. The isolation will then be achieved with a signal to noise ratio of 20 dB. In the field tests performed it was assumed that no obstruction could be placed closer than 10 feet to the track.* In order to achieve signal isolation the directivity of the receiver was maximized. The final setup used is shown in Fig. 3.9. This obviously cumbersome device would be obviated if the receiver could be moved closer to the wheel and housed at ground level. Another aspect of the isolation problem is that excitation of wheels on either side of the axle is necessary. In order to minimize cross talk, it may be desirable to stagger the exciters on either side of the track, in actual practise.

---

* This assumption was due to an erroneous knowledge of the State of Texas Railroad Commission regulations which actually permit objects of graded sizes at various distances from the track.

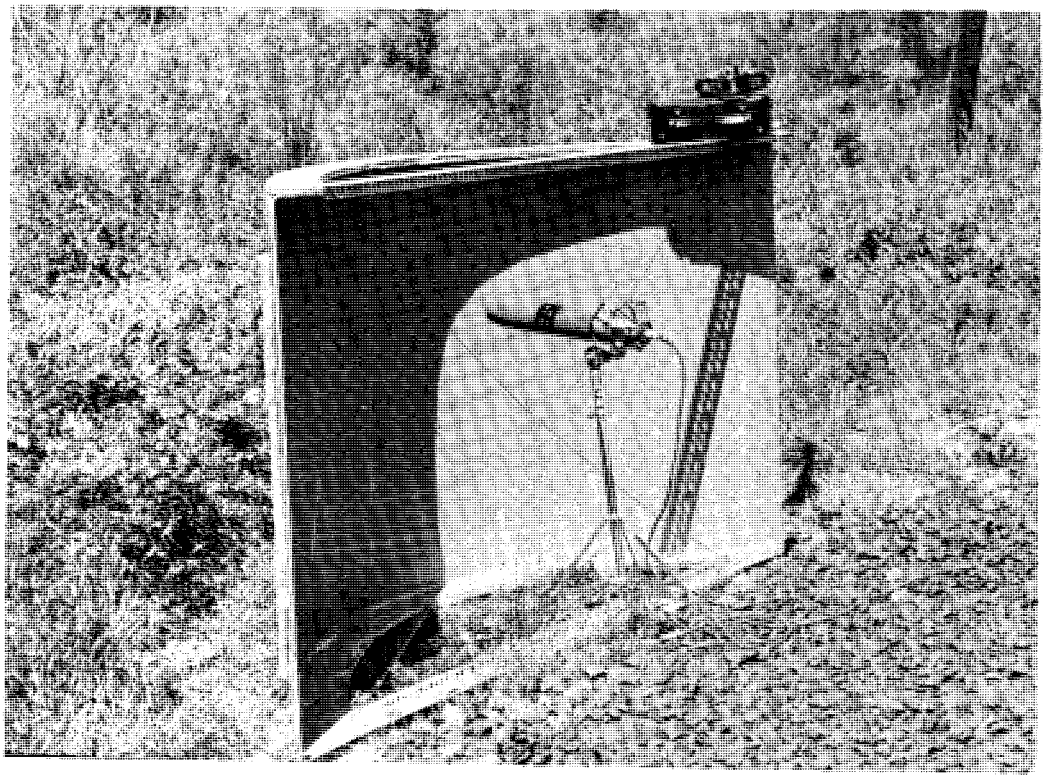

Fig. 3.9 View of the Parabolic Reflector

4. DATA PROCESSING

4.1 INTRODUCTION

Data from analytical work and laboratory tests indicate that there is considerable variation in the signatures of good and flawed wheels. These are temporal, such as decay time differences, and spectral, such as resonance changes. Changes in signature however also occur due to other factors such as the wear of the wheel, manufacturing method, etc. The purpose of the data processing apparatus is to analyze a particular wheel signature and then render a judgement whether the wheel is "good" or "bad". In case of a system malfunction, a "no test" indication is also needed.

On possible approach to accomplish this task may be a "template matching" procedure, where the signature of the wheel under test is compared against a standard signature. Various choices exist for the selection of a standard wheel signature. The first and seemingly easiest choice is what might be termed a "bad wheel" standard signature. If the signatures of all flawed wheels were quite alike, if for instance they contained resonances which were not present in

good wheel signatures, then a bad wheel standard signature would be easy to obtain. In reality however there are a variety of ways in which wheels fail. Crack types that occur in flawed wheels are numerous [25]. It was found in the course of these experiments that signatures of flawed wheels vary considerably from one another. A typical bad wheel signature does not exist.

The next choice of a standard for a template matching procedure is a "good wheel" standard signature. With the use of such a good wheel signature, it is assumed that variations in wheel signature due to wheel material, size, and manufacturing method will always be less than variations due to the presence of flaws. A standard good wheel signature might be arrived at in a deterministic fashion by obtaining wheel signatures analytically and experimentally for all possible variations of good wheels, and then composing a weighted average. However, it is obviously easier to obtain the standard signature by statistical methods.

Another choice of a standard for a template matching procedure might be called a "pseudo" standard. The assumption can be made that when two wheels are pressed onto the same axle they are identical in size, design, material, and age. So their signatures when similarly excited should be identical.

If a flaw is present in one of them their signatures will differ. This simple comparison scheme however leaves the possibility of equally bad wheels on the same axle going undetected.

The wheel signatures are complex time varying signals containing many frequency components. Each frequency channel and time interval sampled is a separate parameter for data processing. Variations of these parameters will be due to a number of causes, some indicative of wheel conditions, some perhaps due to random effects totally unrelated to the wheel. Thus when signatures are matched, the total difference might be more due to the random effects than due to the presence of a flaw.

Comparison problems similar to this one have been encountered before and are dealt with in a discipline known as pattern recognition [26]. Pattern recognition techniques evolved from early attempts to simulate human intelligence with a computer, efforts to machine read and recognize handwritten characters, weather forecasting, photograph sorting, etc. These tasks are accomplished by sorting and classifying data. Nilsson [27] describes the basic model for a pattern classifier as follows: let the pattern that is represented

by a set of real numbers, $x_1, x_2, x_3, \ldots x_n$, be sorted from other patterns by a pattern classifier. The output of the pattern classifier is a single distinct number R for each pattern that is examined. (See Fig. 4.1.) To design an effective pattern recognition system, the input parameters have to be selected such that they are relevant to the recognition problem. Unfortunately no theoretical model exists for such a selection process. It must be based on prior knowledge of the problem, and a trial and error training of the pattern classifier. The operation of the pattern classfier may be described as follows: let the set of input parameters, $x_1, x_2, x_3, \ldots x_n$, that represent the pattern to be classified be the rectangular coordinates of a point in the n dimensional "pattern space". (See Fig. 4.2.) Then regions in the pattern space would be designated and labelled say R_i, such that when a pattern falls into that region R_i, the output of the pattern classifier would be R_i. Functions which describe the surfaces of the regions $R_1, R_2, R_3, \ldots R_n$ are called discriminant functions, and the surfaces are referred to as decision surfaces. In Fig. 4.2 is an example of a two dimensional pattern space with X_1 and X_2 as inputs and R_1, R_2, and R_3 as three regions in pattern space. Point $P(x_1, x_2)$ represents a pattern to be classified. The basic problem in

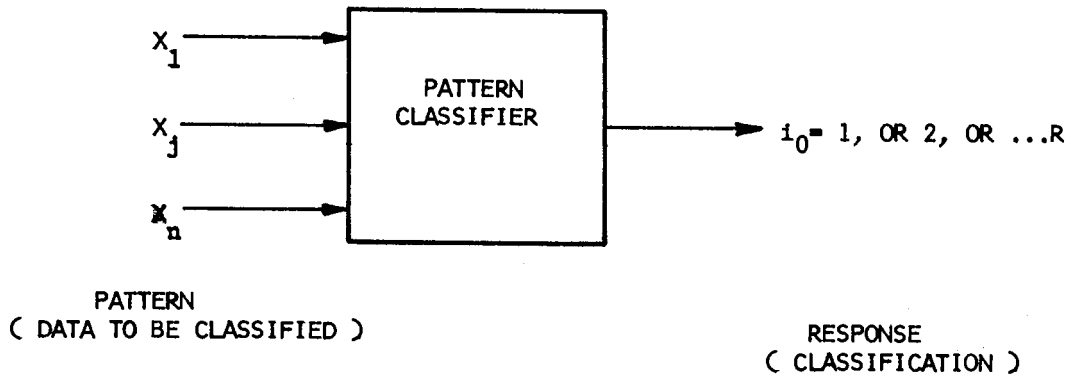

Fig. 4.1 Schematic of a Pattern Classifier

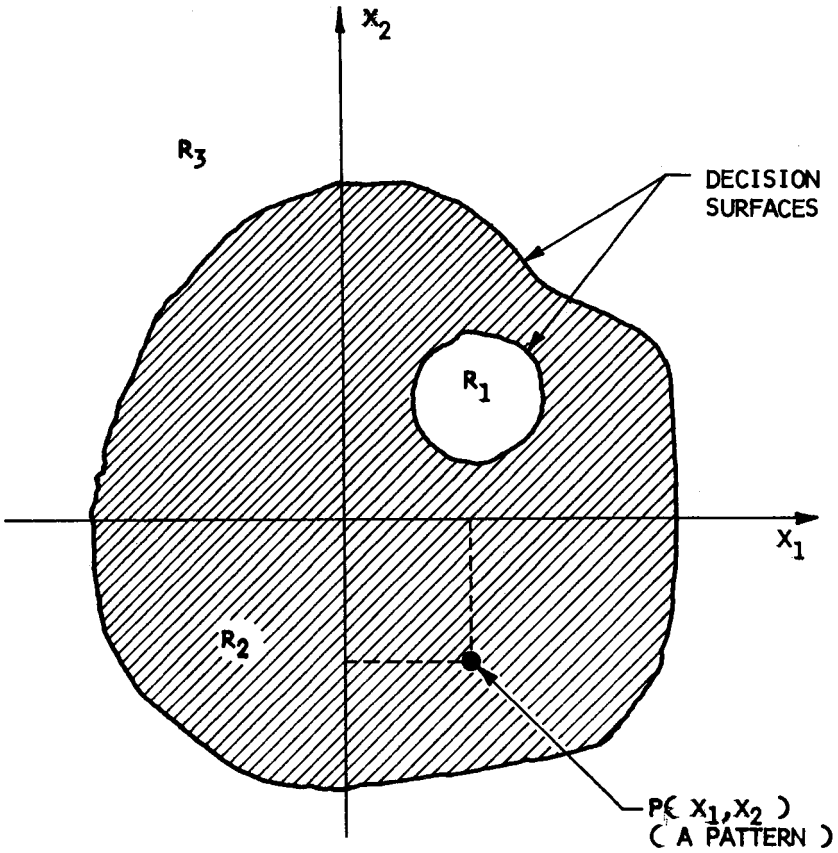

Fig. 4.2 Geometric Representation of a Two Dimensional Pattern Space

pattern recognition is the selection of the discriminant functions so that the patterns are classified into the desired groups.

4.2 WHEEL FLAW DETECTION WITH PATTERN RECOGNITION TECHNIQUES

The wheel flaw detection problem can be adapted to a simple pattern recognition model as discussed in the proceeding section. It consists of a pattern classifier with an input pattern and a single number output per pattern. (See Fig. 4.1.) The input pattern to the model was the wheel signature. The signature was represented by a parameter vector $x_1, x_2, x_3, x_j \ldots x_n$. The values of the parameters were sixteen normalized levels (normalized to the overall sound level) of 1/3 octave bands with center frequencies from 400 Hz to 1.5 KHz, and the decay rate was obtained by taking successive amplitude readings following an impact and calculating the slope. The output of the model was a two state "good" or "bad" indication. Currently there are no provisions for a no test indication.

The pattern classifier was designed as a minimum distance classifier, the operation which is referred to as "template matching". Such a classifier may be used if the patterns fall into groups with well-defined averages and if all patterns in a group tend to cluster closely around their average. "Good" or "bad" judgement then may be made by calculating the distance

between the point P_i representing the standard spectrum and the point $\bar{X}$ representing the signature of the wheel under test as follows:

$$|\bar{X} - \bar{P}_i|^2 = (\bar{X} - \bar{P}_i)\cdot(\bar{X} - \bar{P}_i)$$
$$= \Sigma\Delta_j^2$$

where $\bar{X}$ = the vector from the origin to the point X,

$\bar{P}_i$= the vector from the origin to the point P_i,

and Δ_j is the deviation of the parameter x_j (a one third octave band level or decay time) from the parameter P_{ij}.

Initially, $\bar{X}$ and $\bar{P}_i$ were vectors of 17 components, 16 of which were spectral levels, and 1 was the calculated decay time.

For the values of the vector $\bar{P}_i$, 2 alternate standard spectra were used. In vector P_1 the components were values belonging to an average good wheel signature, whereas in vector P_2 the components were values belonging to the signature of the wheel mounted on the other side of the same axle as the wheel under test. Choice of "good" and "bad" was made by setting a distance limit from the average good wheel pattern point. It was found that some of the spectral levels in the 1/3 octave bands varied even amoung good wheels, probably due to variations in wheel geometry.

These bands were eliminated. In Table 4.1 are tabulated distance values that were calculated for a set of wheel signatures that were obtained from impact tests. Of all the wheels that were tested there was one wheel where the performance of the classifier is questionable. Wheel 8G does not have any apparent cracks, but it is worn beyond serviceable limits.

The data processing task was accomplished with a NOVA 1220 Computer. In Figure 4.3 the schematic of the data processing hardware is shown. The software development for the computer to accomplish these tasks involved the following: An assembly language subroutine was written to interface between the realtime analyzer and the computer. (See Appendix C, Section C.3.) This routine enabled the computer to read the levels in the 39 filters of the real time analyzer. Basic language software was acquired from Data General Corporation with the option of "call", which enabled the use of the assembly language subroutine with any basic language program. Thus, all other software was written in Basic. The development of the pattern recognition program was initiated with the following requirements, that it can operate real time, and that it can update the good wheel average on a continuous basis. In Figure 4.4 a functional diagram is shown for the program, (see Appendix C, Section C.2 for Program Listing),

TABLE 4.1 SUMS OF DIFFERENCES OF WHEEL SPECTRA FROM AVERAGE GOOD WHEEL SPECTRA IMPACT EXCITATION

NOTE: a. Good Wheel Average Based on All Good Wheels.

b. Summing of Differences for 1/3 Octave Bands With Center Frequencies of 1.6 KHz to 8 KHz.

c. All Spectra for this Table Were Obtained by Tapping on the Rim of the Wheels with a Steel Bar.

WHEELS	ACTUAL CONDITION	CONDITION INDICATED BY CLASSIFIER WITH DIST= 70 DISCR LEVEL	DISTANCE IN CLASSIFICATION SPACE TO AVG SIGNATURE POINT	DIFF. IN DISTANCE IN CLASSIFICATION SPACE BETWEEN WHEELS ON SAME AXLE
1G	Good	Good	27	157
1B	Flawed	Flawed	184	
3G	Good	Good	35	49
3B	Flawed	Flawed	84	
4G	Good	Good	41	82
4B	Flawed	Flawed	123	
8G *Mis-pick	Good, Badly Worn	Flawed	128	7
8B	Flawed	Flawed	121	
7A	Good	Good	42	4
7C	Good	Good	38	
9A	Good	Good	51	100
9C	Flawed	Flawed	151	
10A	Good	Good	63	4
10C	Good	Good	67	
11A	Good	Good	28	26
11C	Good	Good	54	

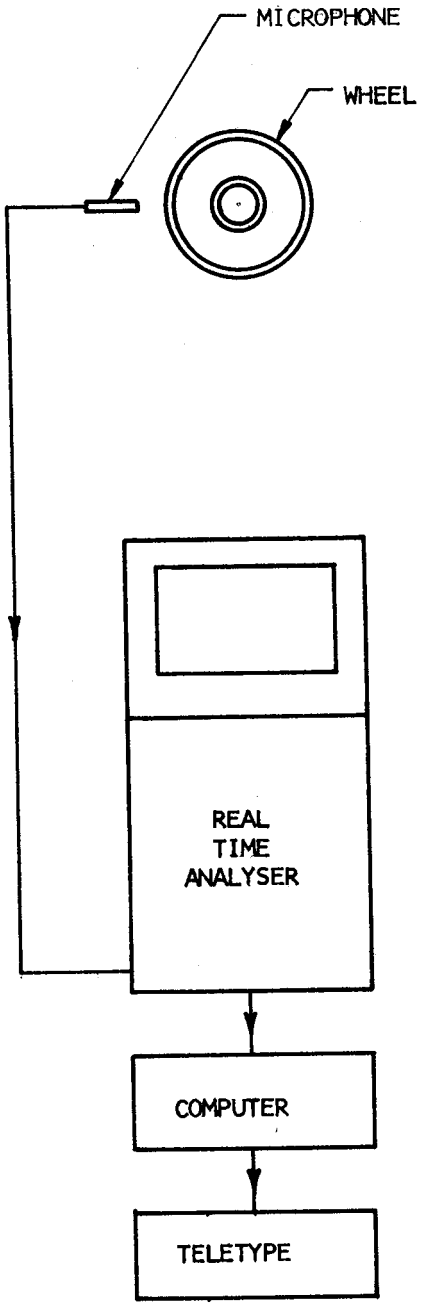

Fig. 4.3 Schematic of Data Processing Hardware

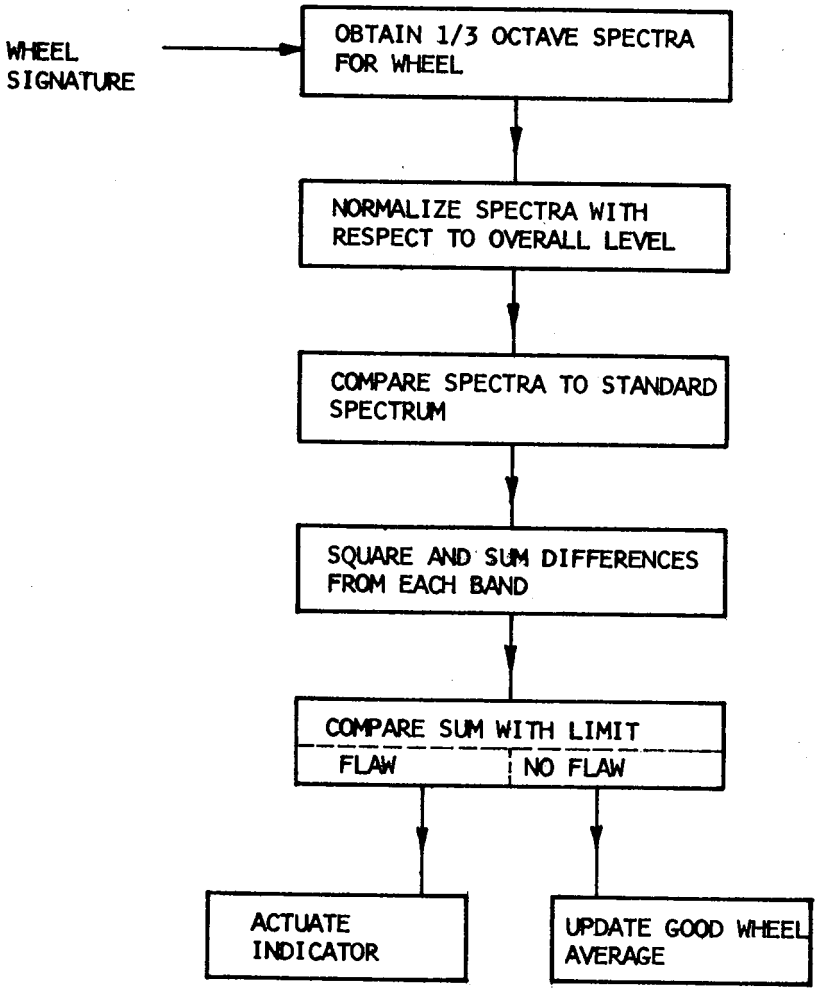

Fig. 4.4 Flow Diagram of Pattern Recognition Software for Flawed Wheel Detection

where the spectral levels are normalized with respect to the overall sound level. This was tried in two ways: in one the level of each 1/3 octave band was subtracted from the overall level, in the other the level of each 1/3 octave band was divided by the value of the overall level. The division method of normalization yielded more consistent results. The use of these two methods of normalization was an attempt to express spectrum levels in a dimensionless fashion, as changes in the shape of the spectrum were of prime interest and not the absolute values of the individual bands.

5. LABORATORY DEMONSTRATION SYSTEM

5.1 DEMONSTRATION SYSTEM DESCRIPTION

The purpose of the work described in this report was to establish the feasibility of the acoustic signature technique in finding flaws in railroad wheels. As a final act in this process it was decided to assemble a laboratory demonstration intended to simulate a field operation as far as possible. It should be emphasized that this system had to be put together within a limited time and budget and that considerable development work will be necessary to translate it into a reliable device in service.

Following the conclusion, as discussed in Chapter 3, that the best form of excitation is an impact generated sound of sufficient intensity to exceed the background noise, some work was undertaken to design a wheel actuated impacter. With this end in view some tests were made to determine the impulse necessary to generate an adequate sound level. Assuming the background level of general train noise is about 85 dB and that a signal to noise ratio of 20 dB is required, a peak radiated sound level of about 105 dB was felt to be a desirable objective.

Five different mild steel cylindrical bars were used to impact a wheel on its rim. The bars were suspended at their center by a string clamped to a supporting sturcture located near the wheel. Different string lengths were used for each bar. Care was taken to see that the flat end portion of each bar struck the rim during the impact. The velocity with which the bar struck the rim of the wheel at the time of impact was calculated from the expression

$$v = \sqrt{2g(\ell - \sqrt{\ell^2 - x^2})}$$

where

ℓ = length of suspension of the bar

x = horizontal distance of the bar from the rim before release

g = acceleration due to gravity

The arrangement is shown schematically in Fig. 5.1. A sound level meter was placed at approximately 10 feet from the wheel rim to record the sound pressure level in dB (C Scale).

A semi-empirical relation between the sound pressure level and impacting velocity can be deduced as follows. Assuming that the system is linear the output acoustic pressure should be proportional to the input force. The input force, assuming all momentum M from the impact is lost should be of

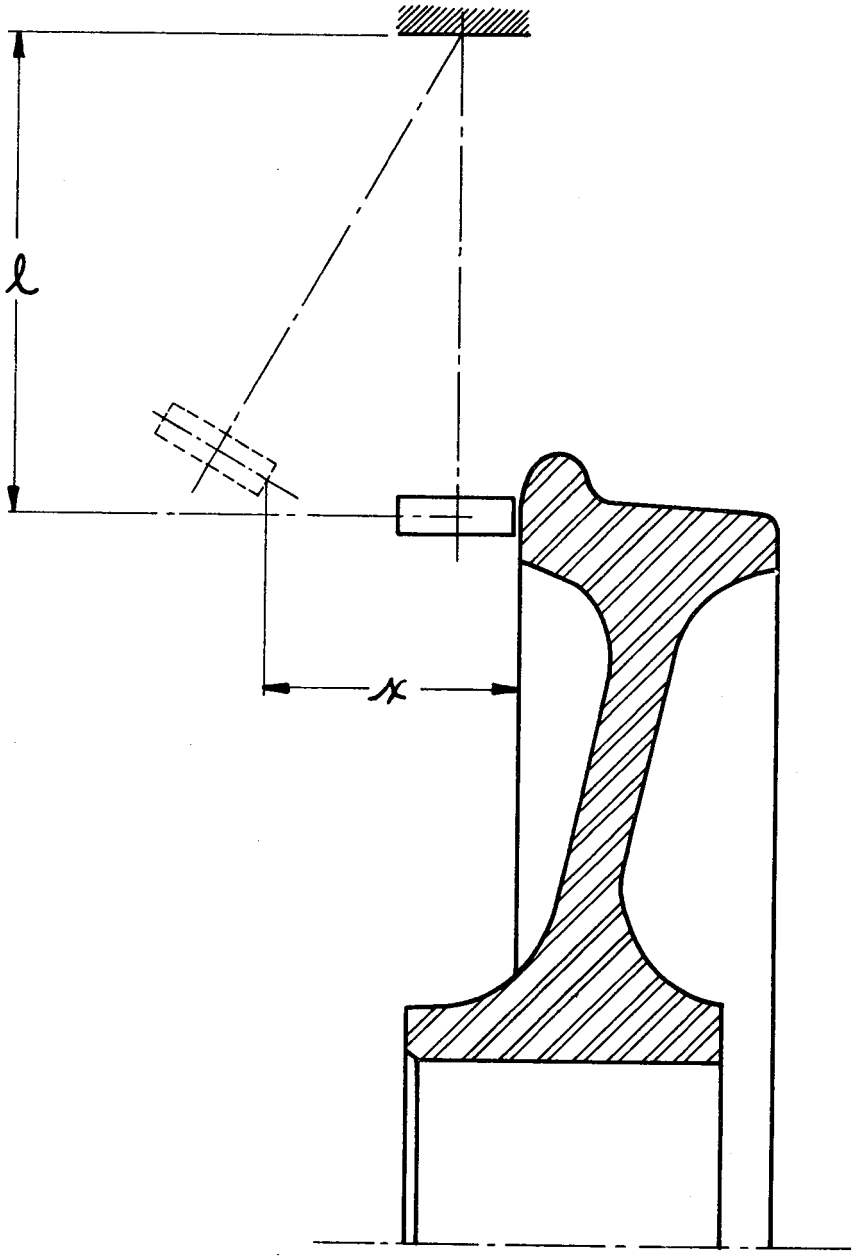

Figure 5.1 Impact Test Schematic

the order $M/\delta t$ where δt is the duration of impact. Assuming this time is determined by the interval for a step wave to travel from the front to the back of the impacting cylinder (length L) and return, $\delta t \simeq \frac{2L}{c}$, where c is the velocity of sound. Hence it is seen that we may expect:

$$\log_{10}\left(\frac{M}{L}\right) = \text{constant} + \frac{SPL}{20}$$

To confirm this relation results are plotted in the form $\log_{10}\left(\frac{M}{L}\right)$ versus SPL in Fig. 5.2, and seem to show a reasonable correspondence to our expectation. A further point of some interest is that the magnitude of the impact force

$$F \simeq \frac{M}{\delta t} = \frac{\rho ALvc}{2L} = \frac{\rho cAv}{2}$$

where A is the area of the impacting cylinder, v its velocity and ρ its density. This suggests that a material of high specific acoustic impedance, ρc, such as steel is required for the impacting head.

Fig. 5.3 is a candidate design and Fig. 5.4 is a photograph of the assembled device for an automatic wheel impacter. The considerations in the design follow the specifications previously outlined. By adjustment of the length of the hammer link, or by inserting an extra out-of-plane link at pin A, the point of impact can be arranged to cover a wide area on the wheel.

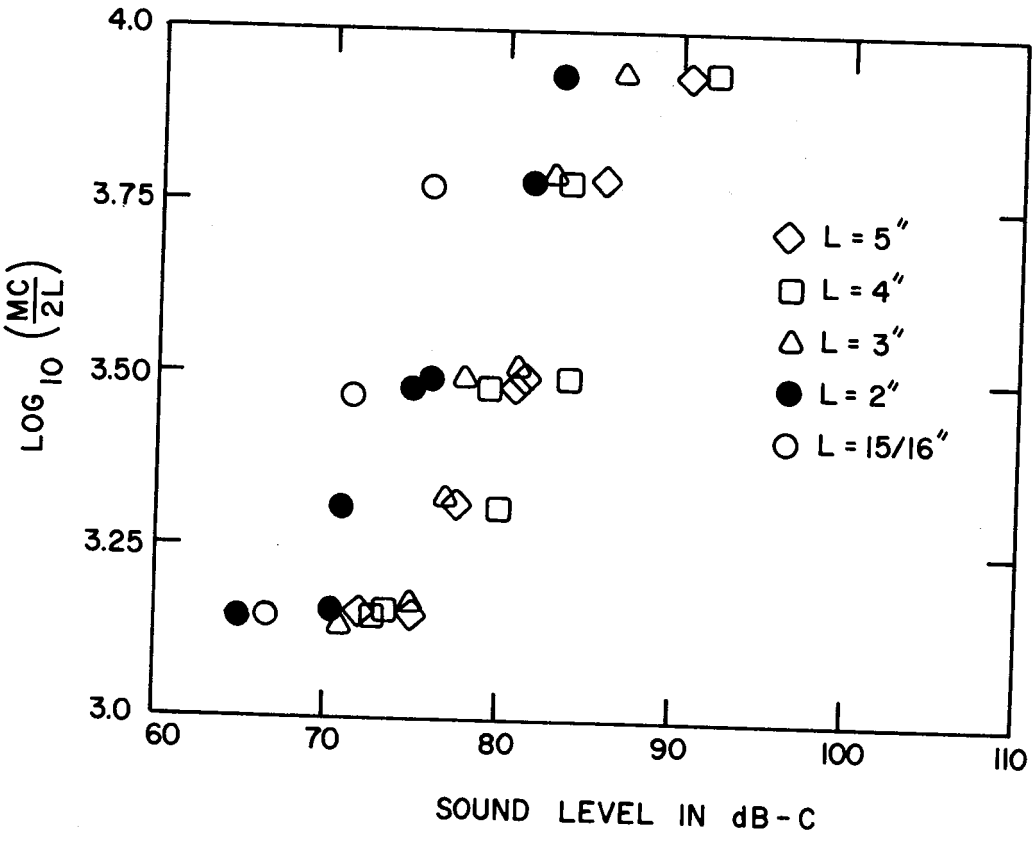

Fig. 5.2 Sound Level versus Logarithm of Impulse

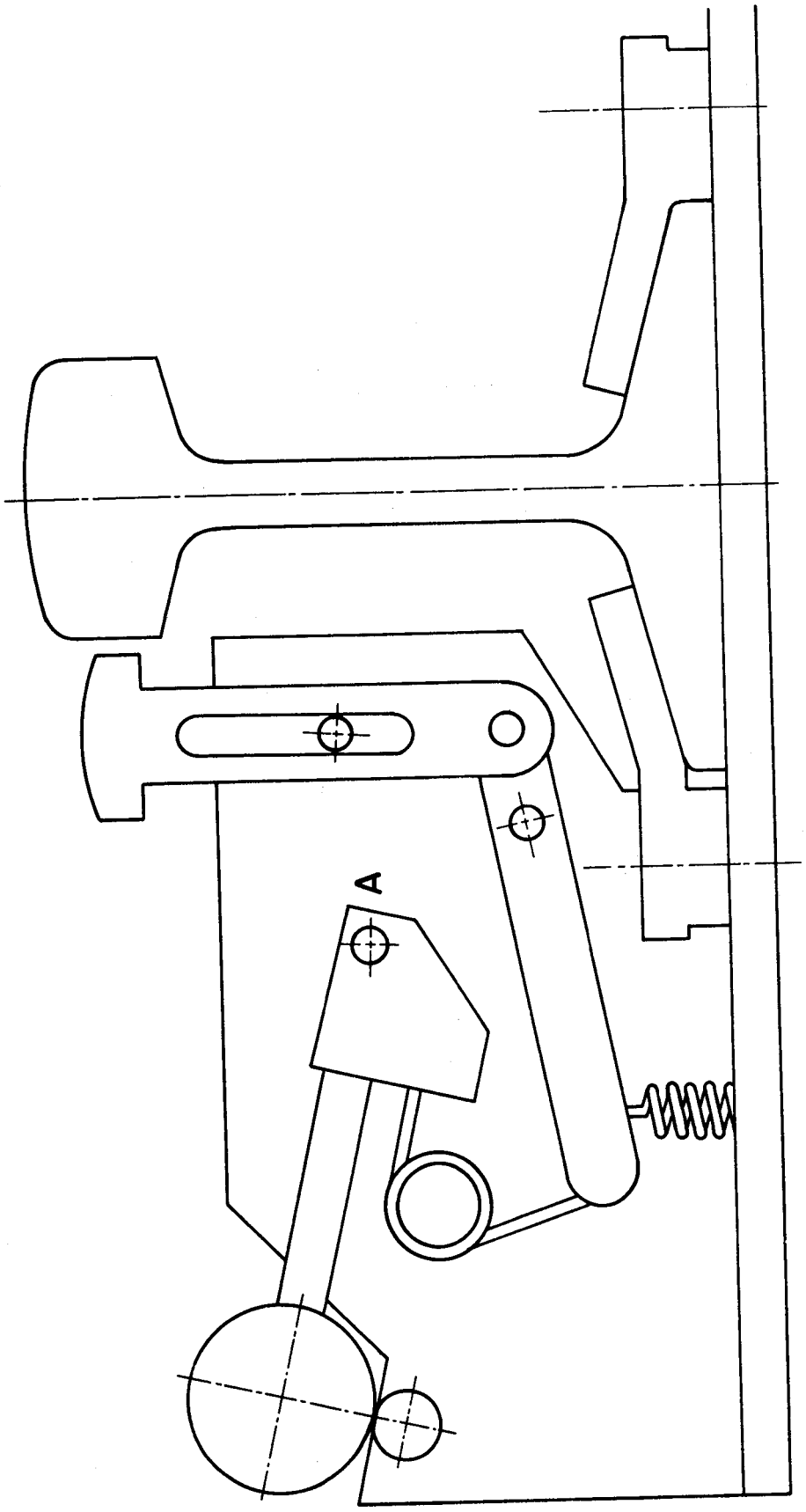

Fig. 5.3 Wheel Impacter Assembly

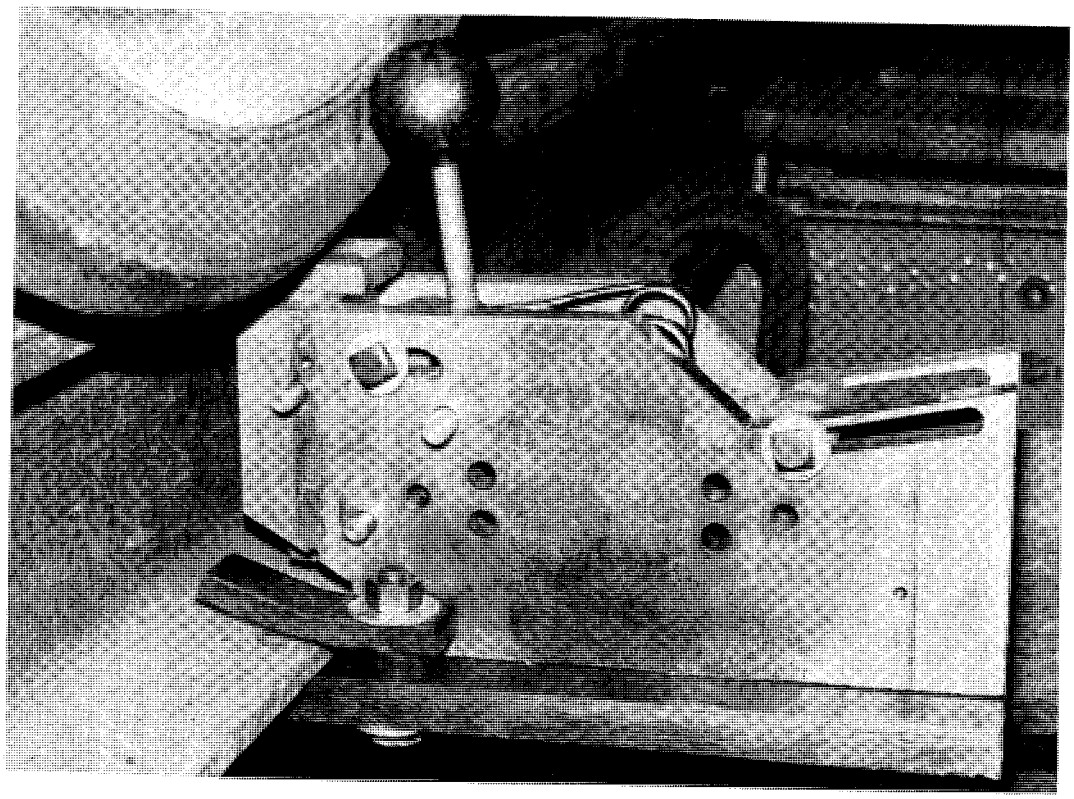

Fig. 5.4 Photograph of Automatic Wheel Impacter

Again following the argument of Chapter 3, to avoid the problem of possible detection of track resonances, it was decided to use a microphone for demonstration purposes.

Since only one exciter was available for the demonstration system, the good wheel standard signature data processing system was used as described in Appendix C. With the exciter mounted on one side of the test track the wheel sets were rolled over it in succession. The sound of each impacted wheel was analyzed in 1/3 octave bands and the difference between the level in each band and a standard normalized good wheel spectrum was obtained using essentially the same software as mentioned in the preceeding chapter and as described in Appendix C, Section C.3. The exciter could then be moved to the other track to obtain values from the wheels on the other side of the axle. In this way, although the difference of spectral band deviations between paired wheels was not computed as part of the program, such calculations could easily be made by hand. Fig. 5.5 is a photograph of the real time analyzer, computer, fast paper tape reader and teletype used.

5.2 TESTS ON THE DEMONSTRATION SYSTEM

The demonstration system was used to test and improve the computer software. In earlier trials, the complete range of

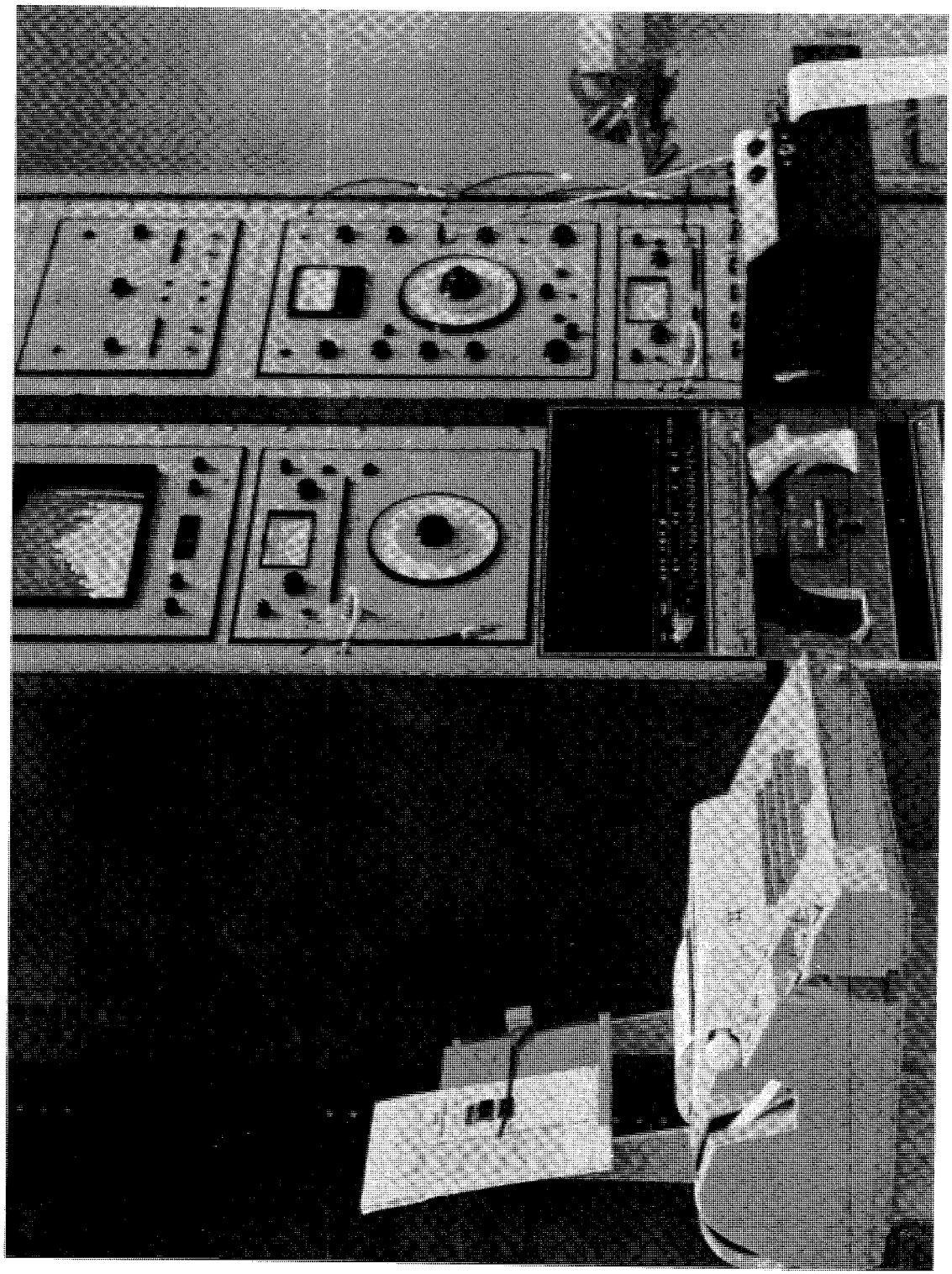

Fig. 5.5 Photograph of Data Processing Apparatus

1/3 octave bands from 20 Hz to 20 KHz was used. It soon became clear that outside of a range from about 1 to 8 KHz the random nature of background noise was prejudicial to the system's operation. Consequently, in later trials only the bands between 1 and 8 KHz were used. This is, as discussed in Chapter 2, the range of the principal wheel resonances affected by cracks. By including a routine to average each good wheel spectrum into the standard spectrum, the program becomes self-training.

The demonstration system was also used to test the effectiveness of hitting the wheel at different points. This was done by using hammer links of different lengths or shapes. These investigations were not thoroughly systematic but it was concluded that hitting the wheel on the rim at the loadline was the least reliable point of excitation. For convenience most subsequent trials were made impacting the plate on the loadline. Some trials were then performed to determine if the spectrum of a cracked wheel varied significantly when impacted at various circumferential positions. Wheel 4B was used for this purpose. Movement of the position of impact was achieved by shifting the impacter to different points along the track. Although some variations in the spectral band levels were found they were not significantly greater than variations

encountered with the exciter impacting at the same circumferential point.

In service, an impacter should deliver the same impulse to the wheel over a practicable range of wheel speeds. Some trials were made to determine the effect of rolling speed on the system's performance. Significant variation was found in normalized spectra. Further development of the excitation device will clearly have to eliminate this problem. For test purposes with the demonstration system the speed was kept constant as far as possible.

As an overall measure of system performance a set of trials was made sequentially. As may be seen in Table 5.1 the total reliability of the demonstration system is 75%.

5.3 DIRECTIONS FOR IMPROVEMENT

The results shown in Table 5.1 serve to illustrate the directions to be taken to improve the system. Inclusion of decay time and across-the-axle comparison in the data processing should go a long way to eliminating the mispicks. The basis for this statement lies in comparison of results from several trials with the exciter mounted on either track. Further improvement should result with a more careful control of impact velocity and the exact point of impact. This involves a redesign of the present exciter which is presently proceeding.

TABLE 5.1 SYSTEM FAILURES IN A TYPICAL TRIAL WITH TOTAL OF 80 RUNS

Failure Nature	Number of Occurences	Percentage of Total Runs
Wheel rode over exciter	1	1.25
Computer Malfunction	1	1.25
Sound level did not trigger system	6	7.5
Wheel Mispicked	12	15.00

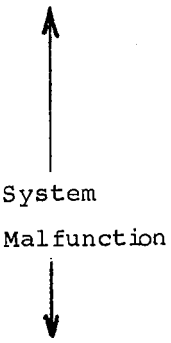

Total reliability = 75%

Reliability excluding system malfunctions = 85%

6. CONCLUSIONS

In these experiments the feasibility of a wayside railway flaw detection device was explored. The basis of the detection scheme is the differences that are found in the acoustic signature of the wheel when cracks are present, where the term acoustic signature means the characteristic sound or vibration emitted by an excited object.

The components of the detection system may be subdivided into subsystems as follows: the excitation, the wheel, the acoustic signature detection, and the data analysis. Three principal types of excitation are possible in the case of a railroad wheel: 1) random shaking, which occurs in rolling and can be modeled in the laboratory with an electromagnetic shaker; 2) slip-stick excitation, which occurs in passage around curves, under the action of retarders or brakes, and 3) impact, which occurs when a wheel crosses a joint and which can be achieved easily in the laboratory by striking a wheel with a suitable object.

Of the various excitation methods rolling is unsuitable since it only excites modes below about 1 KHz. Slip-stick action excites only one or two modes prominently, and although

these lie in the range of interest, they may vary or suddenly change, and furthermore, some wheels do not appear to be excited at all. In the laboratory impact has been shown to excite a rich spectrum of modes in the range of interest and is a convenient way to study sound decay. It is therefore recommended that an impacter be developed to operate automatically upon wheel transit. A demonstration design for an automatic wheel impacter has been described. It is also recommended that airborne sound as a detection method is preferrable to track-borne vibrations since there is evidence that track resonances also occur in the 1 to 5 KHz range.

When the wheel is excited various resonant modes radiate sound into the air and cause vibration in the supporting track. The frequencies at which these resonances occur have been determined experimentally, and to a degree, confirmed theoretically. In 33 inch wheels there are prominent modes at about 450 and 1090 Hz and a series of modes from about 1900 Hz upwards. The presence of large flaws appears to have greatest effect on the number of modes and their resonant frequencies in the range 1 to 5 KHz. When the exciting force is removed the wheel vibration dies away. An unusually fast rate of decay is also an indication of the presence of a flaw. The maximum difference in decay rates between good and bad wheels is also found in the 1 to 5 KHz range.

Various data processing schemes have been considered. The basic requirement is to categorize the signature against a good/bad criterion. The criterion can be based on the average signature of a large number of good wheels, thus allowing for variation of loading, geometry, surface conditions and metallurgy and on the difference between the signatures of wheels on either side of an axle. Each of these procedures can be subdivided according to whether analysis is made in the frequency domain (to find changes in resonant frequency) or in the time domain (to find changes in decay times). A minicomputer, teletype, and fast paper tape reader have been interfaced with a real time frequency analyzer. Software was developed for both frequency and time domain analysis.

Some further research and development is necessary before a preprototype system can be installed in the field. The design of an automatic wheel impacter needs to be tested and consolidated and a variety of software functions have to be accomplished. The system then has to be reviewed for reliability and weather protection.

REFERENCES

1. Bray, D. E., "Pulse Excitation of Railway Wheels," M.S. Thesis, M-2165, University Microfilms, Ann Arbor, Michigan, 48106, 111 pp. 1969.

2. Dalvi, N. G., "Detection of Thermal Cracks in Railway Wheels Using Ultrasonic Surface Waves," M.S. Thesis, University of Houstin, Dec. 1970, 130 pp.

3. Bray, D. E., Finch, R. D., "Flaw Detection in Model Railway Wheels," Report No. FRA-RT-71-75, National Technical Information Services, Springfield, Virginia, 22151, PB-199-956, Feb. 1971.

4. Bray, D. E, Dalvi, N. G. and Finch, R. D., Ultrasonics, II (1973) 66-72.

5. Bray, D. E. and Finch, R. D., Ultrasonics International, 1973 Conference Proceedings 194-198.

6. Schroeer, R., Rowand, R., Kamm, H., "The Acoustic Impact Technique, A Versatile Tool for Nondestructive Evaluation of Aerospace Structures and Components," presented at the 1970 Spring Conference of the American Society for Nondestructive Testing in Los Angeles.

7. Babkin, A. S., Anderson, J. J., "Mechanical Signature Analysis." Sound and Vibration, April 1973.

8. Nagy, K., "The Response of Railroad Wheels to Continuous Excitation and Impact," M.S. Thesis, University of Houston, May 1971.

9. Stappenbeck, Von H., "Das Kurvengerausch Der Strassenbahn." Z VDI bd. 96, Nr. 6, 21 February 1954.

10. Southwell, R. V., "On the Free Transverse Vibrations of a Uniform Circular Disk Clamped At Its Centre and on the Effects of Rotation," Proceedings of the London Royal Society, Series A, Vol. 101, 1922, pp. 133-153.

11. Leissa, A. W., "Vibration of Plates," NASA SP-160, 1969.

12. Timoshenko, S., "Vibration Problems in Engineering," D. Van Nostrand Company, Inc., New York, 1955.

13. Savin, G. N., Fleishman, N. P., "Rib-Reinforced Plates and Shells," NASA TT F-427, 1967.

14. Mote, C. D., Jr., "Free Vibrations of Stressed Circular Disk," ASME Paper No. 64 - WA/MD-4, 1964.

15. Williams, C. J. H., "The Stability of Nodal Patterns in Disk Vibration," Int. J. Mech. Sci., Pergamon Press LTD, 1966.

16. Tobias, S. A., Arnold, R. N., "The Influences of a Dynamical Imperfection of a Rotating Disk," Proc. Inst. of Mech. Eng., Vol. 171, 1957, pp. 669-690.

17. Tobias, S. A., "Free Undamped Non-Linear Vibrations of Imperfect Circular Disks," Proc. Inst. of Mech. Eng., Vol. 171, 1957, pp. 691-715.

18. Zenneck, J., "Über Die Freien Schwingungen Nur Angenahernd Vollkommener Kreis Formiger Platten," 1899, Annalen Der Physik, Vol. 67, p. 164.

19. Rayleigh, J. W. S., "The Theory of Sound," Dover Publications, New York, 1945.

20. Desai, C. S., Abel, J. F., Introduction to the Finite Element Method, Von Nostrand Reinhold Co., 1972.

21. Zienkiewitz, O. C., Cheung, Y. K., The Finite Element Method in Structural and Continuum Mechanics, McGraw-Hill, 1967.

22. Meirovitch, L., Analytical Methods in Vibrations, McMillan Company, New York, 1967.

23. Steele, R. and Lotz, R. (Private Communication).

24. Lyon, R. H., Lectures in Transportation Noise, Grozier Publishing, Cambridge, Mass., 1973.

25. Association of American Railroads, "Wheel and Axle Manual," Ninth Edition, 1968.

26. Andrews, H. C., "Introduction to Mathematical Techniques in Pattern Recognition," Wiley-Inter Science, New York, 1972.

27. Nilsson, N. J., Learning Machines, McGraw-Hill Book Co., New York, 1965.

APPENDIX A

APPARATUS AND EXPERIMENTS

A.1 INTRODUCTION

The experiments for this investigation were primarily designed to obtain acoustic signatures for a number of wheels under various static loading rates, and with various excitation and detection methods. The design of the apparatus was aimed at achieving this goal, as well as to provide wheel storage and handling facilities. The instrumentation was designed to test which method of data acquisition and analysis would be most suited for a prototype device.

A.2 APPARATUS

A.2.1 Test Wheels and Loading Requirements

The test objects for the laboratory studies were full-size railway wheel and axle sets consisting of pairs of 33" (or 36") nominal diameter wheels permanently pressed onto axles. Table A.1 lists the wheel and axle sets that were tested. Figures A.1 through A.6 show views of the defective wheels on axles 1 through 6. On all axles with defective wheels the designation of each wheel is: The axle number followed by the suffix G for good wheel and B for bad wheel. Thus, 1G denotes the good wheel on axle 1. On axles without defective wheels the designation of each wheel is the axle number followed by an A or C, such as Wheel 7A.

TABLE A.1 LIST OF WHEELS ON INVENTORY

AT UNIVERSITY OF HOUSTON

Axle Number	Wheel Size	Good Wheel Description	Bad Wheel Description	Manufacturer
1	33"	No defect, light rusting.	Thermal crack to axle, Fig. A.1.	Southern
2	33"	No defect, light rusting.	Overheated rim, Fig. a.2.	Griffin
3	33"	No defect, heavy coat of dirt and grease on outside of plate.	Large crack running circumferentially in rim fillet, heavy coat of dirt and grease on outside of plate, Fig. A.3.	Southern
4	33"	No defect, light rusting.	Large plate crack, Fig. A.4.	ARMCO
5	36"	No defect, light rusting.	Thermal crack partially extending into plate, Fig. A.5.	Standard
6	36"	No defect, light rusting.	Thermal cracks on outside of tread, extending into rim only, Fig. A.6.	Griffin
7	33"	New wheel	New wheel	Southern
8	33"	No defect	Rim fillet crack	Griffin
9	33"	No defect	Crack on rim face.	Bethlehem
10	33"	No defect	No defect	Griffin
11	33"	No defect	No defect	Southern

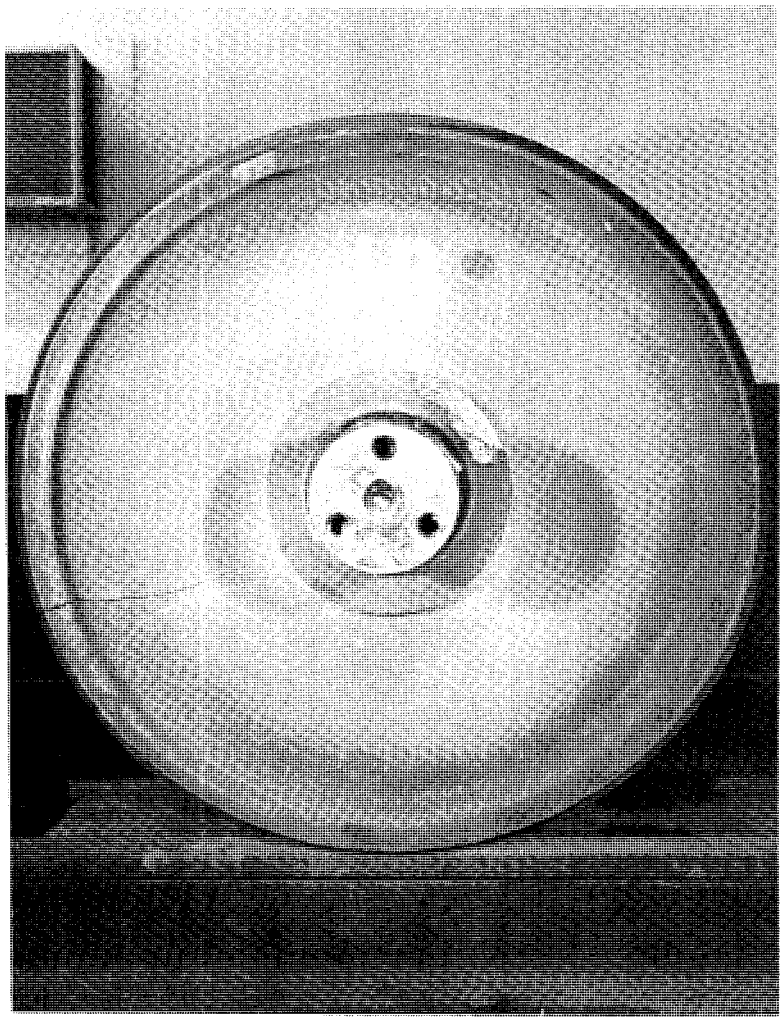

Fig. A.1 View of Wheel 1B with Thermal Crack

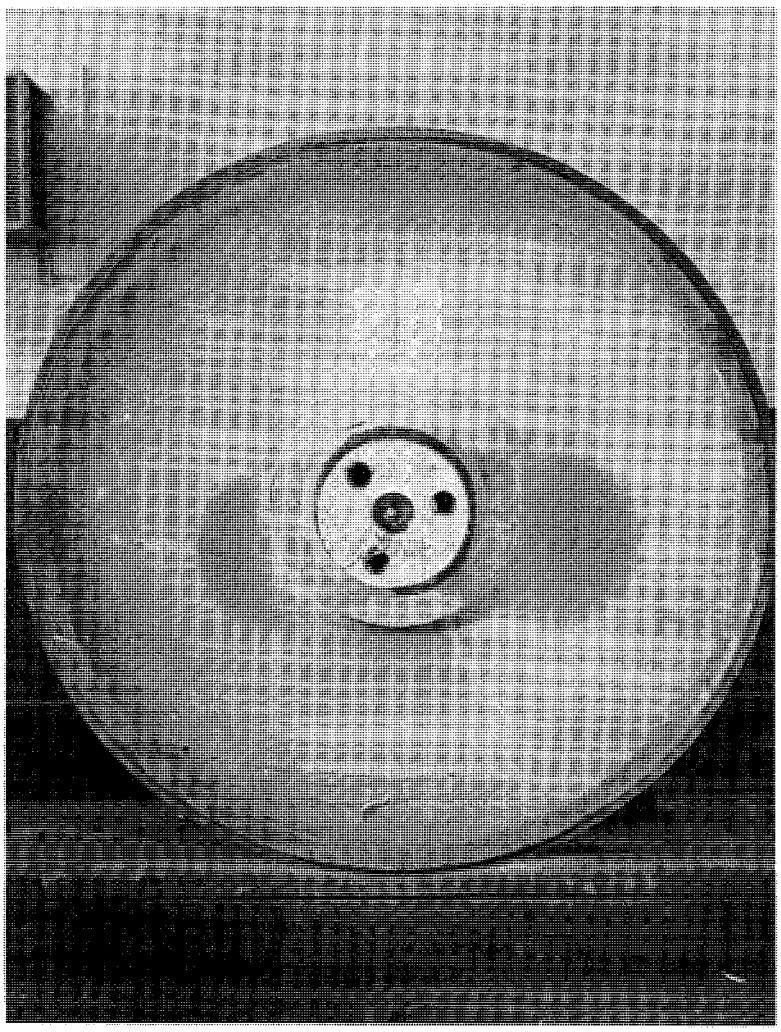

Fig. A.2 View of Wheel 2B with Overheated Rim

Fig. A.3 View of Crack in Rim Fillet of Wheel 3B

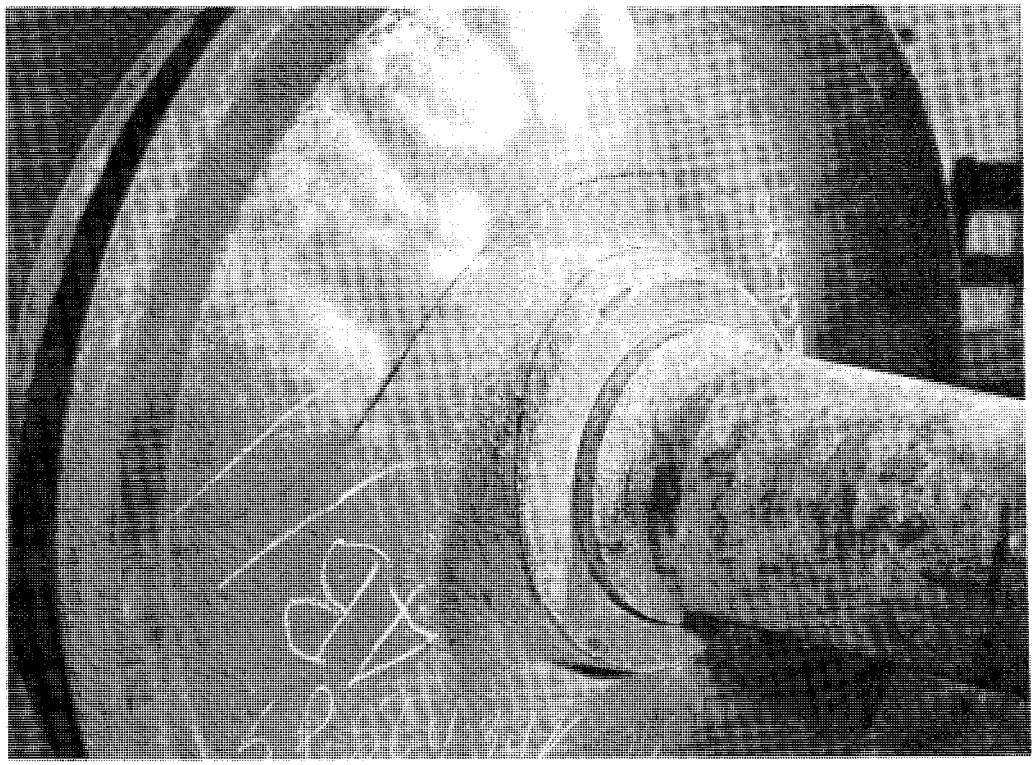

Fig. A.4 View of Wheel 4B with Large Plate Crack

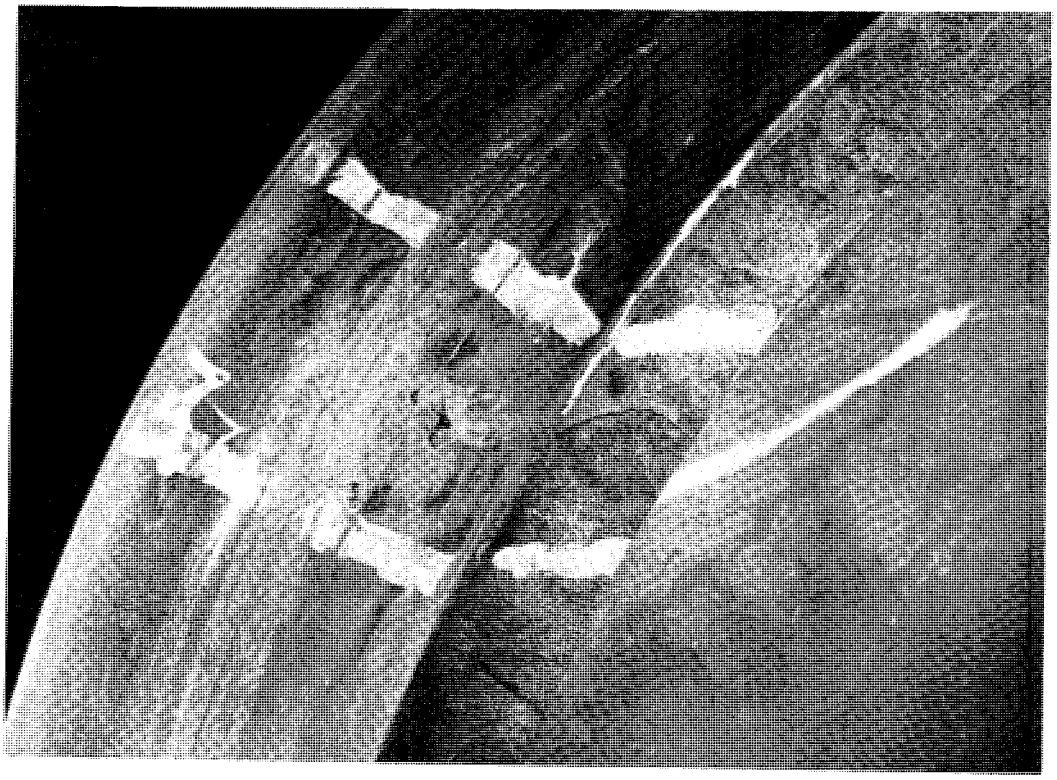

Fig. A.5 View of Crack on Tread of Wheel 5B

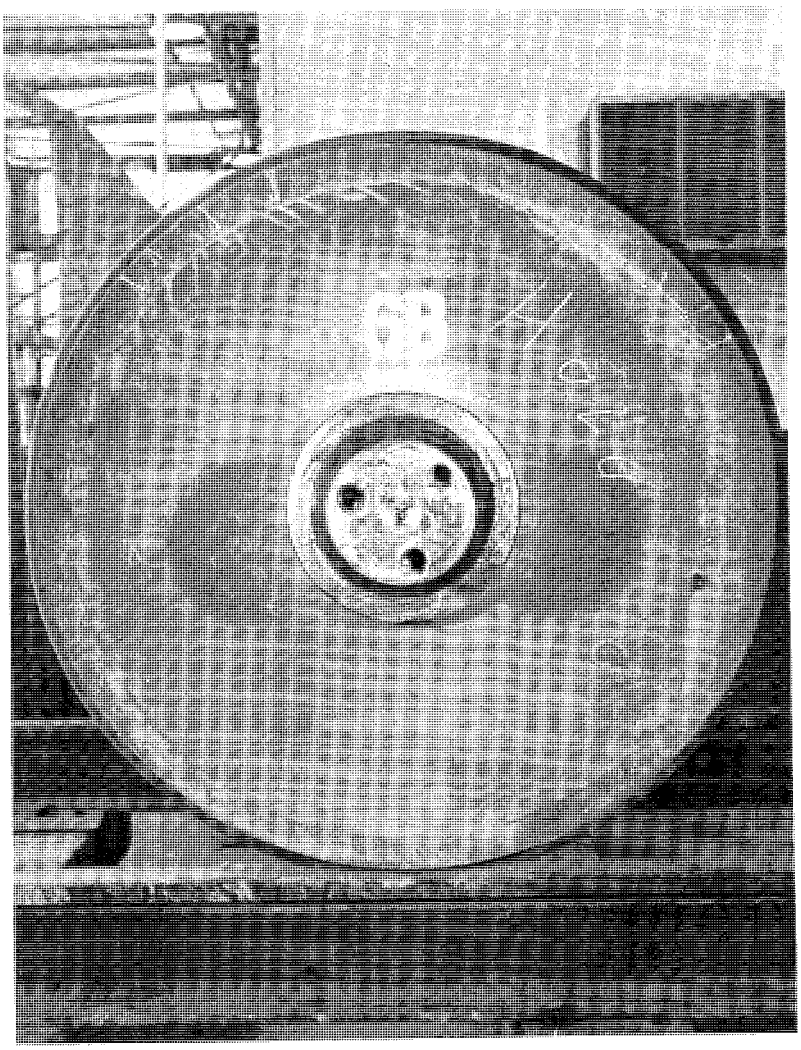

Fig. A.6 View of Wheel 6B, Location of Thermal Cracks Marked by White Lines on Front Face of Rim

The basic test requirements were:

a. The application of a static load (maximum amplitude of 30 tons/wheel, and

b. the application of a dynamic load (50 lbf maximum amplitude).

A.2.2 Test Equipment

The test stand consisted of a rectangular structural steel frame with a 54 foot long storage rack, as shown in Fig. A.7. The steel frame was set across the middle of the track, spanning the track and with the rails running through it. Wheel and axle sets could then be rolled under the frame from either side. Jacking points were constructed on the frame over the axle journals. The static load was applied at these points, with two 30 ton hydraulic jacks (see Fig. A.8) and V blocks to assure that the same load was applied at each journal. The hydraulic jacks were supplied with hydraulic fluid from a common pump. The 4 foot portion of rail fastened to the steel frame was not attached to the 25 foot long storage rails on either side of the test stand. This feature was necessary to assure that during the application of the static load, only the steel frame was loaded.

The excitation system was designed as follows: The dynamic load was applied to the wheel and axle set with a 50 lb.

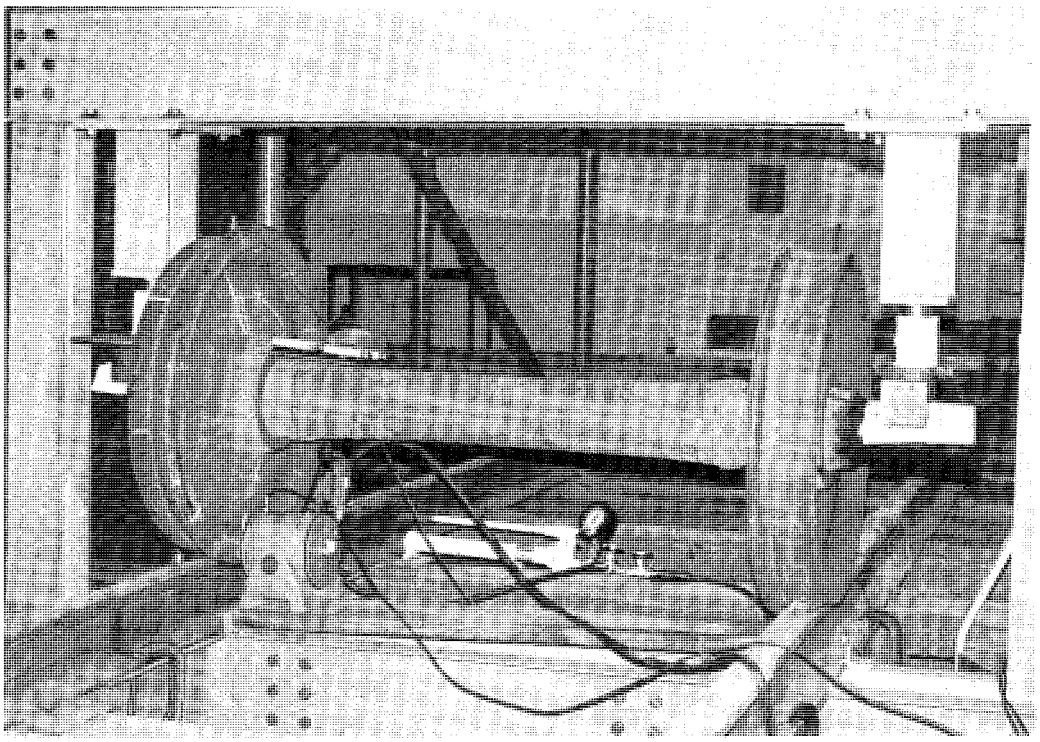

Fig. A.7 View of Test Stand

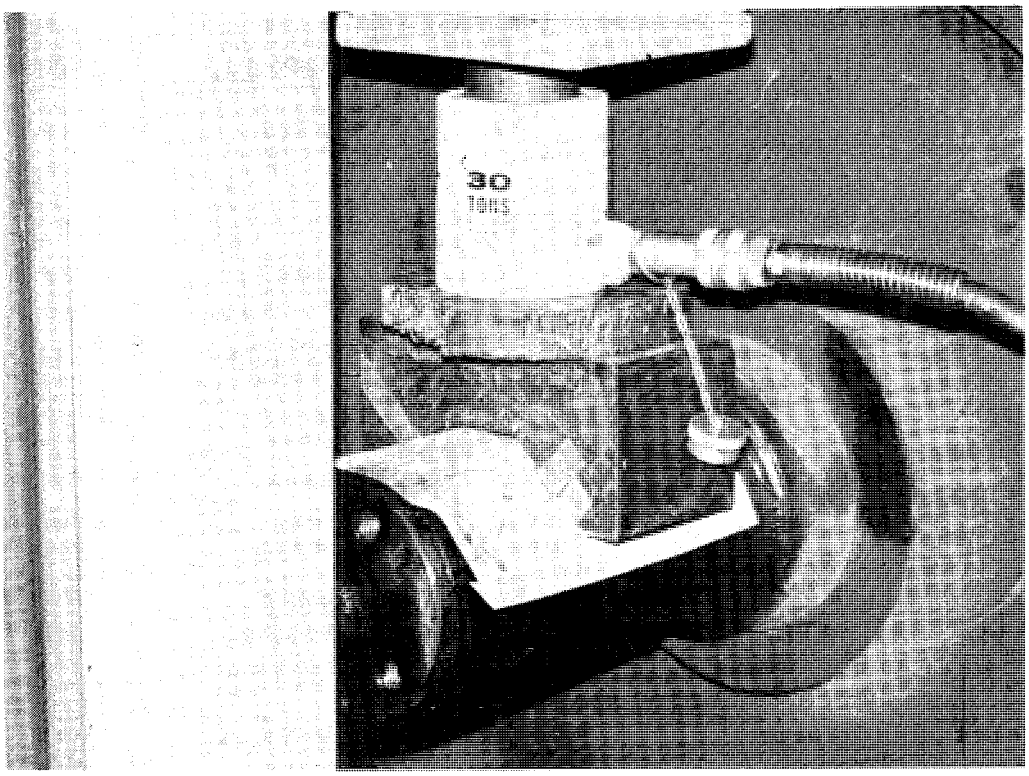

Fig. A.8 View of Hydraulic Jack Applying Static Load

Gilmore Industries Model PM 50 electrodynamic shaker driven by a Gilmore Industries Model 250 MB amplifier. The signal sources for the driving system were as follows:

a. A General Radio Model 1381 Random Noise Generator

b. A Hewlett-Packard Model 651B Sine Wave Generator

c. Rockland Model 5100 Frequency Synthesizer

The schematic of the laboratory excitation system is shown in Fig. A.9 The 50 lb. dynamic load was applied to the wheel and axle set as follows:

a. At the back face of the rim at the lowest point of the wheel, parallel to the axle. (See Fig. A.10.)

b. At the center of the axle and perpendicular to it. (See Fig. A.11.) This excitation point was chosen to simulate the excitation by the rolling of the wheel and axle set on the track. The response of the electrodynamic shaker to 5 KHz bandwidth random noise is shown in Fig. A.12.

The noise and vibration detection system was instrumented such that the airborne noise emitted by the wheel during excitation was picked up by a Shure Bros. Model No. 98108 Microphone and recorded on a Nagra-Kadelski Model Nagra IV, Type L3 Tape Recorder. (See Fig. A.13 for schematic of detection system). During recording, the waveforms were monitored on a Tektronix Model 564B Storage Oscilloscope. Photographs were

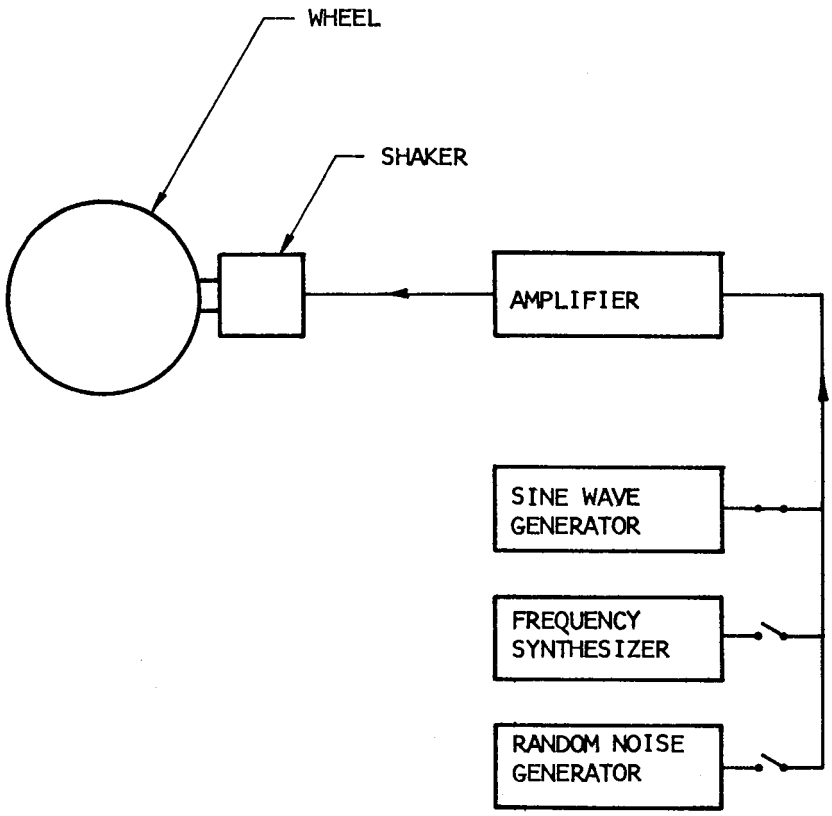

Fig. A.9 Schematic of Laboratory Excitation System

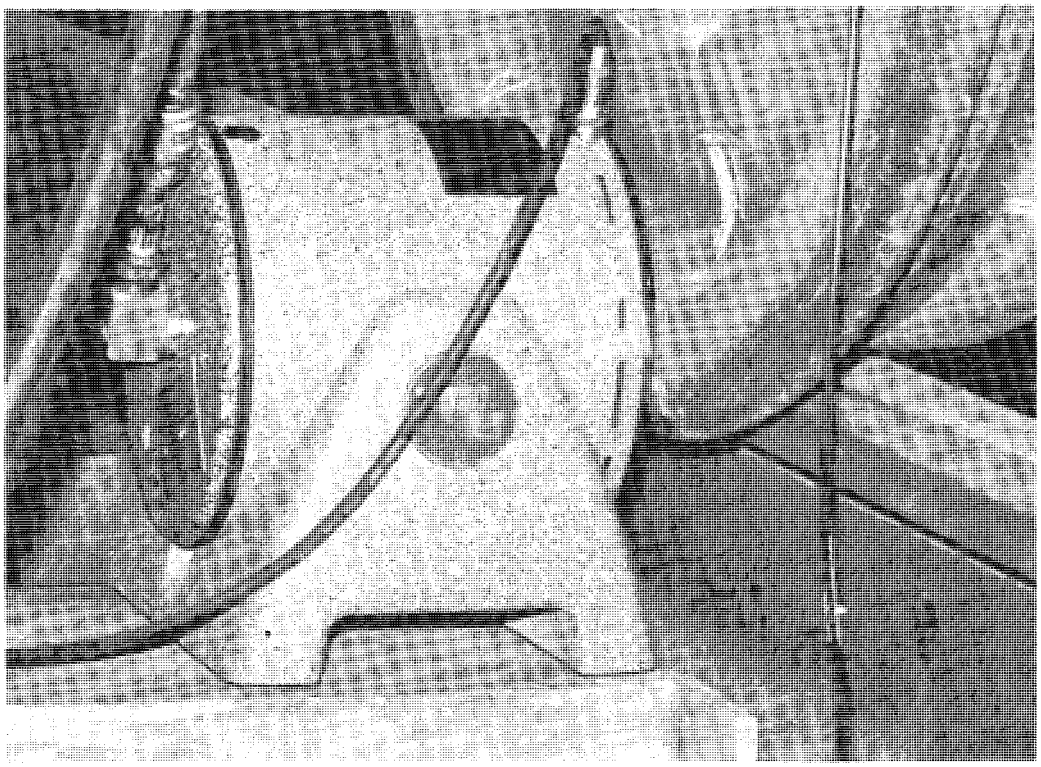

Fig. A.10 View of Shaker at Back Face of Rim

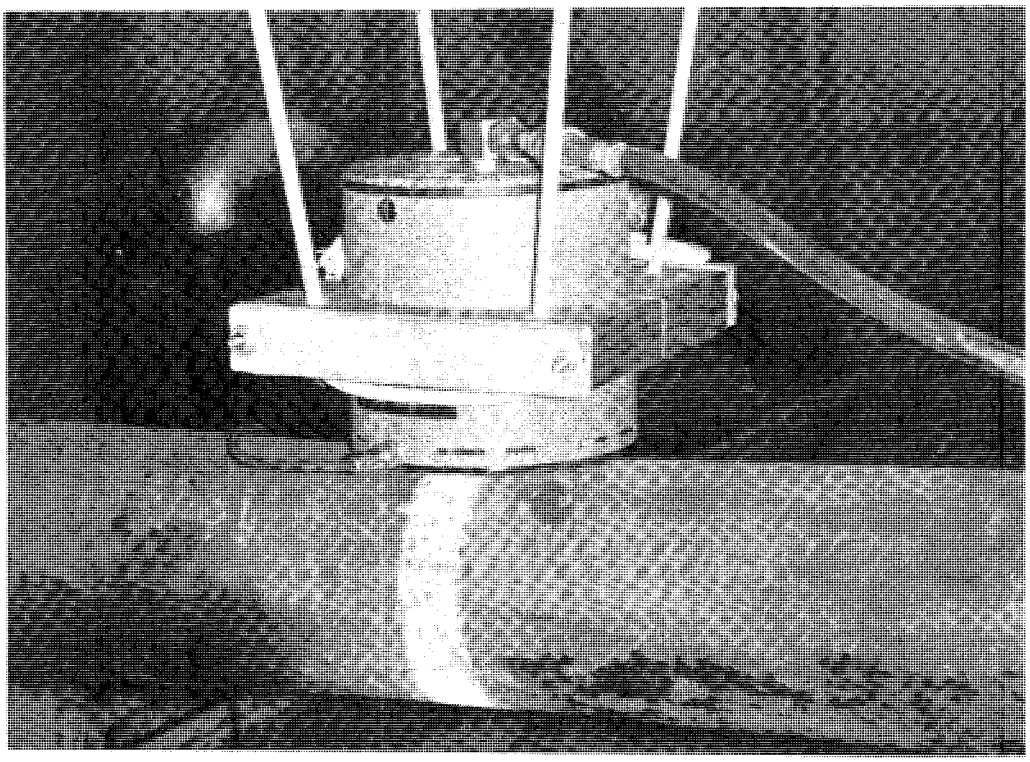

Fig. A.11 View of Shaker at Center of Axle

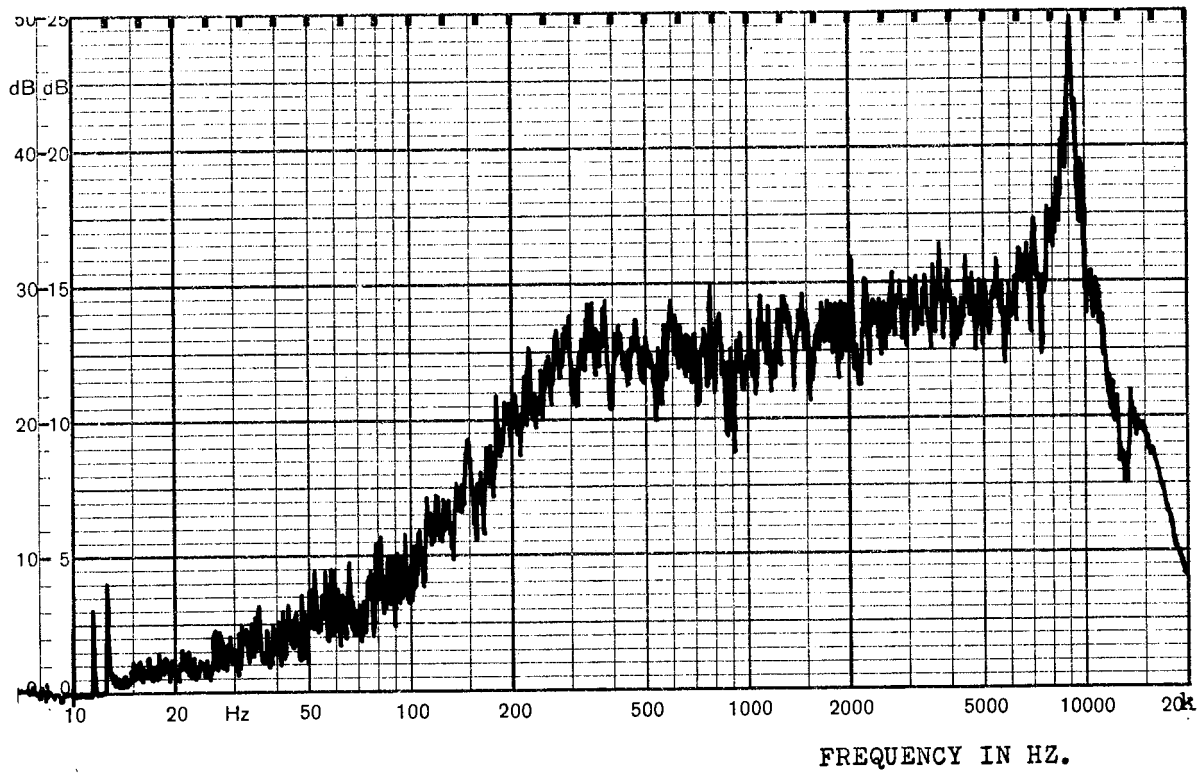

Fig. A.12 The Response of the Electrodynamic Shaker to 5 kHz Bandwidth Random Noise Input

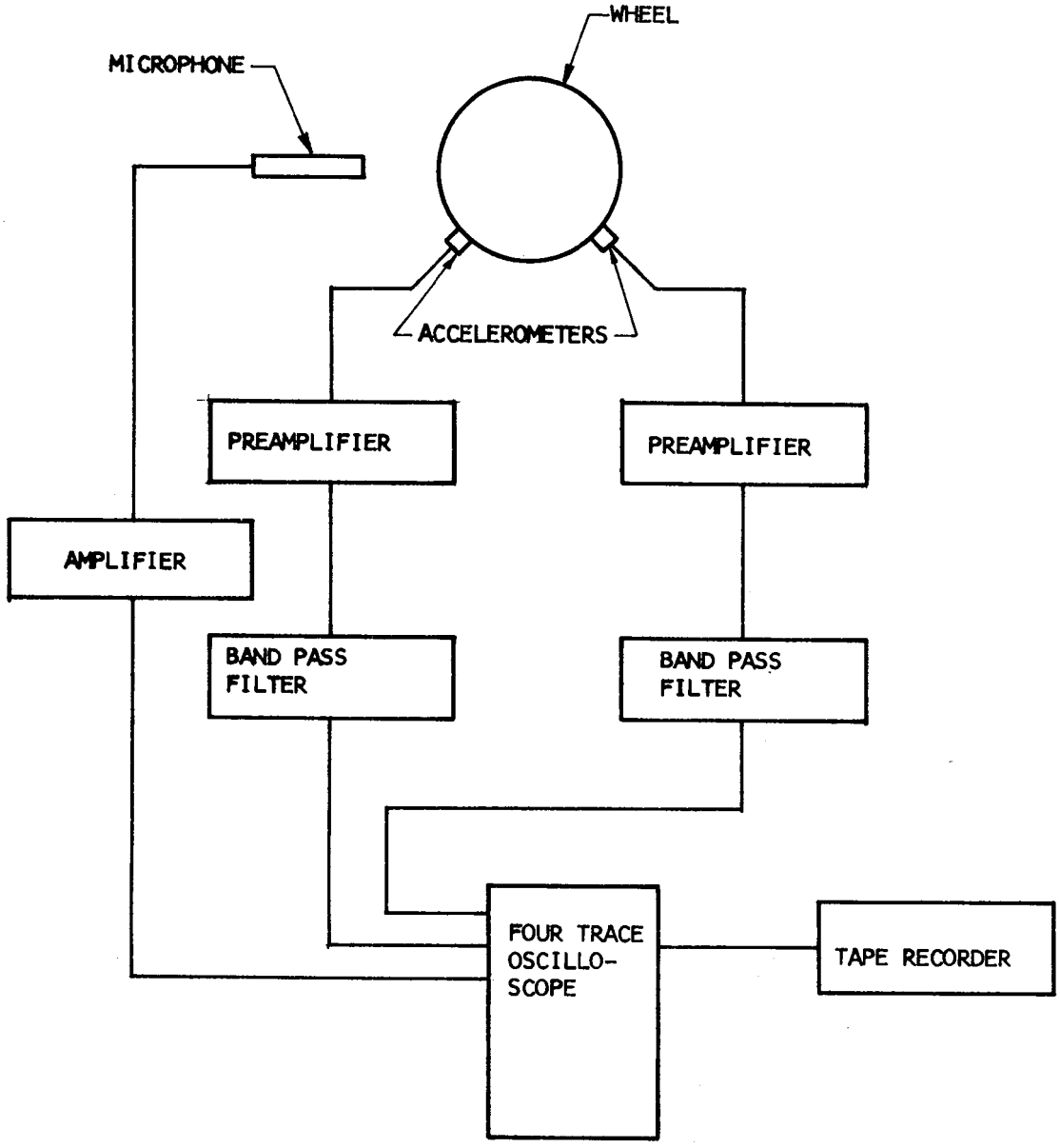

Fig. A.13 Schematic of Laboratory Detection Equipment

made of waveforms displayed on the oscilloscope screen with a Hewlett-Packard Model 196A Oscilloscope Camera. The vibration of the wheel was monitored with accelerometers. Two types of accelerometers were used:

a. An Endevco Model 2242 Accelerometer

b. A General Radio Model 1560-P5 Vibration Pickup.

Each accelerometer was attached to the wheel or track with a magnet, or with a threaded stud. The signal from the accelerometers was amplified with an Endevco Model 2607 Preamplifier. Two Krohn-Hite Model 310 CR Filters were used for signal conditioning. The signal recording and monitoring equipment was the same as for airborne noise.

The Data Processing Apparatus - the response of the wheels to various forms of excitation was recorded on tape. This gave an amplitude vs. time record of the wheel response. For some tests, the signal was a steady state, long time sample, for others it was a short duration, transient decay. The required analysis was as follows:

a. Frequency spectrum analysis, 1/3 octave analysis as well as narrow constant bandwidth analysis.

b. Auto and cross correlation analysis with a correlation function computer.

For the 1/3 octave analysis, the Bruel and Kjaer Real

Time Third Octave Analyzer, Type 3347 was available. This instrument will accept an input signal from a variety of transducers in the 20 Hz to 20 KHz range. It has the capability of providing a real time 1/3 octave frequency spectra of a continuous or a transient signal. The time constant for the response of the analyzer is 0.2 seconds above 200 Hz and 3.15 seconds maximum below 200 Hz.

The 1/3 octave frequency spectrum is displayed on a video screen which shows the sound level in thirty 1/3 octave bands with center frequencies ranging from 25 Hz to 20 KHz. In addition to the 1/3 octave filters, one of the frequency weighting networks A, B, C or D may be selected with the option of displaying overall level in the range from 22.4 Hz to 22.0 KHz. The video display may be stored and subsequently recorded on chart paper with a level recorder. The 1/3 octave real time analyzer is coupled though an interface device to a NOVA 1220 Minicomputer. The rate of data transfer between the two devices is limited by the speed of the 1/3 octave real time analyzer. Although the real time analyzer has analog to digital converters, due to the relatively slow response of the analyzer, the conversion rate is comparatively slow. Thus, sampling rates are not fast enough to supply data for such software tasks as correlation analysis. Data values may be taken at about 0.2 to 0.25 seconds, thus permitting computations such as time decay calculations.

Software was developed to acquire data in real time (continuous as well as transient signals), store and operate on that data, subsequently, under continuous keyboard control and output.

For the narrow band analysis, a Spectral Dynamics Model SD301C Real Time Analyzer was used with a Model SD302C Ensemble Averager, a Model SD42 Memory and a Model 13116-Z X-Y Display. The instrument is a sweep frequency analyzer using digital time compression techniques to speed up the analysis time. In the 0 to 10 KHz range, the analysis time is 0.05 seconds. The spectrum obtained is composed of 500 resolution elements, or "lines" spaced equally across the analysis range. The ensemble averager averages a preselected number of spectra (up to 4096) and stores the average spectrum ready for display. The memory unit allows the storage of one spectrum while another is being obtained. The display is a large oscilloscope screen with logarithmic or linear display option on both X and Y axes. Stored spectra from the analyzer may be fed to an X-Y recorder. A Hewlett-Packard Model 135A X-Y Recorder was used. Some narrow band analyses were also made using a Bruel and Kjaer Slave Filter in a mechanical sweep frequency analysis.

Some correlation analyses were made with a Princeton

Applied Research Model 101 Correlation Function Computer. The computer is a hybid instrument, the correlation function being computed for 100 incrementally increasing values of the time delay selected. Auto or cross correlation may be performed, depending on whether one or two input signals are used. The computed function was displayed on an oscilloscope and on a X-Y recorder.

A.3 EXPERIMENTS

Tests on the full size wheels were acoustic in nature and were performed on the test stand described in Section A.2.2. Some time averaged holograms of vibrating 1/4 scale model wheels were made in the Electro-Optical Laboratory of the Electrical Engineering Department, University of Houston.

For the tests of full size wheels, three methods of excitation were used; impacting of wheels with a striker, excitation with an electrodynamic shaker, and rolling of wheel and axle sets on storage rack.

Microphones and accelerometers were the detection transducers in these experiments. This was necessary in order to compare wheel signatures that are transmitted through the air and wheel signatures that are structure transmitted (i.e., through the rails). The microphone locations in the tests were typically in the order of 1 to 2 feet from the wheel. The accelerometers were placed on the rail and on the surface of the wheels at the rim, on the plate, and on the axle.

A.3.1 Impacting of Wheels

The wheel and axle set to be tested was centered on the test stand. Ordinary railroad spikes were used as wedges to keep the wheels from rolling. The hydraulic jacks were placed over the journals with the V-blocks. (See Figure A.8.) The wheel to be tested was struck with a hammer, (the hammer striking surface was hemispherical) on the back face of the rim approximately at 60° from the load line. The sound emitted from the wheel was picked up by microphone and accelerometer and recorded with the Nagra IV tape recorder. Repeated blows were struck and recorded. This test was performed with and without static load on the journals. Some impact tests were performed with the automatic impacter, while the wheels were rolled on the storage rack.

A.3.2 Excitation of the Wheel with Electrodynamic Shaker

The tests performed with the electrodynamic shaker may be categorized according to the signal source used for the shaker drive.

a. Wide band random noise input was used to obtain characteristic spectra while varying the shaker position and varying the static load on the journals. The shaker position was varied by placing the shaker at different positions on the wheel and axle set (see Figures A.10, A.11).

The response of the wheel in each case was recorded. The static load on the journals was varied with the two 30-ton hydraulic jacks. For the wide band random noise tests, zero and 10-ton/journal loads were used.

b. Pure sine tone input was used to obtain accurate numerical values for resonances obtained with frequency analysis of response to wide band random noise. This was accomplished by varying the frequency of the pure sine tone input while monitoring the amplitude of the wheel response with an accelerometer. The maximum amplitude was picked by observing the signal from the accelerometer on the oscilloscope screen. When resonance was found, a frequency counter was used to measure the exact frequency. Pure sine tone input was also employed to detect resonant frequency and amplitude changes of some of the resonances of wheels when applying different static loads to the journals.

A.3.3 Rolling the Wheel and Axle Set on the Storage Rack

A wheel and axle set was rolled on the storage rack. The purpose of this test was to see if very low velocity rolling generated any detectable wheel response. The sound emitted by the wheel was monitored by microphone (with and without a horn) and accelerometer pickups and recorded with the tape recorder.

A.3.4 Mode Shape Tests

Time average holography was used to determine the mode shape of a vibrating 1/4 size wheel at certain resonances. The experimental setup was assembled from existing optical components, as shown in Figure A.14. The wheel was vibrated with a 2 lb. shaker at a resonant frequency. The laser beam was split into two beams. One beam was used to illuminate the wheel, the other was used as a reference. The reflected light from the vibrating wheel and the reference beam were combined on a photographic plate to form the hologram. The hologram was reconstructed with the same reference beam and photographed with a 35 mm still camera. A typical result is shown in Fig. 2.6.

For mode shape determinations on full sized wheels, which are too large to be illuminated with the holographic set-up, the wheel surface was probed with an accelerometer. Some typical results are shown in Figs. A.15 to A.18. Sine tone excitation was used.

A.4 FIELD TESTING APPARATUS

Field tests were made to record sound from moving railway wheels. Figure A.19 shows the layout plan and Fig. A.20 is a photograph of the actual set-up in the field during recording. It was necessary to isolate the sound coming from only one

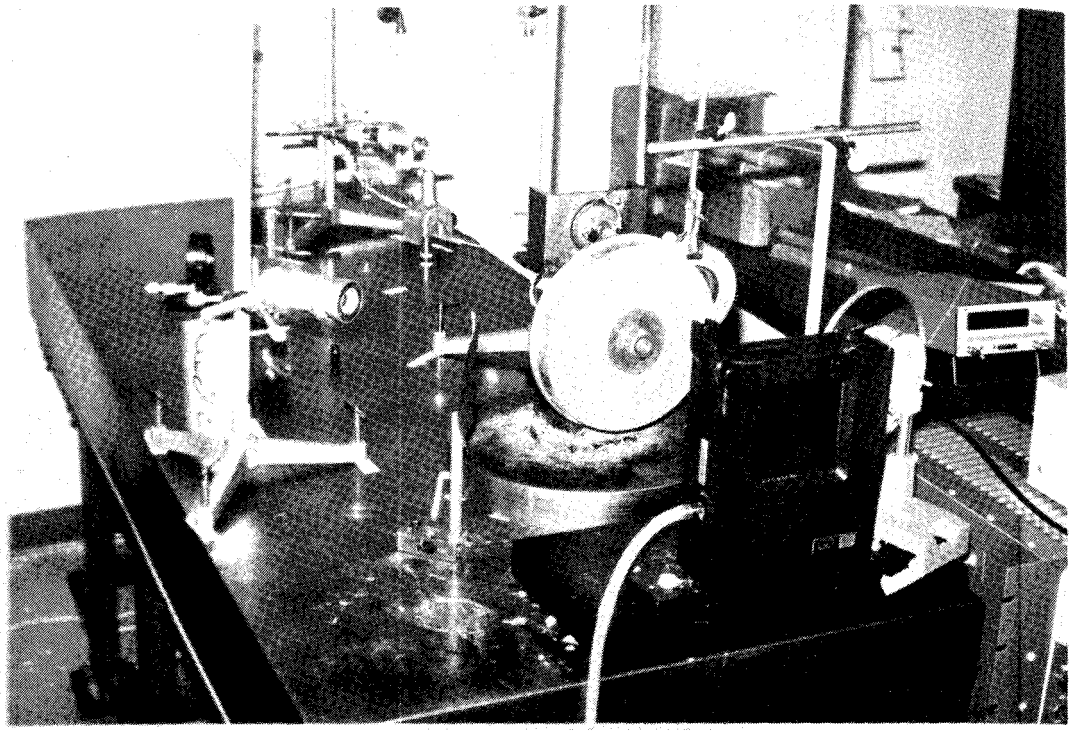

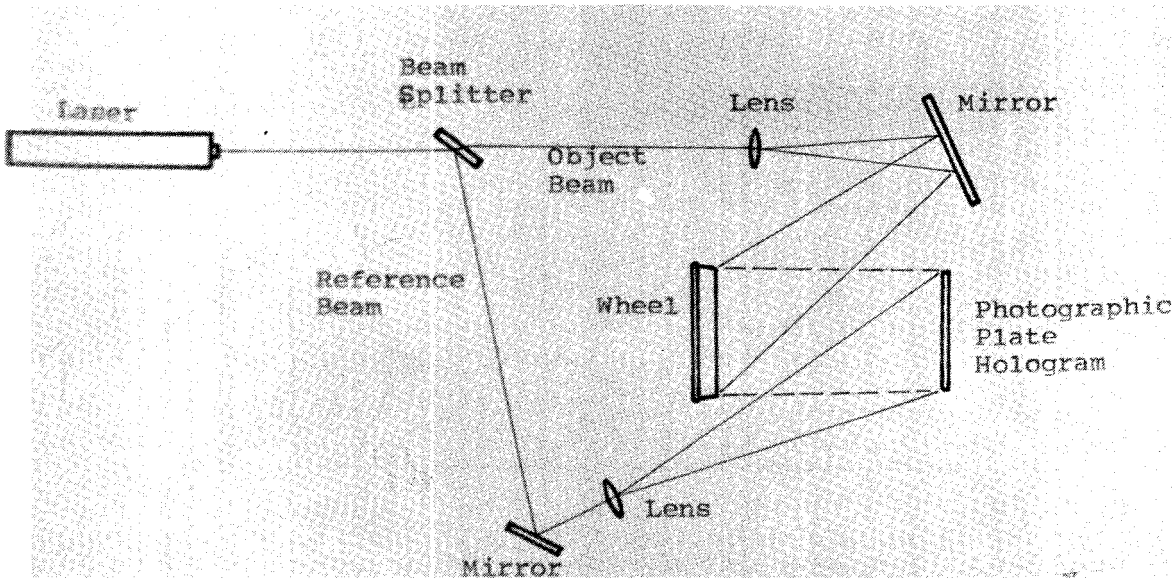

Fig. A.14 View and Schematic of Holography Experiment

Plot of Normalized Amplitude (A/A_{max})
(Measurements Taken at Grid Points
on Surface of Wheel 7A.)

Note: Similar Pattern in Other Three Quadrants of Wheel.

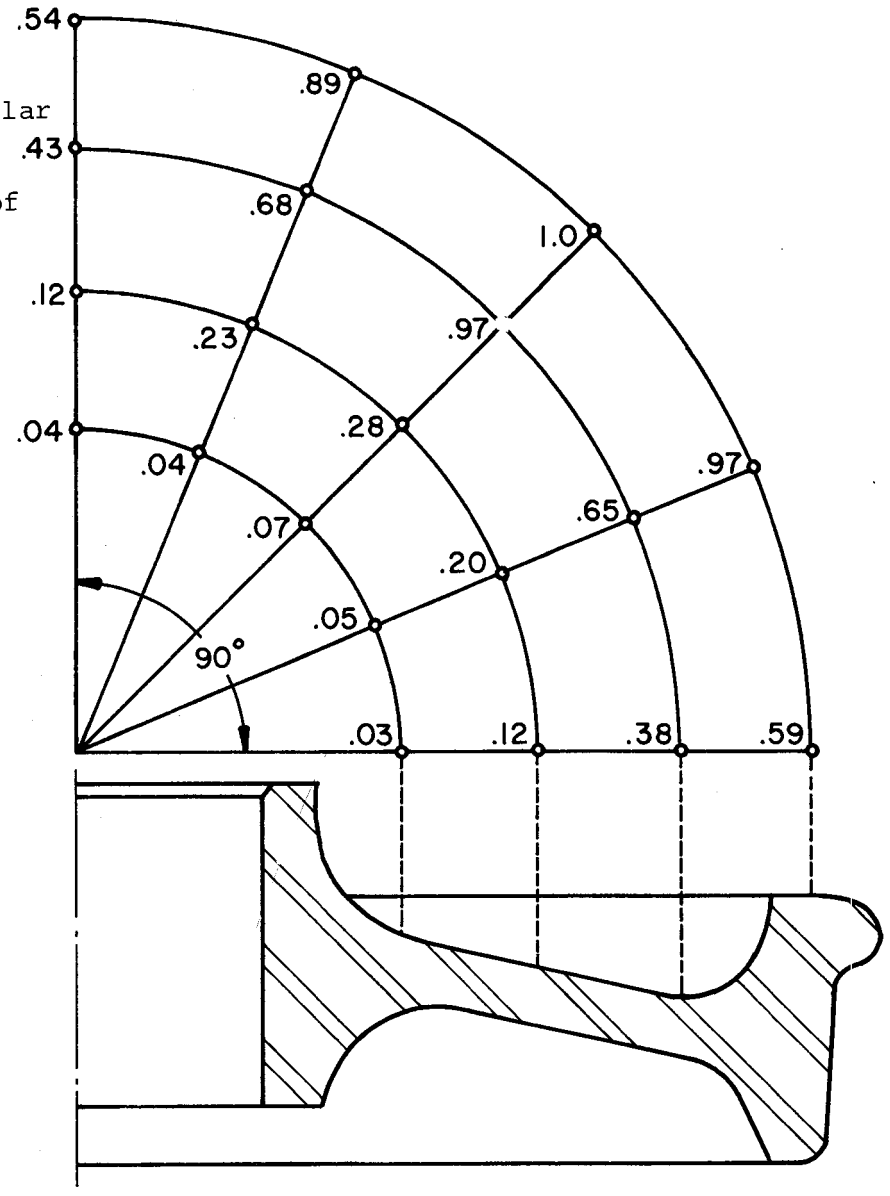

Fig. A.15 Mode Shape for Wheel 7A at 415 Hz
(Sine wave Excitation, Accelerometer Pickup.)

Plot of Normalized Amplitide
(A/A_{max})
(Measurements Taken at Grid
Points on Surface of Wheel 7A)

Note: Similar Pattern
in Other Five Sections
of Wheel.

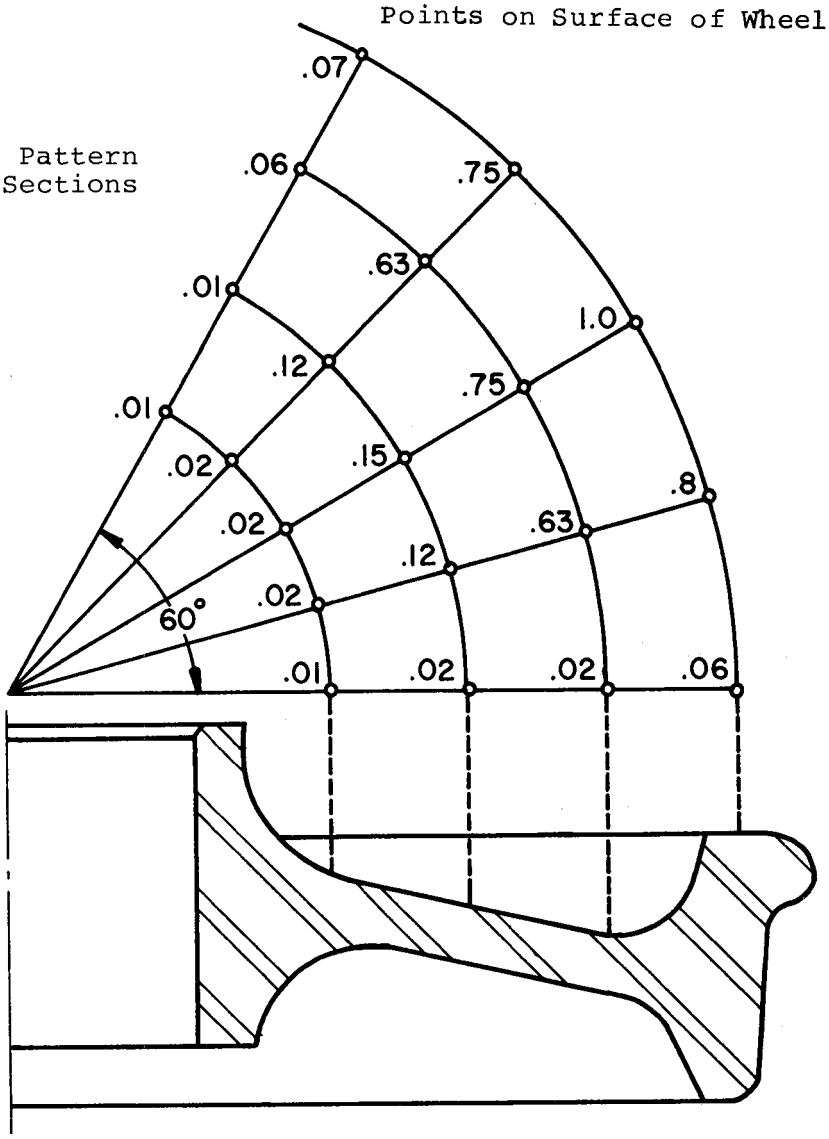

Fig. A.16 Mode Shape for Wheel 7A at 1051 Hz
(Sine Wave Excitation, Accelerometer
Pickup)

Plot of Normalized Amplitide (A/A_{max})
(Measurements Taken at Grid
Points on Surface of Wheel 7A)

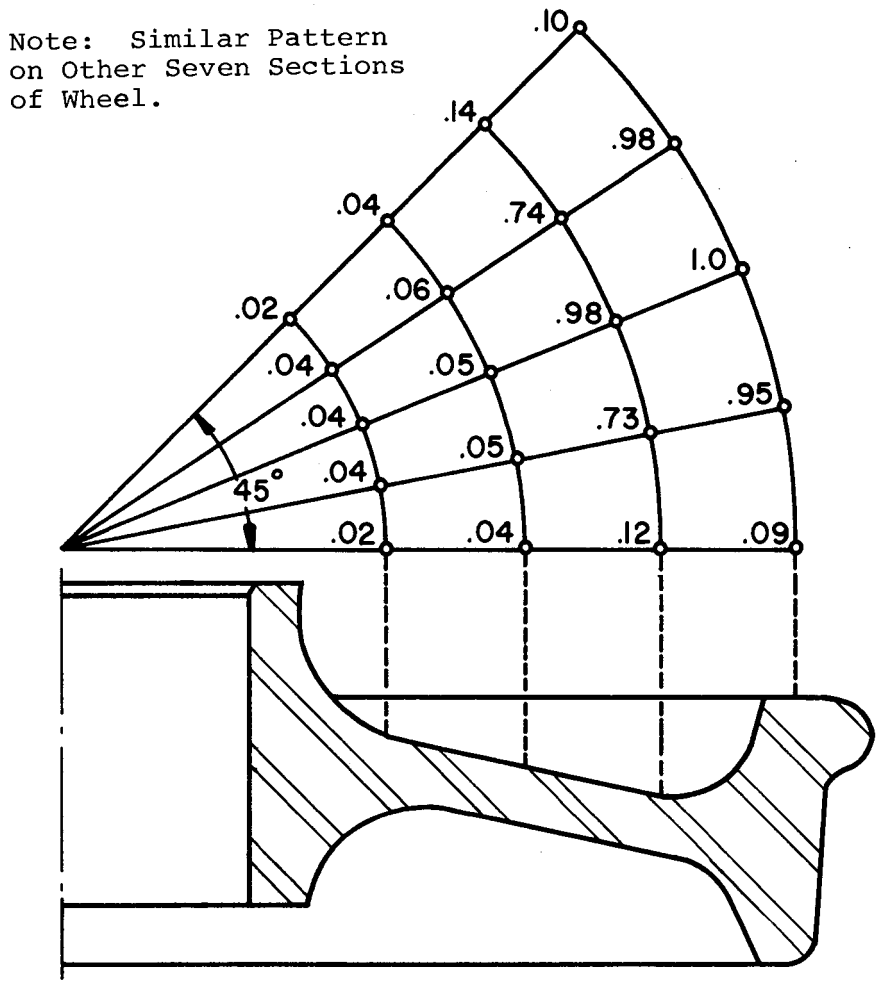

Fig. A.17 Mode Shape for Wheel 7A at 1883 Hz
(Sine Wave Excitation, Accelerometer
Pickup.)

Plot of Normalized Amplitude (A/A_{max})
(Measurements Taken at Points
Along a Radial Line on Survace
of Wheel 7A)

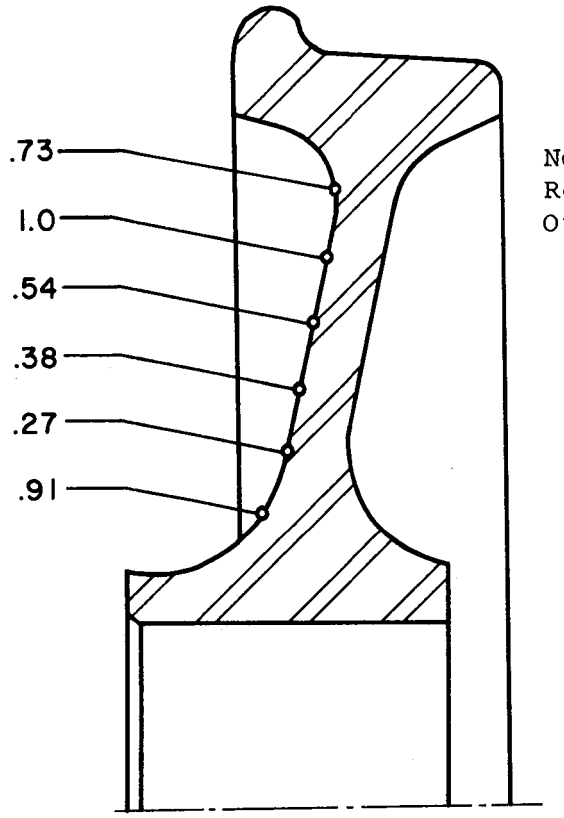

Note: Similar
Readings Taken Along
Other Radial Lines

Fig. A.18 Mode Shape for Wheel 7A at 2417 Hz
(Sine Wave excitation, Accelerometer
Pickup)

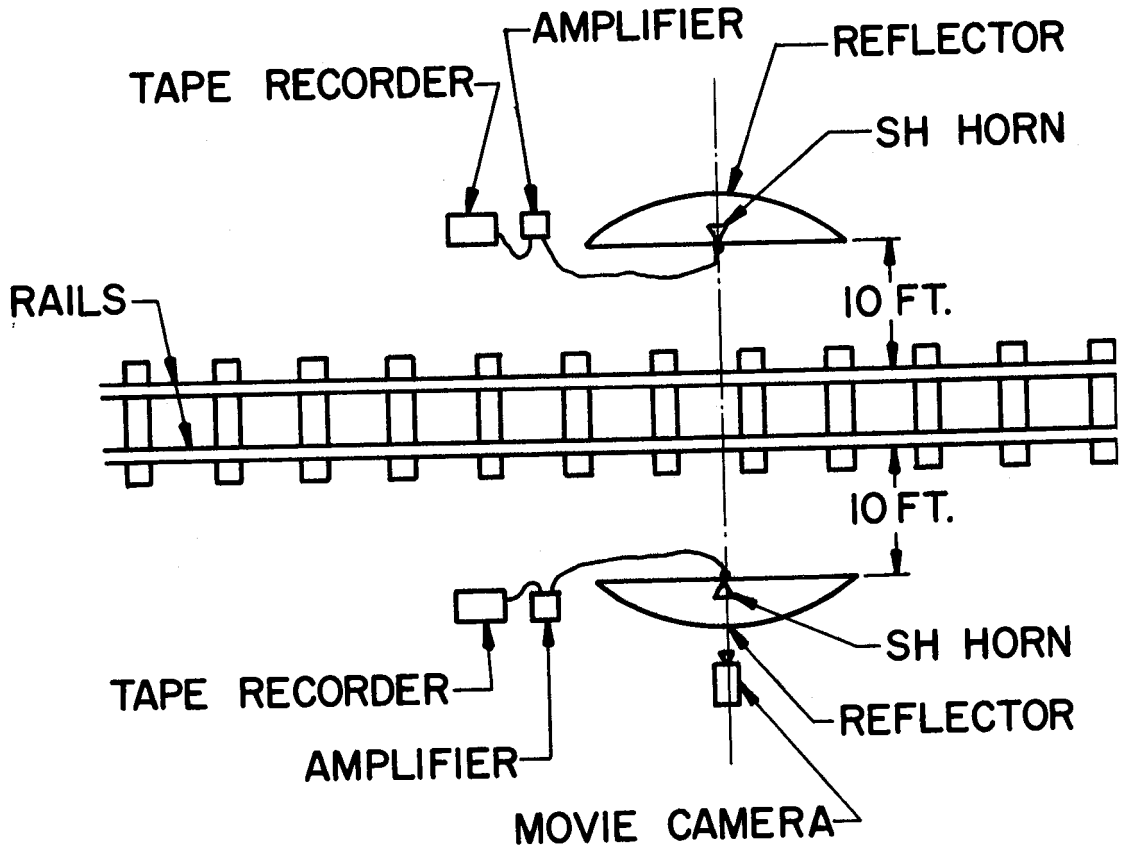

Fig. A.19 Layout Plan for Apparatus Setup in the Field

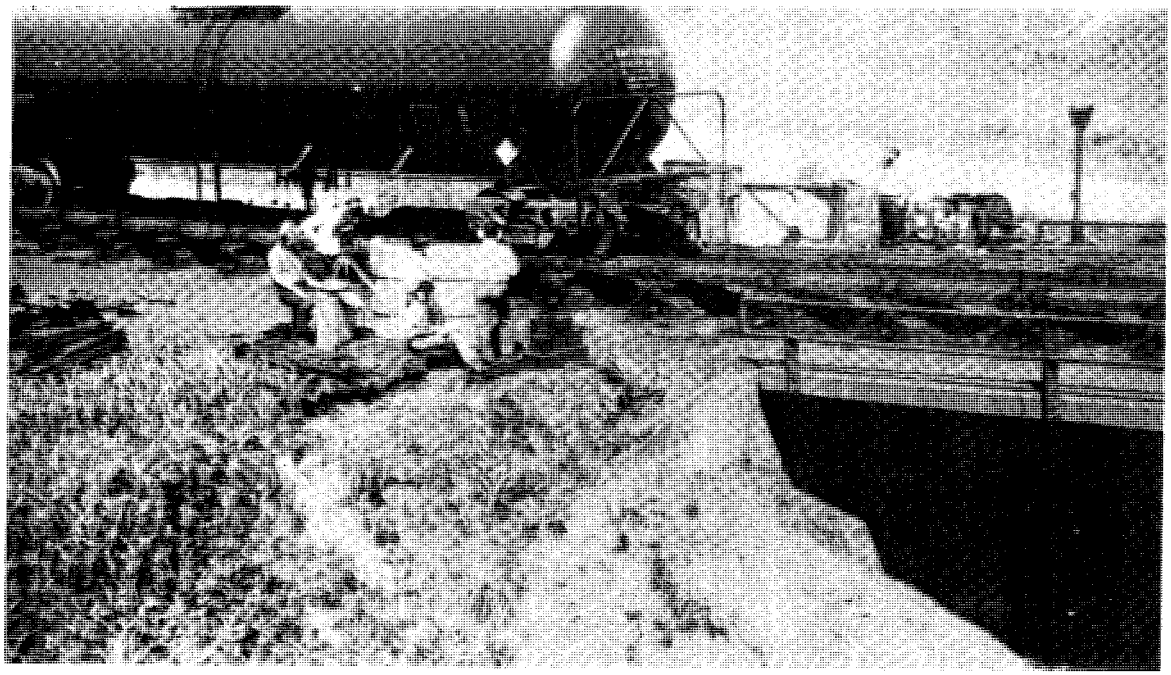

Fig. A.20 View of Apparatus during Field Recording

wheel at a time, and a number of directional receivers were considered, such as a horn or a parabolic reflector in combination with a simple microphone, or a directional microphone. To decide which one of these couplings would be best suited for the purpose, some experimental studies were undertaken, using an anechoic chamber and Bruel and Kjaer polar plotters.

The resulting directional patterns obtained from a University ID60 driver attached to a University SH horn at 2 and 3 KHz, are shown in Figures A.21 and A.22, respectively. Shown in Figures A.23 and A.24 is the additional gain from a parabolic cylindrical reflector approximately 48 in. x 36 in. and with the same horn-driver combination placed on the focal axis, 36 in. distant from the reflector mouth plane. The distance from the mouth plane to the back of the reflector was 3-1/2 in. The reflected sound at 3 kHz has an 8^{o} 3dB beamwidth and side lobes at 110^{o} and 240^{o} which we term "splash" lobes and which are 19dB down from the main beam.

The reciprocity theorem was invoked since it is sometimes more convenient to determine the beam pattern using the coupler connected to a microphone than to a driver. To illustrate the reciprocity theorem, Fig. A.25 shows the beam pattern at 4 kHz with a rectangular cross-section horn attached to a driver, and Fig. A.26 shows the received beam pattern

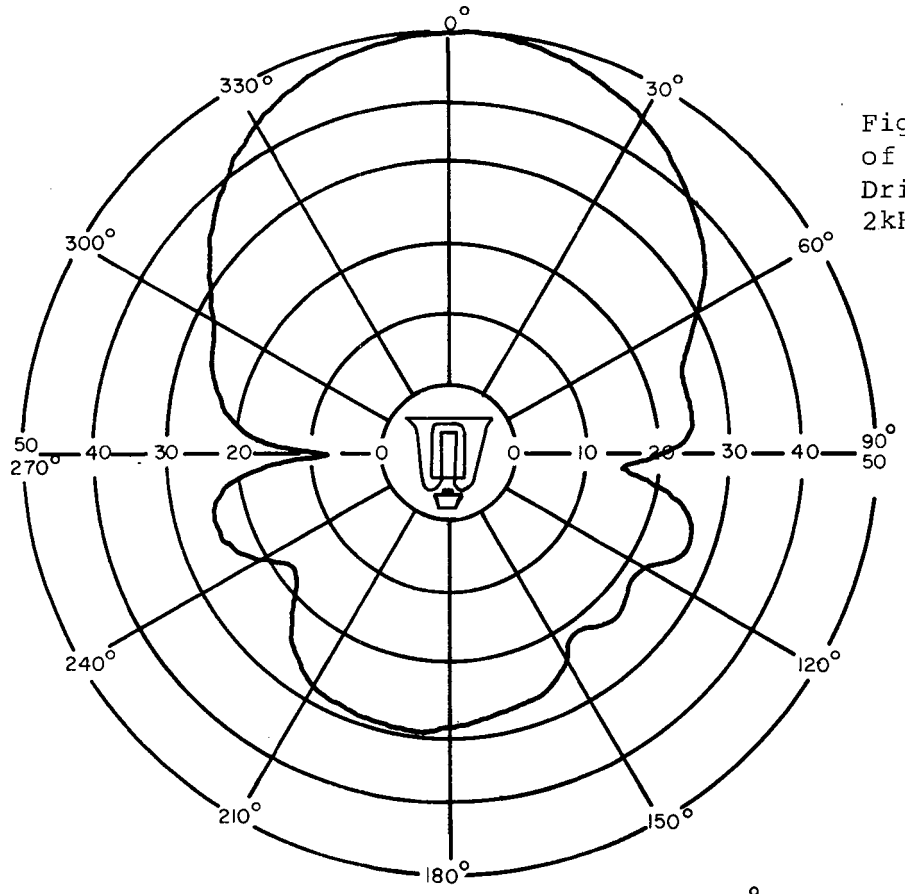

Fig. A.21 Polar Plot of Radiation from ID60 Driver and SH Horn at 2kHz

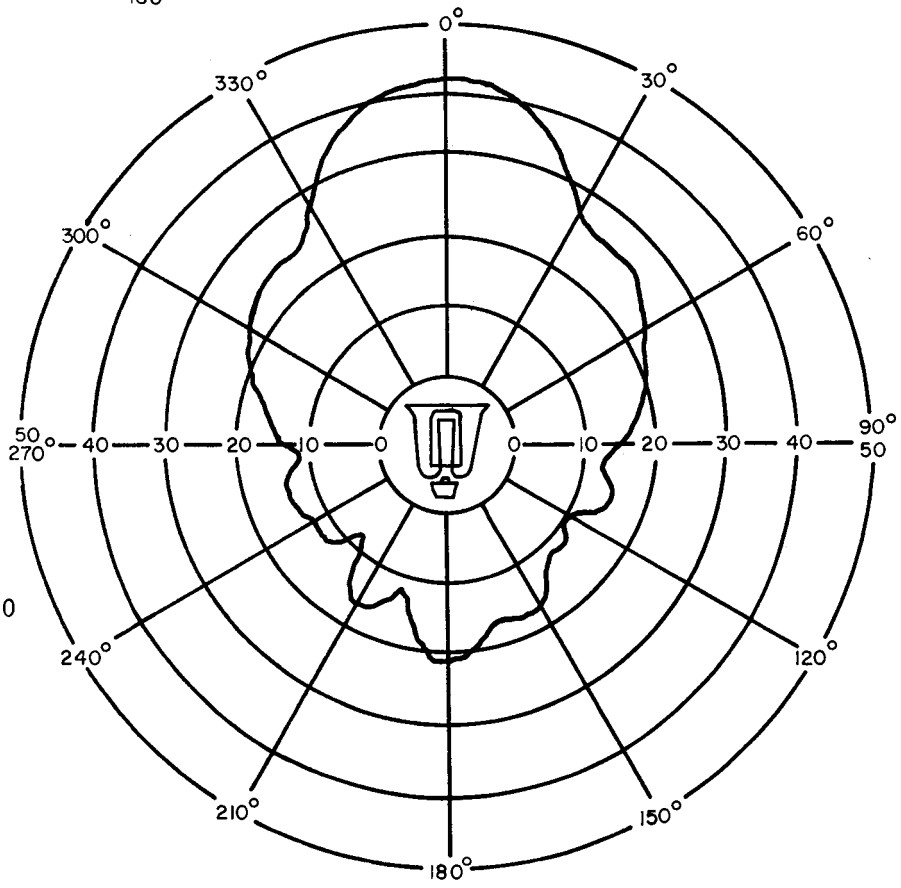

Fig. A.22 Polar Plot of Radiation from ID60 Driver and SH Horn at 3 kHz

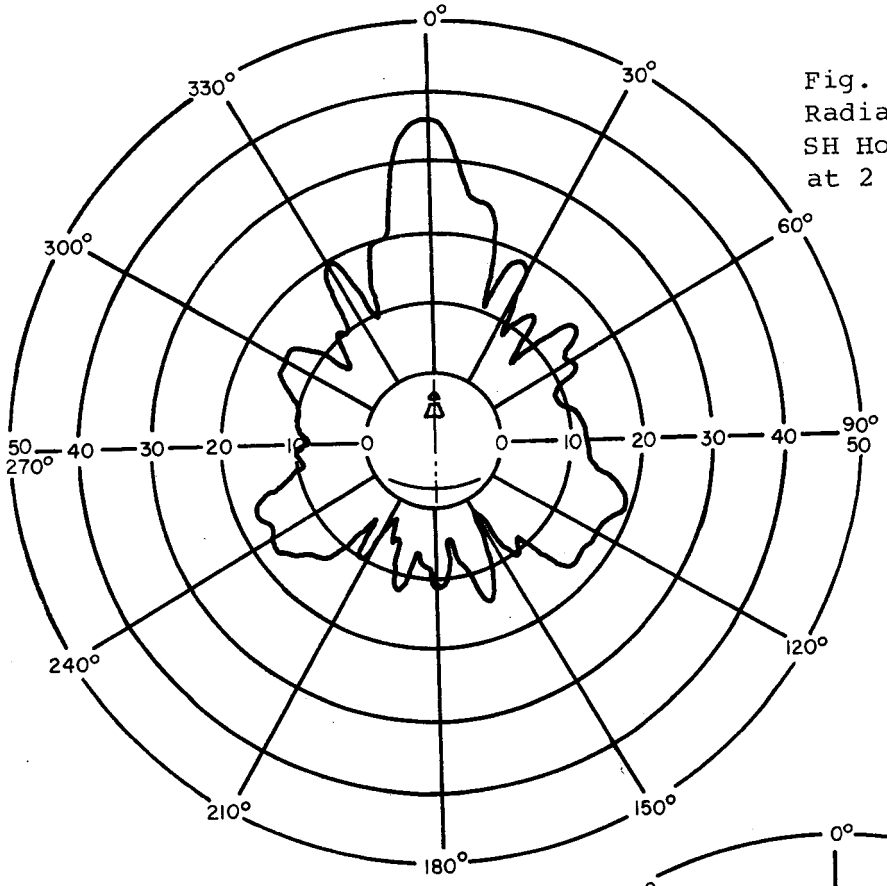

Fig. A.23 Polar Plot of Radiation from ID60 plus SH Horn with Reflector at 2 kHz

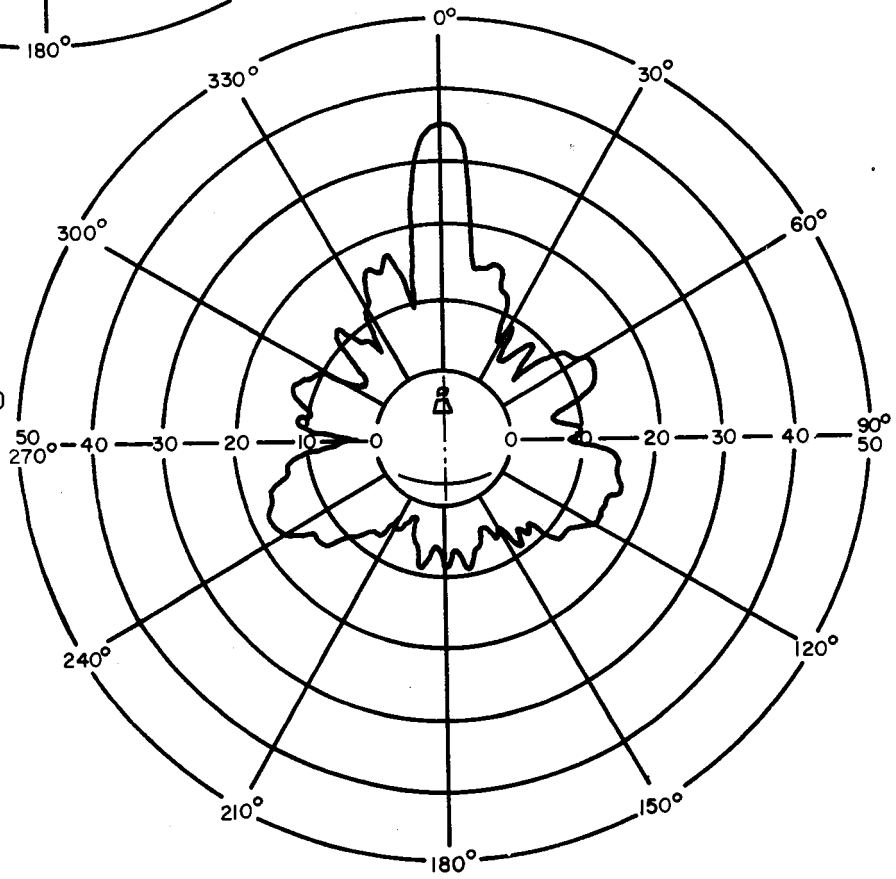

Fig. A.24 Polar Plot of Radiation from ID60 Plus SH Horn with Reflector at 3 kHz

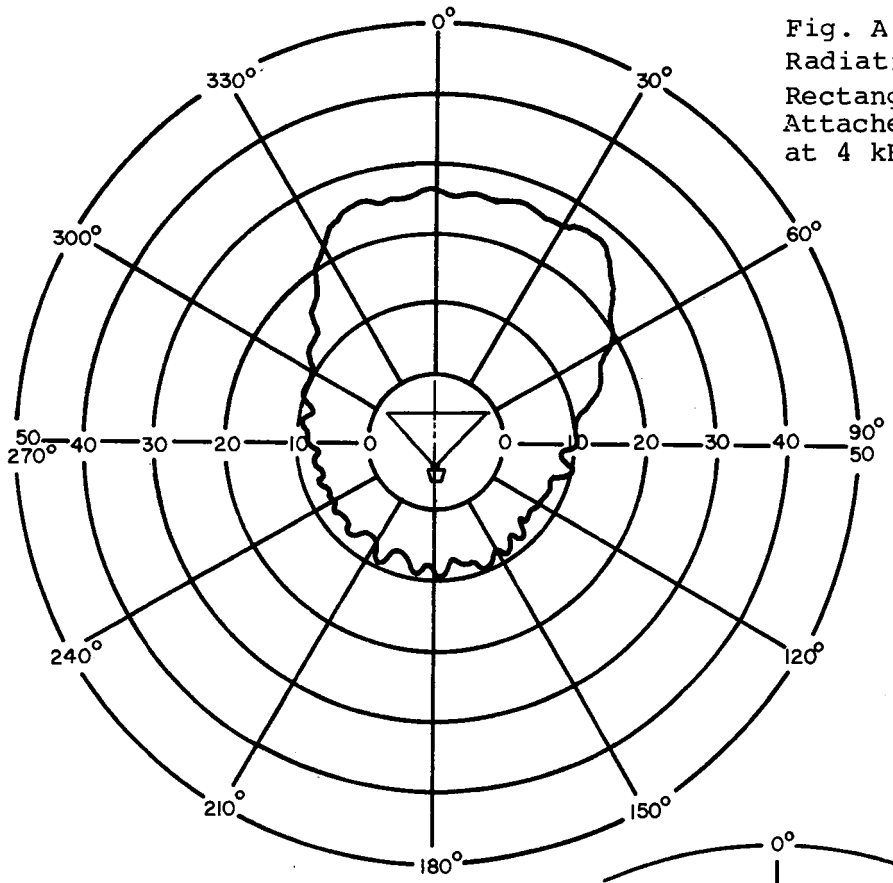

Fig. A.25 Polar Plot of Radiation from 3 ft x 8 in Rectangular Mouth Horn Attached to ID30 Driver at 4 kHz

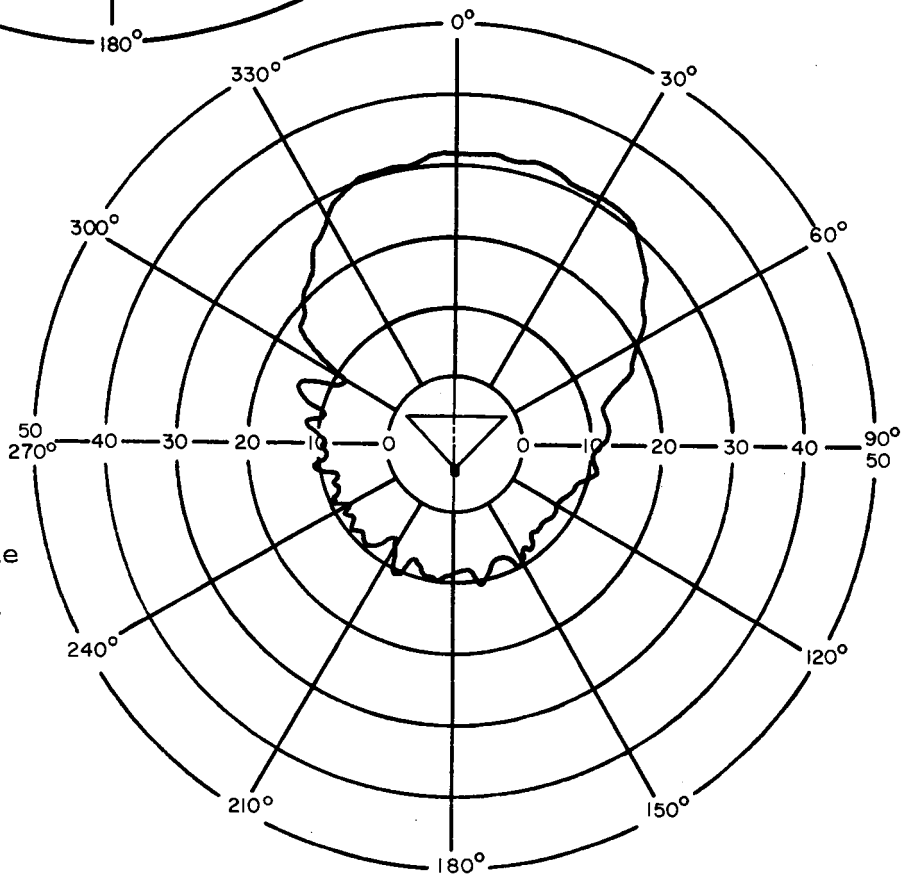

Fig. A.26 Polar Plot of Reception with Same Horn as Used in Fig. A.25 Using B&K Microphone at 4 kHz

at the same frequency with the same horn attached to a microphone. The cross-section of the horn mouth in these experiments was 3 ft. x 8 in. Fig. A.27 shows the beam pattern obtained with a parabolic cylinder having the same mouth cross-section and with a microphone located at the focus, which lies in the plane of the mouth. From these patterns, the following conclusions were drawn: (1) the 3dB beam width from the horn is considerably greater than from the parabolic cylinder; and (2) the "splash" lobes from the cylinder have rotated to approximately 90° and 270°, as compared with those of Figs. A.23 and A.24. It was hypothesized that these "splash" lobes are due to diffraction at the edges of the cylinder. Fig. A.28 shows the beam pattern at 10 kHz for a cylindrical parabola with the focus inside the mouth. The "splash" has moved to the 55° - 305° position. However, the forward beam now shows considerable structure. Some studies were also made of the lateral beamwidth by varying the length of the cylindrical reflector. An Electrovoice directional microphone was rented for the field tests whose 3dB beamwidth is comparable to that of the SH horn, according to manufacturers data. It was concluded that a reflector coupled with a horn or directional microphone at its face should be the best setup. So two parabolic reflectors of face dimensions 7 x 4 ft. were made of fiberglass. Fig. A.29 is the polar plot with one of these

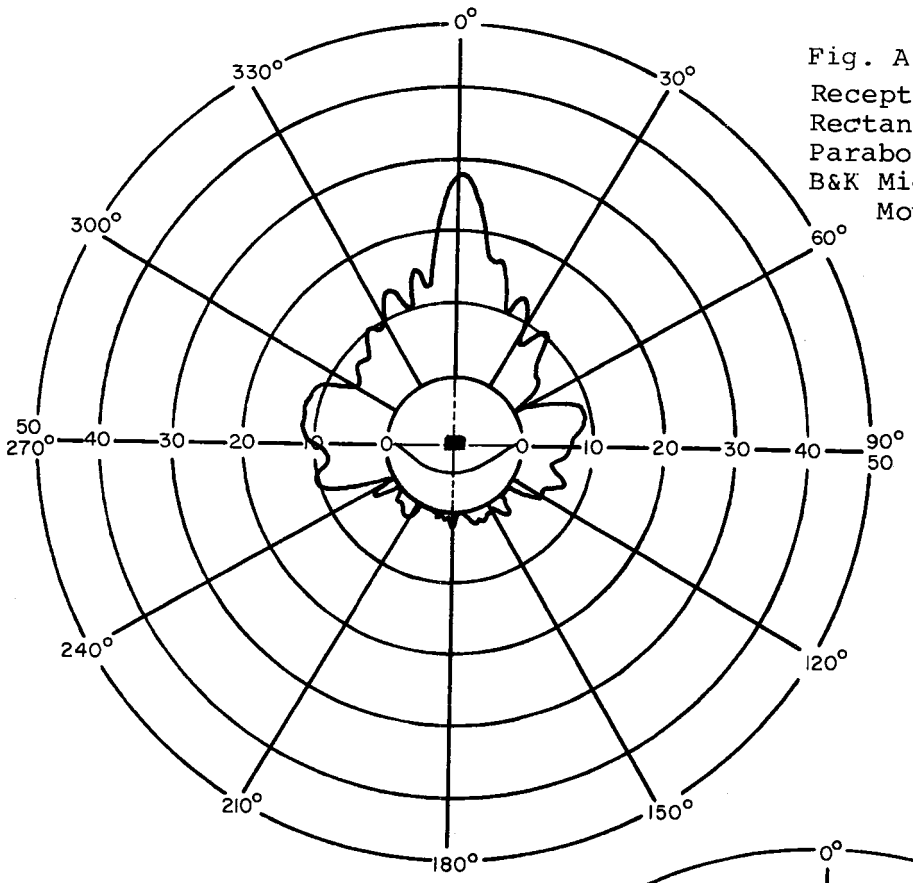

Fig. A.27 Polar Plot of Reception by 3 ft x 8 in Rectangular Mouth Cylindrical Parabolic Reflector at 4 kHz. B&K Microphone at Focus in Mouth Plane

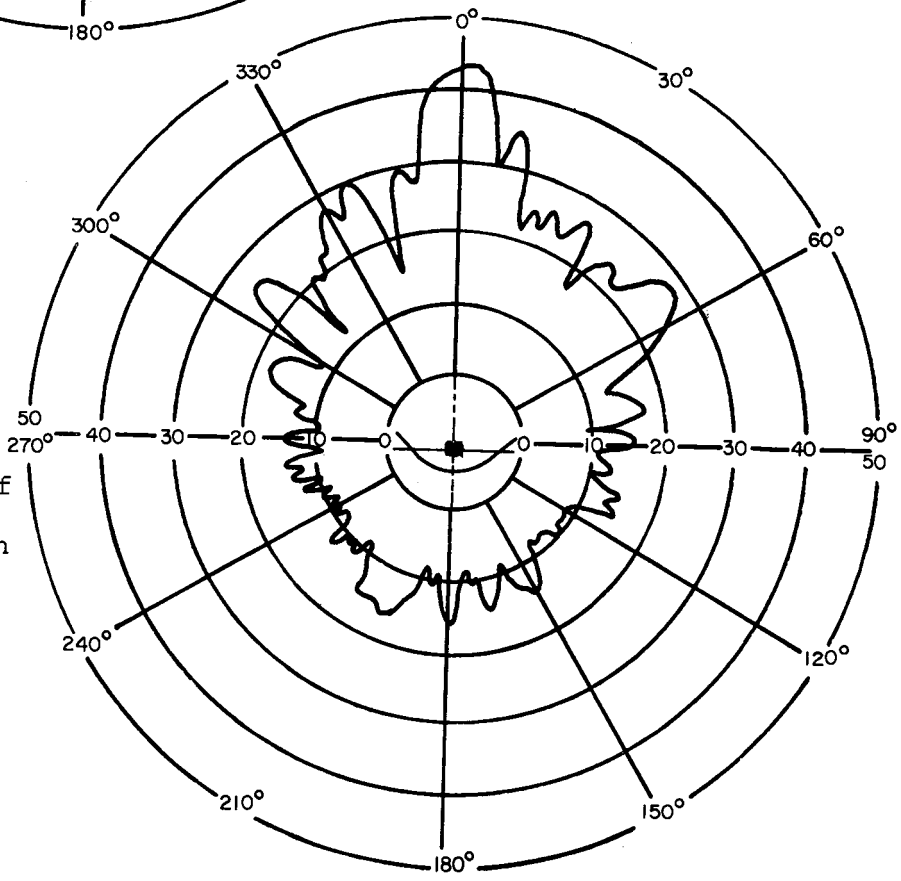

Fig. A.28 Polar Plot of Reception by 2.75 ft x 16 in Rectangular Mouth Cylindrical Parabolic Reflector at 10 kHz. B&K Microphone at Focus inside Mouth Plane

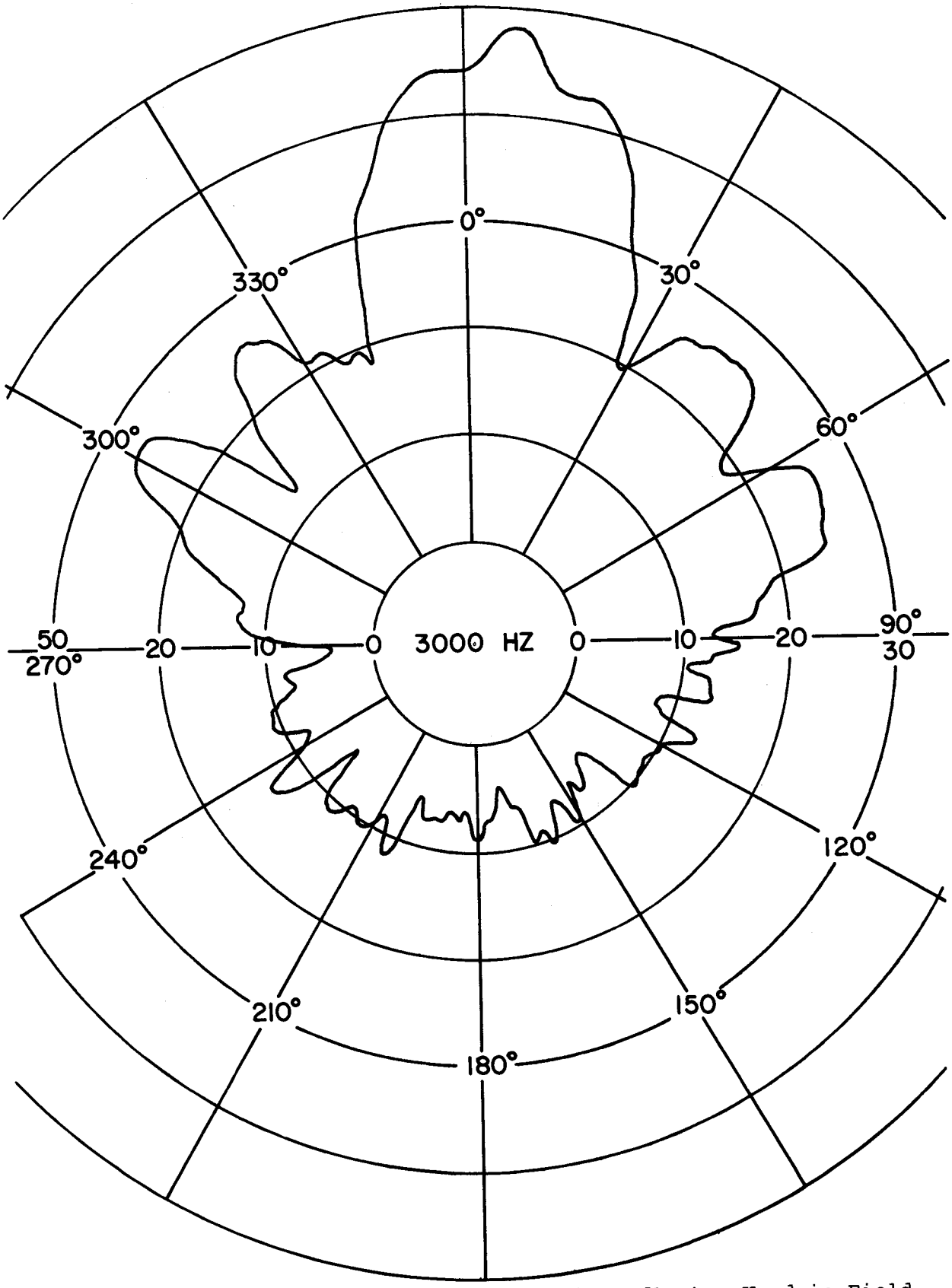

Fig. A.29 Polar Plot of Radiation from Parabolic Reflector Used in Field Tests, at 3000 Hz

reflectors coupled with a University SH horn attached to a University ID 60 driver, and Fig. A.30 is a photograph of the laboratory set-up for the polar plot. This arrangement was used during field recording. Some of the recording in the field was also done with the horn replaced by the Electrovoice Model 642 directional microphone, and Fig. 3.9 is a photograph of this arrangement.

In the field, identical apparatus was set up on both the sides of the track and the reflectors were placed such that they received sound from the two wheels of the same axle of a car simultaneously. The reflectors were placed at a distance of 10 feet from the track to conform with railraod company practice. Figs. A.31 and A.32 are schematic diagrams for these set-ups.

During the recording, a movie camera (Eclair NTR) was used to make a 16 mm movie film showing part of the railway cars and the railway wheels from which the recorded sound was generated. This camera was fixed on a tripod which was placed just behind the reflector and was syncronised with the Nagra IV recorder. To know the approximate speed of the cars, two marker posts were placed 100 ft. apart and the time was recorded for each car to travel that distance. Some recordings were made of the output of an accelerometer attached to the web of the track. The accelerometer used for the purpose was

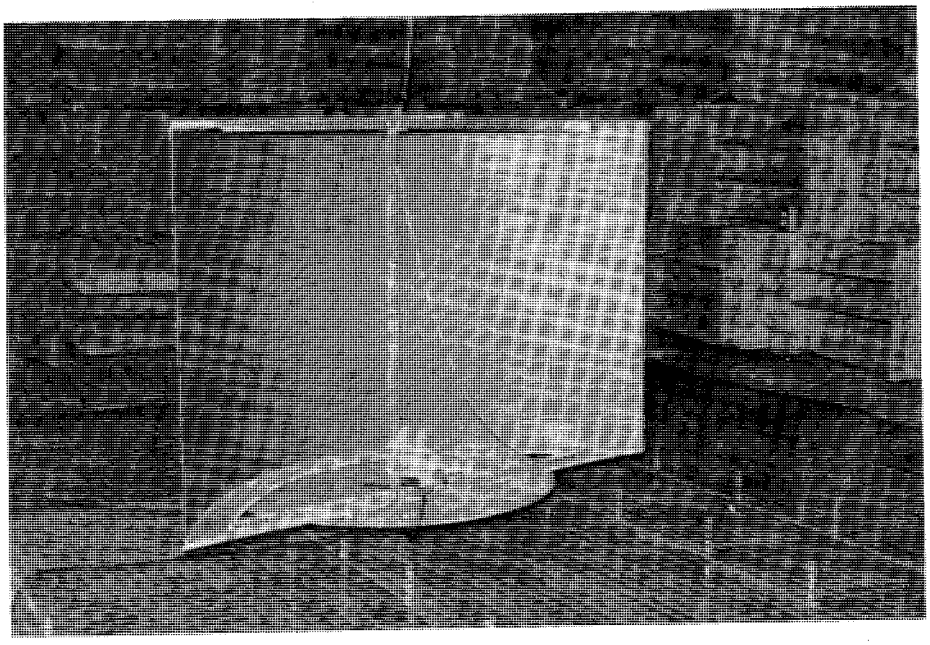

Fig. A.30 View of 7 ft x 4 ft Rectangular Mouth Parabolic Reflector with ID60 Driver and SH Horn, in the Anechoic Chamber

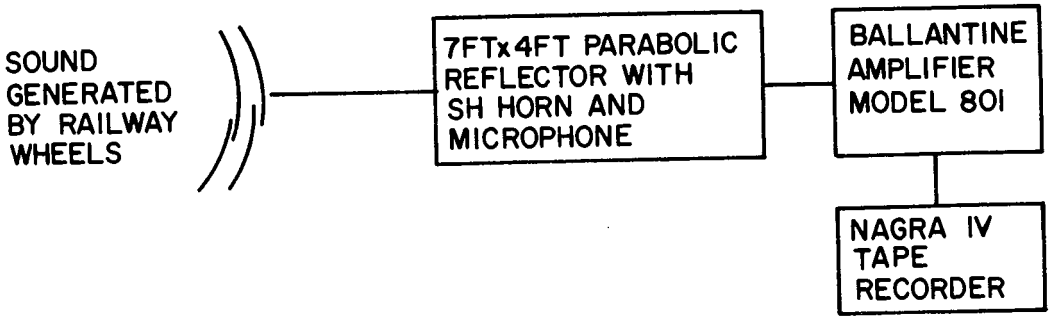

Fig. A.31 Schematic of Field Recording System Using Parabolic Reflector and SH Horn with Microphone

Fig. A.32 Schematic of Field Recording System Using Parabolic Reflector and Directional Microphone

a General Radio, Model 1560-P52, and the recorder was a Sony Type TC800B.

A preliminary field test was made on the Houston Belt and Terminal line, and noise of wheels rolling over a joint was recorded and also sound coming from wheels during braking. For recording, the 7 ft. x 4 ft. fiberglass parabolic reflector attached to the University SH horn was used. A number of extraneous noises, some believed due to electromagnetic pickup were present on these tapes, which were consequently not processed. However, the test served to check out the system.

The principal set of field test results were from the recordings at the main retarder of the Englewood switching yard of the Southern Pacific. After recording the sound for each set of cars released, the recording was stopped and started again when the next set was released. Twenty-eight sets of cars were recorded by a designated "Take Number". Up to "Take Number 11", the recording was done with the reflector coupled with the SH horn, and the remainder of the recording was done with the reflector coupled with the Electro-voice directional microphone. Starting from "Take Number 12" onward, the sound was recorded with an accererometer pickup also for a few takes. One person announced the "Take Numbers" and instructed the others by hand signals as to when to start and stop the tape recorder and movie camera. One person

timed the cars travelling between the marker posts.

These field recordings were used in the laboratory for narrow band analysis. Mainly, the recordings of those takes with retarder screech were analysed trying to capture the highest peak of the sound signature. Plots with a certain number of averages of the spectrum and plots of transient captures at a particular instant were obtained. For the averaged spectra, resultant 16 averages were taken. For both average spectra and transient capture, the highest peak of the sound level was used. The same type of analysis was made for recordings on both sides of the track.

APPENDIX B

LIST OF WHEEL FAILURES FOR 1972

Exhibit F

ANNUAL REPORT OF AAR WHEEL FAILURES JAN. 1, 1972 - DEC. 31, 1972

CAUSE - INTERCHANGE RULE 41 - SEC. F 6

	Wrought Percent of Wheels Shipped 1960 - 1971 Cast Percent of Wheels Shipped 1960 - 1971		Total Failures	Cracked or Broken Flange 66	Cracked or Broken Rim 68	Shattered Rim 71	Thermal Cracks 74	Tread Shelled 75	Burst Hub 82	Cracked or Broken Plate 83	Subsurface Defect 88
28											
1W-CS			1	0	1	0	0	0	0	0	0
1W-WS	2.4		70	0	11	19	0	0	0	39	1
2W&MW-CS			0	0	0	0	0	0	0	0	0
2W&MW-WS	0.1		1	0	0	0	0	0	1	0	0
TOTAL			72	0	12	19	0	0	1	39	1
33											
1W-CS			155	8	31	22	50	1	3	40	0
1W-WS	54.0		220	1	65	94	3	0	0	56	1
2W-MW-CS			23	2	4	5	4	0	0	7	1
2W&MW-WS	13.0		70	1	22	29	5	0	0	12	1
TOTAL			468	12	122	150	62	1	3	115	3
36											
1W-CS			12	0	7	3	1	0	0	1	0
1W-WS	21.0		133	4	35	65	12	0	0	16	1
2W&MW-CS			3	0	1	1	0	0	1	0	0
2W&MW-WS	9.0		21	0	6	12	0	0	0	2	1
TOTAL			169	4	49	81	13	0	1	19	2
38											
1W-CS			0	0	0	0	0	0	0	0	0
1 W-WS	0.6		1	0	0	1	0	0	0	0	0
2W&MW-CS			0	0	0	0	0	0	0	0	0
2W&MW-WS	0.3		0	0	0	0	0	0	0	0	0
TOTAL			1	0	0	1	0	0	0	0	0
GRAND TOTAL	100.0		710	16	183	251	75	1	5	173	6

APPENDIX C

SOFTWARE FOR DATA PROCESSING

C.1 INTRODUCTION

BASIC language compiler software was obtained along with the NOVA 1220 Minicomputer. The BASIC software obtained was a conversational-interpreter language 27, where programs may be input through a teletype, and the computer will generate object code as the program is loaded. After the program is loaded, it can be run immediately. To enable ready interfacing with the real time analyzer it was necessary to write an assembly language subroutine to control the interface device between the two units. The assembly language subroutine then could be called in the BASIC language program as follows:

```
1120      Call 2,A
```

WHERE 1120 is the statement number

2 is the number of the subroutine

A is the variable. Value is read from the device.

When this statement is encountered by the computer during a run, control will be transferred to the assembly language subroutine and a value will be read from the real time analyzer. Two assembly language subroutines were written, one to give a start pulse to the analyzer and another to read the level in one analyzer channel. All thirty-nine analyzer channels then were read with an iterative loop written in BASIC and calling the subroutine repeatedly.

C.2 BASIC LANGUAGE PROGRAM FOR FREQUENCY BAND AND DECAY TIME COMPARISON

```
1  REM        REAL TIME RUNNING AVERAGE PROGRAM
2  REM        IF C=0 INPUT DATA WILL NOT BE PRINTED
3  LET C= 0
6  DIM A[39],L[39],D[39],Q[15]
9  PRINT
65  REM  -------- CONTROL CONSTANTS----------
68  REM      N1 & N2 RANGE OF SPECTRUM AVG.
70  LET N1=18
80  LET N2=27
84  REM      N3 IS NUMBER OF DECAY POINTS READ
85  LET N3=5
86  REM      N4 IS THE VALUE OF DECAY TIME WHERE SPECTRUM IS READ
87  LET N4=2
88  REM      N5 IS THE DECAY TIME CHANNEL #
89  LET N5=24
90  REM      T IS THE TRIGGER LEVEL IN DB.
95  LET T=105
96  REM      T1 IS THE GOOD/BAD LIMIT FOR EACH BAND,SPECTR. DIFF
97  LET T1=5
99  REM      T2 IS THE TRIGGERING CHANNEL #
100  LET T2=27
101  REM      T3 IS THE CHANNEL # FOR THE OVERALL SOUND LEVEL.
102  LET T3=38
103  REM      T4 IS THE GOOD BAD LIMIT FOR TOTAL SUM,SPECTR.DIFF
105  LET T4=20
110  REM      S2 IS A SCALE FACTOR
120  LET S2=100
199  REM  --------SUBR. READ IN IS AT 1000-------------
200  GOSUB  1000
210  REM  --------REMOVING REF. LEVEL------------------
215  LET R5=L[1]
220  FOR I=1 TO 39
225    LET L[I]=L[I]-R5
240  NEXT I
250  REM  --------NORMALIZING TO OVERALL LEVEL---------
252  LET R1=L[T3]
255  FOR I=1 TO 39
260    LET L[I]=L[I]/R1
270  NEXT I
275  IF N<10 GOTO  500
290  REM  --------SUBTRACTING FROM AVG. SPECTRUM-------
295  LET S1= 0
300  FOR I=N1 TO N2
310    LET D[I]=A[I]-L[I]
312    LET S= INT ((D[I]*D[I])*S2)
314    IF S<T1 GOTO  350
315    IF I=18 GOTO  350
316    IF I=23 GOTO  350
317    IF I=24 GOTO  350
340    LET S1=S1+ ABS (S)
350  NEXT I
```

```
354  REM  --------SUBR. DECAY TIME CALC. IS AT 2000----
355  GOSUB  2000
365  PRINT
400  REM  --------GOOD/BAD DECISION--INDICATION PRINTOUT---
410  IF S1<T4 GOTO  430
420  PRINT "BAD WHEEL  SUM=";S1;"DECAY=";G
425  GOTO  600
430  PRINT "GOOD WHEEL  SUM=";S1;"DECAY=";G
498  REM  --------GOOD WHEEL AVERAGE UPDATING----------
500  FOR I=1 TO 39
510    LET A[I]=((A[I]*N)+L[I])/(N+1)
515  NEXT I
516  GOTO  530
519  REM  --------OPTIONAL PRINTOUT OF AVERAGE SPECTR.-
521  FOR I=1 TO 39
522    PRINT A[I]
523  NEXT I
524  PRINT "N=";N
525  STOP
528  REM  --------UPDATE AVG. SPECTR. COUNTER----------
530  LET N=N+1
532  PRINT "N=";N
600  PRINT
601  GOTO  70
999  REM  --------READ LOOP FOR WHEEL UNDER TEST-------
1000  CALL 1,Z
1010  FOR I=1 TO 39
1020    CALL 2,A
1030    IF I=T2 GOTO  1050
1040    GOTO  1060
1050    LET P=A
1060  NEXT I
1062  LET P=P/10
1070  IF P<T GOTO  1000
1075  FOR J=1 TO N3
1100    CALL 1,Z
1110    FOR I=1 TO 39
1120      CALL 2,A
1122      IF J=N4 GOTO  1125
1124      GOTO  1126
1125      LET L[I]=A/10
1126      IF I=N5 GOTO  1128
1127      GOTO  1130
1128      LET Q[J]=A/10
1130    NEXT I
1135  NEXT J
```

```
1140  IF C= 0 GOTO  1200
1142  REM  --------OPTIONAL INPUT SPECTR. PRINTOUT-----
1150  PRINT
1155  PRINT "SPECTRUM READ IN"
1156  PRINT
1160  FOR I=1 TO 39
1165    PRINT L[I];
1170    IF ((I/8)- INT (I/8))> 0 GOTO  1190
1180    PRINT
1190  NEXT I
1200  RETURN
1998  REM  --------DECAY TIME COMPUTATION-------------
2000  FOR I=1 TO N3
2005    LET Q[I]= INT (Q[I]-R)
2020  NEXT I
2030  FOR I=1 TO N3-1
2040    LET Z1=Q[I]-Q[I+1]
2050    IF I=2 GOTO  2052
2051    GOTO  2060
2052    LET G=Z1/.4
2060  NEXT I
2100  RETURN
2198  REM  --------AVERAGE SPECTR. READ IN-------------
2200  FOR I=1 TO 39
2210    INPUT V1
2215    LET A[I]=V1
2220  NEXT I
2230  INPUT N
2240  GOTO  70
```

C.3 ASSEMBLY LANGUAGE PROGRAM FOR INTERFACING WITH REAL TIME ANALYZER

```
        017400                  .LOC 17400
17400   000530  SRTAB:          530
17401   000001                  1
17402   017410                  START
        000004                  .RDX 4
17403   100000                  20000000
        000010                  .RDX 8
17404   000002                  2
17405   017416                  SPECT
        000004                  .RDX 4
17406   140000                  30000000
        000010                  .RDX 8
17407   177777                  -1
17410   054470  START:          STA 3,SAV2
17411   030455                  LDA 2,MASK1
17412   050456                  STA 2,MASK3
17413   004424                  JSR PULSE
17414   034464                  LDA 3,SAV2
17415   001401                  JMP 1,3
17416   054470  SPECT:          STA 3,SV3
17417   004403                  JSR READ
17420   034466                  LDA 3,SV3
17421   001401                  JMP 1,3
17422   054455  READ:           STA 3,SAV1
17423   004432                  JSR GET
17424   030443                  LDA 2,MASK2
17425   050443                  STA 2,MASK3
17426   004411                  JSR PULSE
17427   006456                  JSR @ BCDB
17430   102400                  SUB 0,0
17431   006132                  JSR @ .FLOT
17432   034454                  LDA 3,SV3
17433   031400                  LDA 2,0,3
17434   041000                  STA 0,0,2
17435   045001                  STA 1,1,2
17436   002441                  JMP @SAV1
17437   054442  PULSE:          STA 3,SAV3
17440   030433                  LDA 2,ONE
17441   020427                  LDA 0,MASK3
17442   113400                  AND 0,2
17443   071042                  DOA 2,42
17444   020430                  LDA 0,NUM
17445   040424                  STA 0,CNT
17446   014423                  DSZ CNT
17447   000777                  JMP .-1
17450   030425                  LDA 2,ZERO
17451   020417                  LDA 0,MASK3
17452   113400                  AND 0,2
17453   071042                  DOA 2,42
17454   002425                  JMP @ SAV3
```

```
17455 054421  GET:       STA 3,SAVE
17456 126440             SUBO 1,1
17457 063542             SKPBZ 42
17460 000777             JMP .-1
17461 064442              DIA 1,42
17462 020403             LDA 0, MASK
17463 107400             AND 0,1
17464 002412             JMP @ SAVE
17465 037777  MASK:037777
17466 040000  MASK1:040000
17467 100000  MASK2;100000
17470 000000  MASK3:0
17471 000000  CNT:0
17472 000000  COUNT:0
17473 177777  ONE:177777
17474 000077  NUM:77
17475 000000  ZERO;0
17476 000000  SAVE:0
17477 000000  SAV1:0
17500 000000  SAV2:0
17501 000000  SAV3:0
17502 000000  SAV4:0
17503 000047  CONST:47
17504 000000  CNT1:0
17505 017507  BCDB:.BCDB
      000132  .FLOT=132
      000130  .FIX =130
17506 000000  SV3:0
17507 044443  .BCDB:  STA 1,.EA01
17510 044446  STA 1,.EA11
17511 050442  STA 2,.EA02
17512 054442           STA 3,.EA03
17513 020445  LDA 0,.EA20
17514 040443           STA 0,.EA12
17515 152400           SUB 2,2
17516 004411  .EA98:   JSR .EA50
17517 000405           JMP .EA99
17520 004424           JSR .EA51
17521 010436  ISZ .EA12
17522 000774           JMP .EA98
17523 145021  MOVZ 2,1,SKP
17524 024426  .EA99:   LDA 1,.EA01
17525 030426           LDA 2,.EA02
17526 002426  JMP @.EA03
17527 024431  .EA50:   LDA 1,.EA20
17530 044425           STA 1,.EA10
17531 024425  LDA 1,.EA11
17532 102400           SUB 0,0
17533 125120  MOVZL 1,1
17534 101100           MOVL 0,0
17535 010420           ISZ .EA10
17536 000775           JMP .-3
```

```
17537 044417  STA 1,.EA11      ;
17540 024421  LDA 1,.EA21
17541 106042          ADC0 0,1,SZC
17542 001400          JMP 0,3
17543 001401          JMP 1,3
17544 145120  .EA51:   MOVZL 2,1
17545 125120          MOVZL 1,1
17546 147000  ADD 2,1
17547 131120  MOVZL 1,2
17550 113000  ADD 0,2
17551 001400          JMP 0,3

17552 000000  .EA01:   0
17553 000000  .EA02:   0
17554 000000  .EA03;   0
17555 000000  .EA10:   0
17556 000000  .EA11:   0
17557 000000  .EA12:   0
17560 177774  .EA20:   -4
17561 000012  .EA21:12
      000010              .LOC 10
00010 017400  LOC10:     SRTAB
                         .END
```

```
---
BCDB    017505
CNT     017471
CNT1    017504
CONST   017503
COUNT   017472
GET     017455
LOC10   000010
MASK    017465
MASK1   017466
MASK2   017467
MASK3   017470
NUM     017474
ONE     017473
PULSE   017437
READ    017422
SAV1    017477
SAV2    017500
SAV3    017501
SAV4    017502
SAVE    017476
SPECT   017416
SRTAB   017400
START   017410
SV3     017506
ZERO    017475
.BCDB   017507
.EA01   017552
.EA02   017553
.EA03   017554
.EA10   017555
.EA11   017556
.EA12   017557
.EA20   017560
.EA21   017561
.EA50   017527
.EA51   017544
.EA98   017516
.EA99   017524
.FIX    000130
.FLOT   000132
```

APPENDIX D

ANSYS PROGRAM RESULTS LISTING

D.1 INTRODUCTION

The computer printout for complete set of eigenvalues and the eignevectors for the first 15 modes are included for the 35" good wheel and for the 33" wheel with the plate flaw. UX is the radial displacement and UZ is the displacement along the axis of the wheel.

D.2 RESULTS OF ANSYS RUN FOR 33" GOOD WHEEL

ANSYS - ENGINEERING ANALYSIS SYSTE
SWANSON ANALYSIS SYSTEMS, INC. ELIZABETH, PE

RAIL WHEEL MODES-SOLID ELEMENT

COMPLETE SET OF EIGENVALUES

MODE	FREQUENCY (HERTZ)
1	.31718+003
2	.31719+003
3	.44316+003
4	.44315+003
5	.45501+003
6	.10872+004
7	.10873+004
8	.18972+004
9	.18973+004
10	.19128+004
11	.19998+004
12	.19998+004
13	.23603+004
14	.23603+004
15	.23862+004
16	.23862+004
17	.29456+004
18	.29457+004
19	.30196+004
20	.30197+004
21	.30867+004
22	.30867+004
23	.36406+004
24	.36406+004
25	.37129+004
26	.38856+004
27	.38856+004
28	.39734+004
29	.44598+004
30	.44598+004
31	.47895+004
32	.47895+004
33	.51585+004
34	.52372+004
35	.52372+004
36	.56841+004
37	.59588+004

38	.5468E+004
39	.5998E+004
40	.6116E+004
41	.6116E+004
42	.6432E+004
43	.6432E+004
44	.6869E+004
45	.6869E+004
46	.7335E+004
47	.7335E+004
48	.7608E+004
49	.1014E+005
50	.1014E+005
51	.1020E+005
52	.1020E+005
53	.1022E+005
54	.1022E+005
55	.1026E+005
56	.1038E+005
57	.1038E+005
58	.1045E+005
59	.1045E+005
60	.1075E+005
61	.1181E+005
62	.1181E+005
63	.1190E+005
64	.1190E+005
65	.1208E+005
66	.1208E+005
67	.1224E+005
68	.1224E+005
69	.1249E+005
70	.1294E+005
71	.1294E+005
72	.1309E+005
73	.1309E+005
74	.1346E+005
75	.1361E+005
76	.1361E+005
77	.1402E+005
78	.1402E+005
79	.1439E+005
80	.1439E+005
81	.1460E+005
82	.1473E+005
83	.1473E+005
84	.1492E+005
85	.1502E+005
86	.1502E+005

87	.15065+005
88	.15065+005
89	.15145+005
90	.15164+005
91	.15154+005
92	.15510+005
93	.15510+005
94	.15936+005
95	.15936+005
96	.16195+005

ANSYS - ENGINEERING ANALYSIS SYSTE
SWANSON ANALYSIS SYSTEMS, INC. ELIZABETH, PE

RAIL WHEEL MODES-SOLID ELEMENT

COMPLETE SET OF REDUCED EIGENVECTORS

EIGENVECTOR NUMBER 1 FREQUENCY = .317185+03 HERTZ

NODE	UX	UY	UZ
12	.934504-001		-.151588+000
16	.195527+000		-.599603+000
21	.437633-001		-.107791+001
24	.433623+000		-.918598+000
60	.125334+000		-.203307+000
64	.262236+000		-.804177+000
69	.586944-001		-.144568+001
72	.581566+000		-.123200+001
108	.123635+000		-.200552+000
112	.258635+000		-.793280+000
117	.578959-001		-.142610+001
120	.573697+000		-.121531+001
156	.888069-001		-.144056+000
160	.185814+000		-.569814+000
165	.415855-001		-.102438+001
168	.412094+000		-.872970+000
204	.301808-001		-.489571-001
208	.631480-001		-.193548+000
213	.141382-001		-.348129+000
216	.140046+000		-.296573+000
252	-.365330-001		.592616-001
256	-.764406-001		.234411+000
261	-.171055-001		.421419+000
264	-.169532+000		.359127+000
300	-.934567-001		.151599+000
304	-.195543+000		.599650+000
309	-.437628-001		.107801+001
312	-.433655+000		.918678+000
348	-.125337+000		.203313+000
352	-.262246+000		.804202+000
357	-.586945-001		.144573+001
360	-.581591+000		.123204+001
396	-.123633+000		.200549+000
400	-.258681+000		.793269+000
405	-.578977-001		.142607+001

408	-.573[illegible]+000		.121[illegible]+001
444	-.8[illegible]-001		.14+051+000
448	-.145[illegible]+000		.5[illegible]+001
453	-.415866-001		.102432+001
456	-.412[illegible]+000		.872927+000
492	-.301804-001		.4[illegible]-001
496	-.631[illegible]-001		.193647+000
501	-.141334-001		.348122+000
504	-.140041+000		.295[illegible]+000
540	.365[illegible]-001		-.592543-001
544	.764[illegible]-001		-.234378+000
549	.171[illegible]-001		-.421346+000
552	.169[illegible]+000		-.359070+000

EIGENVECTOR NUMBER 2 FREQUENCY = .317198+03 HERTZ

NODE	UX	UY	UZ
12	-.987939-001		.144033+000
16	-.185780+000		.569714+000
21	-.415981-001		.102416+001
24	-.411[illegible]+000		.872796+000
60	-.301639-001		.469271-001
64	-.631045-001		.193520+000
69	-.141363-001		.347247+000
72	-.139911+000		.296451+000
108	.365373-001		-.592696-001
112	.764508-001		-.234443+000
117	.171057-001		-.421463+000
120	.169561+000		-.359179+000
156	.934445-001		-.151579+000
160	.195510+000		-.599559+000
165	.437654-001		-.107780+001
168	.433563+000		-.918514+000
204	.125321+000		-.203286+000
208	.262203+000		-.804081+000
213	.586974-001		-.144546+001
216	.581456+000		-.123163+001
252	.123630+000		-.200543+000
256	.258670+000		-.793241+000
261	.578478-001		-.142601+001
264	.573650+000		-.121524+001
300	.888164-001		-.144073+000
304	.185438+000		-.569885+000
309	.415847-001		-.102453+001
312	.412164+000		-.873091+000
348	.301974-001		-.489361-001
352	.631[illegible]-001		-.193774+000
357	.141307-001		-.348403+000
360	.140177+000		-.295[illegible]+000

396	-.365241-001	.592459-001
400	-.764178-001	.234343+000
405	-.171073-001	.421270+000
408	-.169452+000	.359010+000
444	-.934528-001	.151609+000
448	-.185559+000	.599596+000
453	-.437616-001	.107812+001
456	-.433724+000	.916761+000
492	-.125350+000	.203336+000
496	-.252281+000	.804303+000
501	-.586906-001	.144596+001
504	-.581708+000	.123222+001
540	-.123638+000	.200558+000
544	-.258695+000	.793308+000
549	-.578955-001	.142617+001
552	-.573731+000	.121536+001

EIGENVECTOR NUMBER 3 FREQUENCY = .443064+03 HERTZ

NODE	UX	UY	UZ
12	-.698746-001		.122314+000
16	-.184346+000		.535390+000
21	.154956-001		.119529+001
24	-.582937+000		.937629+000
60	.139497-001		-.244221-001
64	.367978-001		-.106888+000
69	-.309138-002		-.238601+000
72	.116346+000		-.187177+000
108	.838300-001		-.146749+000
112	.221155+000		-.642326+000
117	-.155563-001		-.143397+001
120	.699307+000		-.112487+001
156	.698864-001		-.122340+000
160	.184369+000		-.535428+000
165	-.154944-001		-.119545+001
168	.582934+000		-.937772+000
204	-.139366-001		.243935-001
208	-.367719-001		.106781+000
213	.309241-002		.238424+000
216	-.116292+000		.187020+000
252	-.838151-001		.146717+000
256	-.221125+000		.642208+000
261	.185883-001		.143377+001
264	-.699244+000		.112470+001
300	-.698596-001		.122306+000
304	-.184336+000		.535360+000
309	.154961-001		.119524+001
312	-.582918+000		.937585+000
348	.139552-001		-.244302-001

352	.369084-001		-.106921+000
357	-.306750-002		-.235636+000
360	.116354+000		-.187225+000
396	.838356-001		-.146757+000
400	.221157+000		-.642360+000
405	-.185531-001		-.143403+001
408	.699334+000		-.112492+001
444	.698906-001		-.122347+000
448	.184376+000		-.535514+000
453	-.154926-001		-.119550+001
456	.583008+000		-.937814+000
492	-.139356-001		.243929-001
496	-.367706-001		.106779+000
501	.309366-002		.238421+000
504	-.116291+000		.187017+000
540	-.838186-001		.146722+000
544	-.221132+000		.642228+000
549	.185581-001		.143381+001
552	-.699261+000		.112473+001

EIGENVECTOR NUMBER 4 FREQUENCY = .443151+03 HERTZ

NODE	UX	UY	UZ
12	.564343-001		-.987797-001
16	.148894+000		-.432392+000
21	-.125153-001		-.965403+000
24	.470855+000		-.757278+000
60	.887190-001		-.155295+000
64	.234072+000		-.579775+000
69	-.196796-001		-.151771+001
72	.740214+000		-.119052+001
108	.322604-001		-.564652-001
112	.851306-001		-.247191+000
117	-.716854-002		-.551996+000
120	.259253+000		-.432969+000
156	-.564915-001		.986957-001
160	-.149007+000		.432828+000
165	.125019-001		.966121+000
168	-.471082+000		.757915+000
204	-.887927-001		.155438+000
208	-.234219+000		.680317+000
213	.196597-001		.151862+001
216	-.740521+000		.119132+001
252	-.323469-001		.566291-001
256	-.853055-001		.247819+000
261	.714401-002		.553069+000
264	-.269636+000		.433904+000
300	.564000-001		-.987239-001
304	.148822+000		-.432170+000

309	-.125301-001		-.964999+000
312	.470696+000		-.756936+000
348	.887056-001		-.155274+000
352	.234044+000		-.679548+000
357	-.196864-001		-.151755+001
360	.740154+000		-.119039+001
396	.322707-001		-.564821-001
400	.851530-001		-.247259+000
405	-.716503-002		-.552124+000
408	.269313+000		-.433076+000
444	-.564611-001		.988461-001
448	-.148944+000		.432633+000
453	.125169-001		.965777+000
456	-.470945+000		.757620+000
492	-.887500-001		.155369+000
496	-.234132+000		.680045+000
501	.196813-001		.151814+001
504	-.740334+000		.119091+001
540	-.323021-001		.565562-001
544	-.852118-001		.247531+000
549	.716496-002		.552552+000
552	-.269429+000		.433465+000

EIGENVECTOR NUMBER · 5 FREQUENCY = .455015+03 HERTZ

NODE	UX	UY	UZ
12	-.826185-001		.166396+000
16	-.164224+000		.629907+000
21	-.173742-001		.105342+001
24	-.341933+000		.929023+000
60	-.826221-001		.166402+000
64	-.164233+000		.629934+000
69	-.173735-001		.105348+001
72	-.341963+000		.929070+000
108	-.825945-001		.166354+000
112	-.164160+000		.629723+000
117	-.173791-001		.105302+001
120	-.341736+000		.928702+000
156	-.825626-001		.166299+000
160	-.164077+000		.629480+000
165	-.173854-001		.105247+001
168	-.341472+000		.928277+000
204	-.825581-001		.166291+000
208	-.164066+000		.629447+000
213	-.173857-001		.105240+001
216	-.341439+000		.928222+000
252	-.825645-001		.166337+000
256	-.164137+000		.629654+000
261	-.173779-001		.105287+001

264	-.341676+000	.925546+000
300	-.825146-001	.166390+000
304	-.164216+000	.629685+000
309	-.173709-001	.105339+001
312	-.341922+000	.926992+000
348	-.826183-001	.166396+000
352	-.164225+000	.629909+000
357	-.173720-001	.105344+001
360	-.341945+000	.929032+000
396	-.825920-001	.166350+000
400	-.164155+000	.629707+000
405	-.173786-001	.105298+001
408	-.341722+000	.928676+000
444	-.825632-001	.166299+000
448	-.164079+000	.629485+000
453	-.173849-001	.105249+001
456	-.341480+000	.928288+000
492	-.825514-001	.166296+000
496	-.164073+000	.629469+000
501	-.173854-001	.105245+001
504	-.341460+000	.928258+000
540	-.825686-001	.166344+000
544	-.164144+000	.629677+000
549	-.173812-001	.105291+001
552	-.341683+000	.928619+000

EIGENVECTOR NUMBER 5 FREQUENCY = .108730+04 HERTZ

NODE	UX	UY	UZ
12	-.435582-001		.936266-001
16	-.160170+000		.464349+000
21	.105279+000		.134894+001
24	-.767739+000		.957895+000
60	-.233825-001		.610066-001
64	-.104366+000		.302567+000
69	.685989-001		.878964+000
72	-.500265+000		.624157+000
108	.435565-001		-.936244-001
112	.160168+000		-.464343+000
117	-.105282+000		-.134894+001
120	.767738+000		-.957890+000
156	.233804-001		-.610041-001
160	.104363+000		-.302560+000
165	-.686021-001		-.878958+000
168	.500284+000		-.624150+000
204	-.435591-001		.936279-001
208	-.160171+000		.464354+000
213	.105279+000		.134895+001
216	-.767791+000		.957901+000

252	-.283827-001		.610077-001
256	-.104366+000		.302571+000
261	.685994-001		.878973+000
264	-.500284+000		.624164+000
300	.435536-001		-.936256-001
304	.160170+000		-.464346+000
309	-.105279+000		-.134894+001
312	.767787+000		-.957890+000
348	.283831-001		-.610072-001
352	.104367+000		-.302570+000
357	-.685986-001		-.878971+000
360	.500289+000		-.624162+000
396	-.435555-001		.936243-001
400	-.160167+000		.464342+000
405	.105281+000		.134893+001
408	-.767784+000		.957885+000
444	-.283813-001		.610055-001
448	-.104364+000		.302564+000
453	.686012-001		.878963+000
456	-.500285+000		.624155+000
492	.435574-001		-.936249-001
496	.160169+000		-.464343+000
501	-.105280+000		-.134893+001
504	.767785+000		-.957886+000
540	.283812-001		-.610047-001
544	.104364+000		-.302561+000
549	-.686004-001		-.878956+000
552	.500282+000		-.624150+000

EIGENVECTOR NUMBER 7 FREQUENCY = .108734+04 HERTZ

NODE	UX	UY	UZ
12	-.283813-001		.610048-001
16	-.104363+000		.302560+000
21	.685996-001		.878952+000
24	-.500279+000		.624147+000
60	.435583-001		-.936269-001
64	.160170+000		-.464351+000
69	-.105280+000		-.134895+001
72	.767791+000		-.957899+000
108	.283822-001		-.610064-001
112	.104365+000		-.302566+000
117	-.685990-001		-.878961+000
120	.500283+000		-.624155+000
156	-.435575-001		.936258-001
160	-.160170+000		.464348+000
165	.105281+000		.134895+001
168	-.767791+000		.957897+000
204	-.283820-001		.610066-001

208	-.104366+000	.302569+000
213	.685011-001	.878975+000
216	-.500291+000	.624165+000
252	.435573-001	-.936246-001
256	.160156+000	-.464342+000
261	-.105279+000	-.134893+001
264	.767782+000	-.957883+000
300	.283814-001	-.610048-001
304	.104365+000	-.302562+000
309	-.685009-001	-.878963+000
312	.500287+000	-.624154+000
348	-.435547-001	.936273-001
352	-.160170+000	.464351+000
357	.105278+000	.134894+001
360	-.767786+000	.957895+000
396	-.283835-001	.610083-001
400	-.104365+000	.302574+000
405	.685994-001	.878980+000
408	-.500293+000	.624169+000
444	.435564-001	-.936237-001
448	.160167+000	-.464339+000
453	-.105281+000	-.134893+001
456	.767783+000	-.957880+000
492	.283812-001	-.610044-001
496	.104364+000	-.302560+000
501	-.685001-001	-.878955+000
504	.500283+000	-.624148+000
540	-.435575-001	.936259-001
544	-.160169+000	.464347+000
549	.105281+000	.134894+001
552	-.767789+000	.957893+000

EIGENVECTOR NUMBER 8 FREQUENCY = .189730+04 HERTZ

NODE	UX	UY	UZ
12	.293021+000		-.297008+000
16	.287535+000		-.576930+000
21	.560652+000		.344505+000
24	-.381637+000		-.273333-001
60	-.106077-002		.108770-002
64	-.103227-002		.210983-002
69	-.202492-002		-.125871-002
72	.141950-002		.102309-003
108	-.294850+000		.296899+000
112	-.289324+000		.580598+000
117	-.563561+000		-.346679+000
120	.384102+000		.275194-001
156	-.509657+000		.516629+000
160	-.500093+000		.100353+001

165	-.974106+000		-.599217+000
168	.663848+000		.475628-001
204	-.597695+000		.595935+000
208	-.576854+000		.115757+001
213	-.112353+001		-.691210+000
216	.765764+000		.545554-001
252	-.508909+000		.515565+000
256	-.499065+000		.100146+001
261	-.972093+000		-.597989+000
264	.662513+000		.474618-001
300	-.293045+000		.247058+000
304	-.287544+000		.577023+000
309	-.560092+000		-.344542+000
312	.381733+000		.273509-001
348	.103517-002		-.103820-002
352	.102313-002		-.201676-002
357	.198094-002		.120915-002
360	-.131510-002		-.918912-004
396	.294437+000		-.298250+000
400	.289316+000		-.560508+000
405	.563523+000		.346640+000
408	-.384005+000		-.275036-001
444	.509634+000		-.516580+000
448	.500089+000		-.100344+001
453	.974054+000		.599180+000
456	-.663784+000		-.475460-001
492	.587872+000		-.595886+000
496	.576859+000		-.115748+001
501	.112359+001		.691160+000
504	-.765687+000		-.548485-001
540	.508585+000		-.515516+000
544	.499059+000		-.100137+001
549	.972059+000		.597947+000
552	-.662417+000		-.474471-001

EIGENVECTOR NUMBER 9 FREQUENCY = .189731+04 HERTZ

NODE	UX	UY	UZ
12	-.509645+000		.516606+000
16	-.500091+000		.100348+001
21	-.974089+000		-.599220+000
24	.663849+000		.475427-001
60	-.587884+000		.595913+000
64	-.576863+000		.115754+001
69	-.112351+001		-.691165+000
72	.765732+000		.548578-001
108	-.508596+000		.515544+000
112	-.499061+000		.100142+001
117	-.972080+000		-.597974+000

120	.662478+000	.474532-001
156	-.293033+000	.297036+000
160	-.287537+000	.576979+000
165	-.560075+000	-.344542+000
168	.381705+000	.273330-001
204	.104809-002	-.105997-002
208	.102519-002	-.205552-002
213	.200400-002	.125493-002
216	-.137575-002	-.824834-004
252	.294549+000	-.298873+000
256	.289322+000	-.580552+000
261	.563540+000	.346647+000
264	-.384040+000	-.275176-001
300	.509644+000	-.516601+000
304	.500091+000	-.100348+001
309	.974077+000	.599161+000
312	-.663816+000	-.475623-001
348	.587831+000	-.595905+000
352	.576858+000	-.115752+001
357	.112351+001	.691206+000
360	-.765751+000	-.548370-001
396	.508597+000	-.515540+000
400	.499063+000	-.100141+001
405	.972076+000	.597956+000
408	-.662458+000	-.474609-001
444	.293034+000	-.297035+000
448	.287542+000	-.576982+000
453	.560071+000	.344507+000
456	-.381674+000	-.273531-001
492	-.104915-002	.106426-002
496	-.103085-002	.207109-002
501	-.200103-002	-.121023-002
504	.135176-002	.112447-003
540	-.294551+000	.298877+000
544	-.289323+000	.580556+000
549	-.563548+000	-.345667+000
552	.384058+000	.275081-001

EIGENVECTOR NUMBER 10 FREQUENCY = .191288+04 HERTZ

NODE	UX	UY	UZ
12	.293633+000		-.594176+000
16	.891023-001		-.110595+001
21	.481904+000		.517272+000
24	-.122555+001		-.172347+000
60	.293621+000		-.594164+000
64	.890922-001		-.110593+001
69	.481876+000		.517229+000
72	-.122551+001		-.172364+000

108	.293610+000	-.594153+000
112	.890807-001	-.110591+001
117	.481856+000	.517226+000
120	-.122550+001	-.172357+000
156	.293604+000	-.594146+000
160	.890734-001	-.110589+001
165	.481848+000	.517238+000
168	-.122551+001	-.172345+000
204	.293603+000	-.594145+000
208	.890745-001	-.110589+001
213	.481841+000	.517206+000
216	-.122548+001	-.172362+000
252	.293605+000	-.594147+000
256	.890764-001	-.110589+001
261	.481847+000	.517221+000
264	-.122549+001	-.172356+000
300	.293613+000	-.594154+000
304	.890823-001	-.110591+001
309	.481864+000	.517246+000
312	-.122552+001	-.172346+000
348	.293626+000	-.594169+000
352	.890971-001	-.110594+001
357	.481884+000	.517231+000
360	-.122551+001	-.172366+000
396	.293639+000	-.594182+000
400	.891049-001	-.110596+001
405	.481911+000	.517259+000
408	-.122554+001	-.172360+000
444	.293648+000	-.594192+000
448	.891163-001	-.110598+001
453	.481932+000	.517288+000
456	-.122557+001	-.172350+000
492	.293650+000	-.594195+000
496	.891202-001	-.110599+001
501	.481931+000	.517262+000
504	-.122555+001	-.172368+000
540	.293645+000	-.594188+000
544	.891143-001	-.110597+001
549	.481922+000	.517265+000
552	-.122555+001	-.172361+000

EIGENVECTOR NUMBER 11 FREQUENCY = .199986+04 HERTZ

NODE	UX	UY	UZ
12	.190790-001		-.631844-001
16	.135173+000		-.400338+000
21	-.259386+000		-.169531+001
24	.112156+001		-.106227+001
60	-.426479-002		.141342-001

64	-.304756-001	.895935-001
69	.580702-001	.379477+000
72	-.251051+000	.237771+000
108	-.148004-001	.490298-001
112	-.105653+000	.310707+000
117	.201343+000	.131585+001
120	-.870543+000	.824498+000
156	.190779-001	-.631813-001
160	.136174+000	-.400333+000
165	-.259390+000	-.169531+001
168	.112157+001	-.106227+001
204	-.426599-002	.141367-001
208	-.304760-001	.895968-001
213	.580674-001	.379467+000
216	-.251049+000	.237766+000
252	-.148037-001	.490337-001
256	-.105691+000	.310715+000
261	.201337+000	.131585+001
264	-.870542+000	.824497+000
300	.190725-001	-.631754-001
304	.136168+000	-.400323+000
309	-.259400+000	-.169531+001
312	.112158+001	-.106226+001
348	-.427162-002	.141408-001
352	-.304832-001	.896052-001
357	.580563-001	.379464+000
360	-.251050+000	.237768+000
396	-.148055-001	.490331-001
400	-.105694+000	.310714+000
405	.201333+000	.131585+001
408	-.870544+000	.824495+000
444	.190752-001	-.631812-001
448	.136169+000	-.400331+000
453	-.259395+000	-.169531+001
456	.112157+001	-.106225+001
492	-.426623-002	.141341-001
496	-.304786-001	.895931-001
501	.580669-001	.379474+000
504	-.251061+000	.237768+000
540	-.148001-001	.490274-001
544	-.105688+000	.310702+000
549	.201342+000	.131585+001
552	-.870549+000	.824492+000

EIGENVECTOR NUMBER 12 FREQUENCY = .19998E+04 HERTZ

NODE	UX	UY	UZ
12	.609189-002		-.201564-001
16	.434323-001		-.127678+000

21	-.827012-001	-.540608+000
24	.357647+000	-.338747+000
60	-.195506-001	.647761-001
64	-.139630+000	.410501+000
69	.266021+000	.173650+001
72	-.115016+001	.108932+001
108	.134840-001	-.446453-001
112	.962214-001	-.282874+000
117	-.183272+000	-.119786+001
120	.792477+000	-.750577+000
156	.608664-002	-.201513-001
160	.434265-001	-.127668+000
165	-.827113-001	-.540612+000
168	.357652+000	-.338745+000
204	-.195584-001	.647823-001
208	-.139536+000	.410514+000
213	.266006+000	.173650+001
216	-.115015+001	.108932+001
252	.134753-001	-.446399-001
256	.962113-001	-.282861+000
261	-.183289+000	-.119788+001
264	.792485+000	-.750579+000
300	.607736-002	-.201443-001
304	.434165-001	-.127655+000
309	-.827302-001	-.540626+000
312	.357661+000	-.338749+000
348	-.195664-001	.647892-001
352	-.139547+000	.410528+000
357	.265991+000	.173649+001
360	-.115015+001	.108932+001
396	.134721-001	-.446368-001
400	.962081-001	-.282854+000
405	-.183295+000	-.119787+001
408	.792485+000	-.750576+000
444	.608123-002	-.201477-001
448	.434206-001	-.127661+000
453	-.827226-001	-.540622+000
456	.357658+000	-.338749+000
492	-.195564-001	.647801-001
496	-.139636+000	.410509+000
501	.266010+000	.173650+001
504	-.115016+001	.108932+001
540	.134844-001	-.446474-001
544	.962216-001	-.282876+000
549	-.183272+000	-.119786+001
552	.792477+000	-.750579+000

EIGENVECTOR NUMBER 13 FREQUENCY = .236033+04 HERTZ

NODE	UX	UY	UZ
12	-.172733+000		.199582+000
16	-.171344+000		.372530+000
21	-.323999+000		-.149240+000
24	.194718+000		.619568-001
60	.465036+000		-.537322+000
64	.461297+000		-.100293+001
69	.872277+000		.401894+000
72	-.524224+000		-.166805+000
108	.637770+000		-.736900+000
112	.632645+000		-.137546+001
117	.119627+001		.551169+000
120	-.718929+000		-.228762+000
156	.172736+000		-.199570+000
160	.171358+000		-.372511+000
165	.324009+000		.149274+000
168	-.194680+000		-.619514-001
204	-.465029+000		.537340+000
208	-.461275+000		.100296+001
213	-.872257+000		-.401893+000
216	.524276+000		.166819+000
252	-.637763+000		.736921+000
256	-.632622+000		.137549+001
261	-.119625+001		-.551174+000
264	.718991+000		.228774+000
300	-.172733+000		.199589+000
304	-.171340+000		.372541+000
309	-.323997+000		-.149283+000
312	.194734+000		.619607-001
348	.465031+000		-.537330+000
352	.461283+000		-.100295+001
357	.872264+000		.401897+000
360	-.524256+000		-.166809+000
396	.637765+000		-.736925+000
400	.632622+000		-.137550+001
405	.119626+001		.551177+000
408	-.719000+000		-.228776+000
444	.172731+000		-.199604+000
448	.171326+000		-.372567+000
453	.323989+000		.149283+000
456	-.194770+000		-.619720-001
492	-.465035+000		.537311+000
496	-.461307+000		.100292+001
501	-.872283+000		-.401885+000
504	.524191+000		.166802+000
540	-.637771+000		.736903+000
544	-.632646+000		.137546+001
549	-.119628+001		-.551170+000
552	.718933+000		.228763+000

EIGENVECTOR NUMBER 14 FREQUENCY = .236033+04 HERTZ

NODE	UX	UY	UZ
12	-.636697+000		.735703+000
16	-.631555+000		.137322+001
21	-.119425+001		-.550255+000
24	.717824+000		.228402+000
60	-.467945+000		.540672+000
64	-.464191+000		.100919+001
69	-.877737+000		-.404400+000
72	.527474+000		.167844+000
108	.168746+000		-.195041+000
112	.167350+000		-.364042+000
117	.316504+000		.145855+000
120	-.190381+000		-.605640-001
156	.636685+000		-.735749+000
160	.631506+000		-.137329+001
165	.119421+001		.550272+000
168	-.717961+000		-.228425+000
204	.467926+000		-.540756+000
208	.464105+000		-.100933+001
213	.877673+000		.404422+000
216	-.527714+000		-.167894+000
252	-.168772+000		.194944+000
256	-.167453+000		.363886+000
261	-.316584+000		-.145831+000
264	.190100+000		.605065-001
300	-.636709+000		.735665+000
304	-.631599+000		.137316+001
309	-.119429+001		-.550248+000
312	.717711+000		.228378+000
348	-.467941+000		.540707+000
352	-.464160+000		.100925+001
357	-.877718+000		-.404414+000
360	.527572+000		.167852+000
396	.168770+000		-.194944+000
400	.167450+000		-.363884+000
405	.316579+000		.145829+000
408	-.190101+000		-.605068-001
444	.636718+000		-.735614+000
448	.631646+000		-.137307+001
453	.119432+001		.550232+000
456	-.717566+000		-.228348+000
492	.467958+000		-.540617+000
496	.464246+000		-.100910+001
501	.877775+000		.404387+000
504	-.527316+000		-.167811+000
540	-.168748+000		.195048+000

544	-.167345+000		.364053+000
549	-.316507+000		-.145863+000
552	.190399+000		.605642-001

EIGENVECTOR NUMBER 15 FREQUENCY = .238623+04 HERTZ

NODE	UX	UY	UZ
12	-.392537-001		-.155957+000
16	-.162157+000		-.252999+000
21	-.123130+000		.423763-001
24	-.452425+000		-.911147-001
60	.555945-001		.221577+000
64	.230056+000		.359490+000
69	.174631+000		-.602761-001
72	.642480+000		.129412+000
108	.135586+000		.539694+000
112	.560720+000		.875569+000
117	.425727+000		-.146737+000
120	.156516+001		.315251+000
156	.179244+000		.713201+000
160	.741104+000		.115704+001
165	.562744+000		-.193877+000
168	.206849+001		.416622+000
204	.174833+000		.695656+000
208	.722659+000		.112657+001
213	.548895+000		-.189113+000
216	.201760+001		.406370+000
252	.123536+000		.491758+000
256	.510905+000		.797802+000
261	.387898+000		-.133707+000
264	.142615+001		.287249+000
300	.391390-001		.156093+000
304	.162045+000		.253253+000
309	.122967+000		-.424683-001
312	.452556+000		.911624-001
348	-.557035-001		-.221446+000
352	-.230192+000		-.359247+000
357	-.174835+000		.601759-001
360	-.642341+000		-.129372+000
396	-.135581+000		-.539697+000
400	-.560713+000		-.875576+000
405	-.425717+000		.146737+000
408	-.156517+001		-.315254+000
444	-.179131+000		-.713335+000
448	-.740993+000		-.115729+001
453	-.562532+000		.193980+000
456	-.206862+001		-.416662+000
492	-.174725+000		-.695787+000
496	-.722765+000		-.112882+001

501	-.548694+000	.189205+000
504	-.201773+001	-.406414+000
540	-.123541+000	-.491754+000
544	-.510911+000	-.797794+000
549	-.387910+000	.133699+000
552	-.142614+001	-.267250+000

ROUTINE TERMINATED AT MFDRS

RUN TERMINATED FOR MAX TIME AT 167630

B	000000	000000	000001	413744	000000	000001	00000
	000000	000001	000000	040406	000000	000000	00000
A	777777	777776	000000	000000	743000	000000	00000
	200663	036643	564404	547275	777600	012403	60626
R	000000	010363	000000	000077	163014	576344	00034
	000000	000030	000000	000000	000000	020464	00000

DATA CARDS ENCOUNTERED BY SYSTEM - IGNORED

D.3 RESULTS OF ANSYS RUN FOR 33" FLAWED WHEEL

ANSYS - ENGINEERING ANALYSIS SYSTEM
SWANSON ANALYSIS SYSTEMS, INC. ELIZABETH, PENN

RAIL WHEEL MODES-SOLID ELEMENT

COMPLETE SET OF EIGENVALUES

MODE	FREQUENCY (HERTZ)
1	.14852+003
2	.25513+003
3	.37432+003
4	.42170+003
5	.42963+003
6	.76453+003
7	.87615+003
8	.10164+004
9	.10831+004
10	.10839+004
11	.13517+004
12	.18089+004
13	.19395+004
14	.19597+004
15	.19988+004
16	.20003+004
17	.21951+004
18	.23803+004
19	.24156+004
20	.25946+004
21	.26497+004
22	.27166+004
23	.29951+004
24	.30773+004
25	.30865+004
26	.30883+004
27	.33902+004
28	.34135+004
29	.35844+004
30	.36944+004
31	.37234+004
32	.39392+004
33	.40999+004
34	.44243+004
35	.44448+004
36	.47692+004
37	.48069+004
38	.51195+004
39	.52510+004
40	.54056+004
41	.58545+004
42	.59829+004
43	.60456+004
44	.60575+004
45	.61127+004

46	.62450+004
47	.64307+004
48	.64815+004
49	.68287+004
50	.68888+004
51	.72051+004
52	.72053+004
53	.74901+004
54	.90264+004
55	.90791+004
56	.92226+004
57	.92293+004
58	.93605+004
59	.95444+004
60	.10102+005
61	.10132+005
62	.10167+005
63	.10204+005
64	.10242+005
65	.10300+005
66	.10340+005
67	.10460+005
68	.10478+005
69	.10627+005
70	.10687+005
71	.10842+005
72	.11847+005
73	.11901+005
74	.12183+005
75	.12316+005
76	.12604+005
77	.12697+005
78	.12768+005
79	.13188+005
80	.13371+005
81	.13424+005
82	.13789+005
83	.13834+005
84	.14150+005
85	.14224+005
86	.14258+005
87	.14368+005
88	.14454+005
89	.14554+005
90	.14640+005
91	.14680+005
92	.14743+005
93	.14837+005
94	.14927+005
95	.14987+005
96	.15038+005
97	.15045+005
98	.15108+005
99	.15216+005
100	.15377+005
101	.15683+005
102	.15769+005

103	.15860+005	
104	.16092+005	180
105	.16710+005	
106	.17402+005	

ANSYS - ENGINEERING ANALYSIS SYSTEM
SWANSON ANALYSIS SYSTEMS, INC. ELIZABETH, PEN

RAIL WHEEL MODES-SOLID ELEMENT

COMPLETE SET OF REDUCED EIGENVECTORS

EIGENVECTOR NUMBER 1 FREQUENCY = .148517+03 HERTZ

NODE	UX	UY	UZ
12	-.403551-001		.861516-001
16	-.553776-001		.231653+000
21	-.441261-001		.247166+000
24	-.213414-001		.260894+000
60	.768486-002		-.137547-001
64	.332532-001		-.863131-001
69	-.143604-001		-.249524+000
72	.138341+000		-.184160+000
108	.368032-001		-.607211-001
112	.850622-001		-.252237+000
117	.114827-001		-.490836+000
120	.213295+000		-.407529+000
156	.459368-001		-.743408-001
160	.100246+000		-.300217+000
165	.206010-001		-.555169+000
168	.230508+000		-.469530+000
204	.368025-001		-.607197-001
208	.850583-001		-.252227+000
213	.114850-001		-.490805+000
216	.213277+000		-.407508+000
252	.768714-002		-.137580-001
256	.332542-001		-.863203-001
261	-.143548-001		-.249514+000
264	.138326+000		-.184159+000
300	-.403445-001		.861348-001
304	-.553577-001		.231594+000
309	-.441165-001		.247074+000
312	-.213084-001		.260810+000
348	-.219529-001		.440765-001
352	-.707729-001		.763333+000
357	-.125877-001		.958982+000
360	-.169473+000		.896196+000
396	.175747-002		-.436068-002
400	-.630670-001		.124992+001
405	.514383-001		.162547+001
408	-.277947+000		.148669+001
444	-.520231-003		-.357230-003
448	-.611408-001		.143842+001
453	.782832-001		.189895+001
456	-.329763+000		.172600+001
492	.175793-002		-.436142-002
496	-.630939-001		.125002+001
501	.514392-001		.162566+001

504	-.278033+000	.148685+001
540	-.219559-001	.440826-001
544	-.708074-001	.763449+000
549	-.125934-001	.959195+000
552	-.169564+000	.896373+000
626	-.266768-001	.550060+000
674	.184705-002	.924650+000
722	.173429-001	.105748+001
770	.183471-002	.924693+000
818	-.266938-001	.550101+000

EIGENVECTOR NUMBER 2 FREQUENCY = .255127+03 HERTZ

NODE	UX	UY	UZ
12	.142580+000		-.218799+000
16	.281918+000		-.816668+000
21	.982286-001		-.141331+001
24	.574302+000		-.121707+001
60	.980108-001		-.156142+000
64	.195277+000		-.602026+000
69	.620166-001		-.101942+001
72	.387647+000		-.887305+000
108	.498428-001		-.803394-001
112	.977636-001		-.306494+000
117	.336613-001		-.505173+000
120	.184305+000		-.445261+000
156	.513469-005		-.839705-005
160	.118848-004		-.345989-004
165	.136761-005		-.689850-004
168	.311470-004		-.563512-004
204	-.498361-001		.803287-001
208	-.977475-001		.306448+000
213	-.336597-001		.505079+000
216	-.184262+000		.445186+000
252	-.980122-001		.156145+000
256	-.195280+000		.602039+000
261	-.620167-001		.101944+001
264	-.387653+000		.887323+000
300	-.142590+000		.218819+000
304	-.281938+000		.816739+000
309	-.982296-001		.141344+001
312	-.574354+000		.121718+001
348	-.261034-001		.518071-001
352	-.281447+000		.885725+000
357	-.116433+000		.143844+001
360	-.596526+000		.123787+001
396	.476095-002		-.767398-002
400	-.175108+000		.590994+000
405	-.732630-001		.927829+000
408	-.375237+000		.800047+000
444	-.149197-006		.114486-006
448	-.150371-005		.490164-004
453	-.141592-005		.486172-004
456	.311270-006		.497629-004
492	-.476071-002		.767321-002
496	.175102+000		-.590889+000
501	.732620-001		-.927707+000

504	.375223+000	-.799930+000
540	.261004-001	-.518011-001
544	.281431+000	-.885621+000
549	.116434+000	-.143828+001
552	.596481+000	-.123774+001
626	-.174066+000	.421650+000
674	-.117190+000	.327132+000
722	-.106967-005	.426048-004
770	.117187+000	-.327052+000
818	.174060+000	-.421592+000

EIGENVECTOR NUMBER 3 FREQUENCY = .374319+03 HERTZ

NODE	UX	UY	UZ
12	-.838937-001		.144302+000
16	-.156493+000		.501443+000
21	-.776628-001		.754093+000
24	-.253376+000		.687720+000
60	-.117250+000		.192104+000
64	-.225935+000		.724762+000
69	-.730476-001		.118818+001
72	-.425755+000		.104788+001
108	-.143495+000		.237581+000
112	-.285582+000		.913680+000
117	-.765282-001		.155625+001
120	-.581092+000		.135340+001
156	-.154331+000		.255906+000
160	-.310041+000		.988486+000
165	-.790088-001		.170123+001
168	-.643319+000		.147365+001
204	-.143473+000		.237542+000
208	-.285525+000		.913515+000
213	-.765307-001		.155589+001
216	-.580918+000		.135312+001
252	-.117226+000		.192064+000
256	-.225874+000		.724587+000
261	-.730472-001		.118781+001
264	-.425577+000		.104758+001
300	-.838812-001		.144296+000
304	-.156473+000		.501414+000
309	-.776448-001		.754049+000
312	-.253348+000		.687681+000
348	-.791862-002		.214795-001
352	.251588-001		.377077+000
357	.337600-001		.423799+000
360	.423376-002		.415971+000
396	.623350-002		-.541312-002
400	.241250+000		.296000+000
405	.231454+000		.258320+000
408	.273374+000		.275949+000
444	.327952-002		-.846973-003
448	.328866+000		.263951+000
453	.313507+000		.210442+000
456	.369099+000		.232832+000
492	.623380-002		-.541306-002
496	.241251+000		.295858+000
501	.231407+000		.258018+000

504	.273476+000	.275712+000
540	-.791608-002	.214739-001
544	.251555-001	.376950+000
549	.337079-001	.423508+000
552	.433102-002	.415746+000
626	.464695-001	.298061+000
674	.234424+000	.287118+000
722	.318293+000	.268801+000
770	.234401+000	.287084+000
818	.464421-001	.298048+000

EIGENVECTOR NUMBER 4 FREQUENCY = .421696+03 HERTZ

NODE	UX	UY	UZ
12	.329160-001		-.273818-001
16	.636496-001		-.137678+000
21	.290984-001		-.259563+000
24	.133659+000		-.215706+000
60	.951093-001		-.161196+000
64	.240445+000		-.700342+000
69	-.737159-002		-.151561+001
72	.722748+000		-.120239+001
108	.855027-001		-.149142+000
112	.220368+000		-.645705+000
117	-.113476-001		-.140900+001
120	.675016+000		-.111443+001
156	-.106522-003		.182252-003
160	-.269960-003		.786398-003
165	.872554-005		.170228-002
168	-.812712-003		.135057-002
204	-.856242-001		.149347+000
208	-.220670+000		.646584+000
213	.113494-001		.141088+001
216	-.675902+000		.111593+001
252	-.950427-001		.161073+000
256	-.240261+000		.699805+000
261	.734647-002		.151438+001
264	-.722135+000		.120144+001
300	-.327375-001		.270666-001
304	-.631880-001		.136335+000
309	-.291253-001		.256606+000
312	-.132230+000		.213376+000
348	.111642-001		-.240259-001
352	.801374-001		-.510033+000
357	-.971383-001		-.110512+001
360	.455397+000		-.863977+000
396	.805250-004		.751616-003
400	.939231-001		-.583845+000
405	-.925267-001		-.121020+001
408	.495056+000		-.953550+000
444	.830325-006		.200190-006
448	-.158574-003		.531297-003
453	.164029-004		.112641-002
456	-.553664-003		.876306-003
492	-.831109-004		-.742911-003
496	-.940558-001		.584235+000
501	.925376-001		.121108+001

504	-.495530+000		.954220+000
540	-.111336-001		.239670-001
544	-.798866-001		.509148+000
549	.971206-001		.110332+001
552	-.454580+000		.862539+000
626	-.128086-001		-.109524+000
674	-.229760-002		-.198980+000
722	-.685099-004		.221555-003
770	.223758-002		.199157+000
818	.129051-001		.109237+000

EIGENVECTOR NUMBER 5 FREQUENCY = .429635+03 HERTZ

NODE	UX	UY	UZ
12	-.103013+000		.180256+000
16	-.260927+000		.759338+000
21	.447692-002		.163777+001
24	-.782287+000		.130009+001
60	-.503763-001		.881474-001
64	-.126186+000		.373667+000
69	.229411-002		.795237+000
72	-.374637+000		.633441+000
108	.429129-001		-.745226-001
112	.116352+000		-.332485+000
117	-.129892-001		-.761055+000
120	.378110+000		-.592532+000
156	.883785-001		-.154039+000
160	.235116+000		-.678691+000
165	-.212635-001		-.152629+001
168	.748473+000		-.119495+001
204	.427531-001		-.742436-001
208	.115938+000		-.331272+000
213	-.129643-001		-.758394+000
216	.376830+000		-.590431+000
252	-.505509-001		.884442-001
256	-.126632+000		.374964+000
261	.231328-002		.798067+000
264	-.375994+000		.635680+000
300	-.103064+000		.180293+000
304	-.261029+000		.759548+000
309	.443233-002		.163818+001
312	-.782510+000		.130043+001
348	-.160937-001		.318860-001
352	-.125543+000		.486142+000
357	.173421-001		.973411+000
360	-.428690+000		.782850+000
396	.220581-002		-.509840-002
400	.108953+000		-.215632+000
405	.301813-001		-.487254+000
408	.296864+000		-.369300+000
444	-.361645-003		-.276526-003
448	.219998+000		-.583826+000
453	.292935-001		-.123230+001
456	.651461+000		-.959635+000
492	.220611-002		-.510040-002
496	.108757+000		-.214475+000
501	.303464-001		-.484881+000

504	.295889+000	-.367426+000
540	-.161168-001	.319354-001
544	-.125720+000	.487173+000
549	.175111-001	.975604+000
552	-.429598+000	.784573+000
626	-.414562-001	.160671+000
674	.688398-001	-.101180+000
722	.121717+000	-.249344+000
770	.688302-001	-.100770+000
818	-.414499-001	.160916+000

EIGENVECTOR NUMBER 6 FREQUENCY = .764528+03 HERTZ

NODE	UX	UY	UZ
12	-.189710+000		-.153144-001
16	-.255200+000		-.289614-001
21	-.387666+000		-.244221+000
24	-.206873+000		-.188163+000
60	-.111738-001		-.356359-001
64	.617019-002		-.118320+000
69	-.669564-001		-.319072+000
72	.124851+000		-.252350+000
108	.172848-001		-.269999-001
112	.425258-001		-.123727+000
117	-.212998-001		-.312502+000
120	.154985+000		-.241801+000
156	.224313-006		-.567121-005
160	.222256-005		-.223263-004
165	-.719272-005		-.485678-004
168	.162159-004		-.391953-004
204	-.172857-001		.269914-001
208	-.425260-001		.123696+000
213	.212888-001		.312445+000
216	-.154975+000		.241751+000
252	.111702-001		.356308-001
256	-.617673-002		.118305+000
261	.669462-001		.319054+000
264	-.124863+000		.252329+000
300	.189706+000		.153076-001
304	.255193+000		.289355-001
309	.387644+000		.244166+000
312	.206874+000		.188117+000
348	.101097-001		-.183479-001
352	.958605+000		.214755-001
357	.108313+001		.379291+000
360	.807265+000		.266940+000
396	-.139164-001		.615682-002
400	.873019+000		.687078-002
405	.993653+000		.367277+000
408	.726864+000		.248254+000
444	.477866-006		-.881714-007
448	.510911-004		.809080-005
453	.558585-004		.255974-004
456	.393194-004		.172380-004
492	.139175-001		-.615696-002
496	-.872942+000		-.687574-002
501	-.993578+000		-.367284+000

504	-.726785+000		-.248262+000
540	-.101083-001		.183458-001
544	-.958586+000		-.215082-001
549	-.108313+001		-.379367+000
552	-.807225+000		-.267000+000
626	.965252+000		-.516891+000
674	.913522+000		-.477610+000
722	.529218-004		-.736428-006
770	-.913446+000		.477609+000
818	-.965236+000		.516894+000

EIGENVECTOR NUMBER 7 FREQUENCY = .876151+03 HERTZ

NODE	UX	UY	UZ
12	.936057-001		.437315-001
16	.186264+000		.121095+000
21	.333624+000		.304464+000
24	.194311+000		.255753+000
60	.869587-001		.178504-001
64	.127503+000		.788181-001
69	.222476+000		.281228+000
72	.426923-001		.228333+000
108	.715750-001		.217054-001
112	.964820-001		.111051+000
117	.207975+000		.369739+000
120	-.246574-001		.292274+000
156	.686452-001		.256687-001
160	.873595-001		.135787+000
165	.211409+000		.436967+000
168	-.615924-001		.341251+000
204	.715737-001		.217088-001
208	.964771-001		.111068+000
213	.207980+000		.369785+000
216	-.246809-001		.292308+000
252	.869608-001		.178523-001
256	.127503+000		.788269-001
261	.222484+000		.281261+000
264	.426784-001		.228357+000
300	.936218-001		.437288-001
304	.186287+000		.121086+000
309	.333654+000		.304463+000
312	.194334+000		.255751+000
348	-.202099-001		.287066-001
352	-.137241+000		.236652+000
357	-.999795-001		.202367+000
360	-.931142-001		.207710+000
396	-.169705-001		.287593-002
400	-.108605+001		.229539+000
405	-.119793+001		-.143684+000
408	-.929649+000		-.164995-001
444	-.138454-001		.150796-002
448	-.153100+001		.223562+000
453	-.170006+001		-.336085+000
456	-.128388+001		-.142552+000
492	-.169694-001		.287532-002
496	-.108611+001		.229543+000
501	-.119799+001		-.143704+000

504	-.929694+000	-.165108-001
540	-.202110-001	.287089-001
544	-.137308+000	.236664+000
549	-.100054+000	.202360+000
552	-.931761-001	.207708+000
626	-.227718+000	.445880+000
674	-.116508+001	.777452+000
722	-.163079+001	.965992+000
770	-.116514+001	.777488+000
818	-.227784+000	.445923+000

EIGENVECTOR NUMBER 8 FREQUENCY = .101636+04 HERTZ

NODE	UX	UY	UZ
12	-.677635-001		.150707+000
16	.653731-002		.160048+000
21	-.116216+000		-.288232+000
24	.327740+000		-.115009+000
60	-.346801-001		.408619-001
64	-.415166-001		.987985-001
69	-.525328-001		.625146-001
72	-.175290-001		.664472-001
108	-.186763-001		.226833-002
112	-.164021-001		-.176723-001
117	-.506748-001		-.117830+000
120	.439613-001		-.827361-001
156	-.917575-002		-.181313-001
160	.966552-002		-.101789+000
165	-.625262-001		-.325282+000
168	.152443+000		-.235346+000
204	-.186774-001		.227025-002
208	-.164052-001		-.176635-001
213	-.506742-001		-.117808+000
216	.439493-001		-.827200-001
252	-.346817-001		.408628-001
256	-.415192-001		.988021-001
261	-.525355-001		.625190-001
264	-.175319-001		.664512-001
300	-.677674-001		.150705+000
304	.653183-002		.160043+000
309	-.116227+000		-.288249+000
312	.327739+000		-.115021+000
348	-.444691-001		.950361-001
352	.336553+000		.673671+000
357	-.146647+000		-.779907+000
360	.987375+000		-.324382+000
396	.896654-002		-.107128-001
400	.582194+000		.111766+001
405	-.462117-001		-.807254+000
408	.144399+001		-.220411+000
444	.311139-002		-.171574-002
448	.693029+000		.130890+001
453	.422632-001		-.683800+000
456	.156787+001		-.917169-001
492	.896613-002		-.107127-001
496	.582213+000		.111766+001
501	-.461965-001		-.807260+000

504	.144402+001	-.220413+000
540	-.444695-001	.950369-001
544	.336574+000	.673681+000
549	-.146626+000	-.779898+000
552	.987396+000	-.324373+000
626	.471740-001	.279529+001
674	.169804+000	.373699+001
722	.254388+000	.407565+001
770	.169820+000	.373700+001
818	.471932-001	.279531+001

EIGENVECTOR NUMBER 9 FREQUENCY = .108313+04 HERTZ

NODE	UX	UY	UZ
12	.748743-002		-.236144-001
16	-.178863-002		-.152698-001
21	.248501-001		.699701-001
24	-.610227-001		.365865-001
60	-.407962-001		.105061+000
64	-.177686+000		.546641+000
69	.152453+000		.163862+001
72	-.923304+000		.116045+001
108	.114274-001		-.183854-002
112	.146068-001		.142618-002
117	.275942-001		.344021-001
120	-.348967-002		.235443-001
156	.631193-001		-.111986+000
160	.204790+000		-.547486+000
165	-.964858-001		-.156241+001
168	.906284+000		-.111040+001
204	.116719-001		-.235498-002
208	.154901-001		-.111943-002
213	.270391-001		.270514-001
216	.697190-003		.183220-001
252	-.407709-001		.105055+000
256	-.177659+000		.546634+000
261	.152513+000		.163870+001
264	-.923334+000		.116050+001
300	.734529-002		-.231383-001
304	-.255579-002		-.127497-001
309	.256443-001		.775824-001
312	-.652383-001		.419706-001
348	.191566-001		-.427828-001
352	.868366-001		-.668786+000
357	-.152300+000		-.150897+001
360	.724094+000		-.110663+001
396	-.380608-002		.401103-002
400	-.142122+000		-.153888+000
405	-.641507-001		.840039-001
408	-.248428+000		.133024-001
444	-.146052-002		.676209-003
448	-.321684+000		.418570+000
453	.623332-001		.168803+001
456	-.115331+001		.115388+001
492	-.380138-002		.401658-002
496	-.143088+000		-.151001+000
501	-.638652-001		.911617-001

APPENDIX E

EQUIPMENT LIST

Signal Generation Equipment

Frequency Synthesizer	Rockland	Model 5100
Random Noise Generator	General Radio	1381
Sine Wave Generator	Hewlett-Packard	651B
Amplifier	MB Electronics (Gilmore Ind.)	2250MB
Shaker, 50 lbs	"	PM-50

Detection Equipment

Vibration Pickup	General Radio	1560-P52
Vibration Analyzer	" "	1564-A
Accelerometer	Endevco	2242
Acc. Preampl.	"	2607
Acc. " Power Supply	"	2622
Acc. " DC " "	Kepco	CK36-1.5M
Filter	Krohn-Hite	310CR
Storage Oscilloscope	Tektronix	564B
Oscilloscipe Camera	Hewlett-Packard	196A
Tape Recorder	Nagra-Kudelski	Type L3, (Nagra IV)
Frequency Counter	Hewlett-Packard	Model 523 DR
Microphone	Shure Bros.	9810B
Microphone	Bruel & Kjaer	½" Condenser

Analysis Equipment

Real Time Analyzer	Bruel & Kjaer	Type 3347
Real Time Analyzer	Spectral Dynamics	Model SD301C
Ensemble Averager	" "	SD302C
Memory	" "	SD 42
X-Y Display	" "	13116-Z
X-Y Recorder	Howlett-Packard	135A
Correlation Function Computer	PAR	101
Minicomputer	Data General	NOVA 1220
Teletype	Teletype Corp.	ASR33
Fast Paper Tape Reader	Data General	

APPENDIX F

REPORT OF INVENTIONS

In the opinion of the authors of this report the following items may or may not be patentable but are considered as improvements made under the contracts:

1) The system for Acoustic Inspection of Railroad Wheels or other manufactured components.
2) The mechanical impacter actuated by the movement of a railroad wheel, such as the variations of the design presented in this report.
3) The computer programs developed for analysis of acoustic signatures.

360 copies

☆U. S. GOVERNMENT PRINTING OFFICE: 1976--700-486--80

B21

24